WP3000 Deliverable:

WP3000: An investigation of the error characteristics of the GOCE geoid models

14 November 2011

GUT 2

VERSION 2 OF THE GOCE USER TOOLBOX

Ref:

ESA/XGCE-DTEX-EOPS-SW-09-0001 "**GUTS Phase 3: GUT Development and Supporting Scientific Studies**"

Coordinator: Per Knudsen (DNSC)

WP3000: "**An investigation of the error characteristics of the GOCE geoid models**"

Responsible partner: Newcastle University

Prepared by: Dr. Rory J. Bingham

DOCUMENT CHANGE LOG				
Rev.	Date	Sections modified	Comments	Changed by
1	14/11/11	All	Updated to include SPW2	Rory Bingham

Table of Contents

Applicable and Reference Documents

AD1 XGCE-DTEX-EOPS-SW-09-0001: "GUTS Phase 3: GUT Development and Supporting Scientific Studies". Response to ESA Intended Extension to ESRIN/Contract No. 19568/06/I-OL Statement of Work XGCE-DTEX-EOPS-SW-09-0001, 26 November 2009.

AD2 ESA-GUT2-SAD-001. GUT2 Technical Specification and Architectural Design v1.1, 21 September 2010.

AD3 ESA/XGCE-DTEX-EOPS-SW-04-0001 "GOCE User Toolbox Specifications (GUTS)", GUTS Final Report, 20 July 2007.

AD4 ESA/XGCE-DTEX-EOPS-SW-04-0001 "GUTS Phase 2: GUT Implementation and Supporting Scientific Studies", GUTS Final Report, 21 August 2009.

AD5 ESA/XGCE-DTEX-EOPS-SW-09-0001 "GUTS Phase 3: GUT Development and Supporting Scientific Studies", 26 November 2009

RD1 "GOCE High level processing facility – GOCE Level 2 Data Handbook", GO-MA-HPF-GS-0110, iss. 4.1, 23-June-2010

RD2 "Efficient propagation of error covariance matrices of gravitational models: application to GRACE and GOCE", G. Balmino, Journal of Geodesy, 83, 989-995 (2009).

RD3 "GUT The covhsmp and covhs2p software - User's guide", G. Balmino, 14 January, 2009

RD4 "Using the GOCE MDT in Ocean Data Assimilation", K. Haines, D. Lea and R.J. Bingham, Proceedings of the 4th International GOCE User Workshop, 31 March - 1 April, Munich, Germany

Abbreviations

CLS	Collecte Localisation Satellites
ECF	Error Covariance Function
GUT	GOCE User Toolbox
GOCE	Gravity and Ocean steady-state Circulation Explorer
HPF	High level Processing Facility
MSS	Mean Sea Surface
MDT	Mean Dynamic Topography
SLA	Sea Level Anomaly

Executive summary

The availability of the full error variance-covariance matrices for the GOCE gravity field models is an important feature of the GOCE mission. Potentially, it will allow users to evaluate the accuracy of a geoid or mean dynamic topography (MDT) derived from the gravity field model at any particular location, design optimal filters to remove errors from the surfaces, and rigorously assimilate a geoid/MDT into ocean models, or otherwise combine the GOCE gravity field with other data. This report presents an initial investigation into the error characteristics of the GOCE gravity field models as they are realised in the calculated geoid anomalies. The work was completed under the framework of GOCE User Toolbox (Phase 3) project as a supporting scientific study. The error calculations were performed using a set of routines developed by George Balmino. The computational issues associated with using these routines are described. The initial challenge was to convert the ascii form in which the GOCE error variance-covariance information is supplied into a format useable by the Balmino routines. How this challenge was met is described in the report.

The report then examines the error fields associated with the GOCE geoids. As expected, errors depend primarily on latitude and so zonal mean errors are discussed. Zonal mean errors are at their greatest at low latitudes – some hemispheric asymmetry, with errors somewhat greater in the Southern Hemisphere, resulting from the elliptical satellite orbit, is seen. For the timewise models, where the impact of the additional GOCE data is clearly seen, the error reduction grows from 0.5 cm (peak) at degree and order (d/o)=50 to 6 cm (peak) at d/o=224 – about 50% in each case. The ranking of the models in terms of errors varies with maximum truncation. Up to degree and order 150 the second direct solution has the largest errors and the second timewise model the smallest, with a factor of 2 difference. At d/o=240, the errors in the second timewise solution are 20 cm (peak) – 8-10 cm greater than the direct solutions.

Next, error covariances are described. It is shown that for all of the models and over all truncations, the error covariance functions (ECFs) at any latitude can be closely approximated by the zonal mean ECF at that latitude. In terms of zonal and meridional cross sections, within about 60 degrees of the equator the form of the ECFs does not change much with latitude. The form of the ECFs seems to depend on the solution method. The ECFs of the two timewise models are essentially identical, and at low degree and order quite distinct from the other models. The ECFs of the two direct solutions are less similar, with the second model having a more meridionally elongated pattern. Moving to higher d/o truncations, the ECFs of the various models converge on a similar rotationally symmetric pattern. The second direct solution, however, is an exception, maintaining its meridionally elongated pattern even at high degree and order. An attempt is made to characterise the ECFs in terms of zonal and meridional e-folding length scales, with the results generally confirming the preceding analysis.

With regard to the GOCE User toolbox and the initial aims of this work package, the main conclusions of this report are that once the initial challenges of handling the large ECFs are met, the efficiency of the Balmino routines are such that the error calculations are likely to be feasible for most users. This is fortunate, since it is unlikely the fast approximations to the error covariance functions, as originally suggested, can be easily found. Without substantial recoding effort it would not be possible to fully integrate all of the error calculation functionality of the Balmino routines in the GUT toolbox, and so they will likely remain as standalone tools. However, the small conversions routines developed as part of this work package could, without too much effort be incorporated into the toolbox. Thus providing a convenient entry point for those wishing to explore the error characteristics of the GOCE gravity models. The most useful, and perhaps feasible, next step would be to include the ability to calculate error fields on an arbitrary grid or set of points and to an arbitrary degree and order.

1 Introduction

The GOCE satellite was successfully launched in March 2009. The first level 2 datasets, based on two months of observations, were released to the scientific community in June 2010, with a second release, based on 8 months of observations following in March 2011. The primary products of the GOCE mission are the earth gravity models (EGMs), of which three variants are provided. The EGMs allow the geoid to be computed. A distinguishing feature of the GOCE mission is that, for the first time, the full error variance-covariance information associated with the EGMs will be also be provided to the user community, allowing, for instance, the error characteristic of the geoid, or other derived products to be studied and accounted for in subsequent applications. Because this error information has never previously been available to the user community, the tools and methods to fully exploit this information have yet to be developed. Some potential applications include the design of optimal filters and the characterization of errors magnitudes and length scales in mean dynamic topographies (MDT) derived from the gravity field models to enable the rigorous assimilation of an MDT into an ocean model. However, it may well be many years before the user communities have gained sufficient knowledge and experience to fully exploit the potential of the variance covariance information.

The European Space Agency have funded the development of the GOCE User Toolbox (GUT) to facilitate and ease the use of the GOCE products. In mind, has been the wider scientific community who may wish to use these products in their particular scientific area but who may be deterred by the unfamiliar nature of the spherical harmonic expression of many of the gravity field products. Supplied as part of the GUT package, but standing alone from GUT itself, is a set of tools developed by G Balmino (see RD2) to enable a range of error calculations using the GOCE error variance covariance information. (So far, it has been considered beyond the scope of the GUT project to fully integrate these tools into GUT, but this may be done at a later date.)

The original intention of WP3000 (see AD5) was to investigate the error characteristics of the *simulated* GOCE gravity model, with the first part considering the error characteristics of the geoid derived from the simulated model and the second part looking at the error characteristics of the geostrophic currents obtained from an MDT based on the simulated GOCE geoid (assuming that the errors in the mean sea surface could be neglected). In both cases the original plan was to examine how the error characteristics depended on geographical position, with changes expected primarily with latitude, and on maximum truncation. It was also hoped that the error covariances could somehow be approximated to allow a more rapid characterisation of the errors.

Due to events subsequent to the writing of the proposal, this final report has deviated with respect to the original aims. First, the most important change, caused by a delay in the start of the project, is that rather than describe the errors of a simulated GOCE model, this report presents an analysis of the error characteristics of actual GOCE gravity fields. This clearly is a positive development. Also unexpected was the release of three different versions of the GOCE gravity model, based on only two months of data, and a subsequent release of a second generation of the models, based on 8 months of data. This report compares the error characteristics of all six of these models, thereby shedding new light on how the solution method and the number of observations used may affect the error characteristics of the gravity fields. This is a further positive development. However, the analysis of six actual models is obviously a more difficult task than the analysis of one simulated model. For this reason the scope of this report is limited to considering the error characteristics of the GOCE geoids, with a similar analysis from geostrophic currents as originally intended left outstanding.

The use of the Balmino routines, and, in particular the interfacing of them with the ascii format in which the error variance covariance information is delivered, has also thrown up some unsuspected challenges and issues. Dealing with these has also placed an additional workload on the work package. Yet, what has come from meeting these challenges may be one of the most useful aspects of this work package. First, a set of routines have been developed to convert the raw ascii files delivered to ESA into a form that can be used by the Balmino routines. Second, the Balmino routines have been modified to work more easily. These interfaces and the modified Balmino routines, as well as a firsthand account of the use of the handling of the very large files, from a third party, non-specialist perspective will be made available to the wider user community. Third, through the delivery of this work package, errors and issues with the supplied data have been identified and corrected. These can be considered to be unforeseen additional deliverables of this work package.

The remainder of this report is structured as follows: In Section 2, the practical computational issues associated with the handling and processing of the GOCE error variance covariance models are described and the solutions to these problems are presented. The use of the Balmino routines is also discussed. Hopefully this will be of some use to others wishing to use the error information. In section 3, an examination of the error magnitudes of the GOCE geoids is given. The differences between the models and how the accumulated errors depend on truncation degree and order (d/o) and on geographical location are considered. The error covariances of the GOCE geoids are analysed in Section 4. In Sections 5 the conclusions of this work package are given and recommendations for further developments of GUT are made.

2 Computational issues

2.1 Handling the GOCE VCM files

The GOCE variance-covariance matrices (VCMs) are obtained from the ESA virtual server as compressed tarballs (*.TGZ). The key properties of the VCM files are given in Table 1.

Model	Filename: GO_CONS_EGM_GVC_2__*	d/o	Order	Form	File size (GB) *.TGZ	*.TAR	*.DAT
DIR1	20091101T000000_20100110T235959_0001	240	I	e20.14	11	35	13
DIR2	20091101T000000_20100630T235959_0001	240	I	e20.14	11	35	13
TIM1	20091101T000000_20100111T000000_0002	224	B	e25.20	13	34	10
TIM2	20091101T000000_20100705T235500_0001	250	B	e25.20	20	52	16
SPW1	20091030T005757_20100111T073815_0001	210	B	e11.8	3	13	8
SPW2	20091031T000000_20100705T235959_0001	240	B	e11.8	5	22	13

*Table 1: Key properties of the GOCE error covariance models available at the time of writing. For "order" I=interleaved denotes models for which the C and S coefficients are supplied as pairs and B=blocked denotes models for which the coefficients are supplied as all C's and then all S's within each order. The order can be determined from the header file *.IIH in each case. "Form" gives the number format in which the coefficients are supplied in the ascii files, defined in standard Fortran notation. Note for the first generation of models the tar file containing the coefficient files for each order had the suffix *.DBL rather than *.TAR. The *.DAT file is the full square matrix (in single precision).*

File sizes for the initial compressed tarballs range from just 3GB for the SPW1 model to 20GB for the TIM2 model. To some extent this obviously depends on the d/o of the model with SPW1 being the smallest at 210 and TIM2 being the largest at 250. However, it is in fact largely due to the number of decimal places to which the coefficients are given – 16 for the timewise models, but only 3 for the SPW models. If the latter precision is in fact adequate it would seem sensible to restrict all of the models to this thereby greatly reducing the size of the files the user must download.

Uncompressing and unpacking one of these files yields a header file (*.HDR) containing basic meta data for the model and another tarball (*.DBL in release 1, now *.TAR). For this tarball, the size differential between the models, due to the number of decimal places supplied, becomes even more pronounced, with sizes ranging from 13GB for the SPW1 model to 52 GB for TIM2. Again, it would be desirable to avoid this if possible, especially since for some users disk space may be limited. Unpacking the second tarball, gives a set of ascii files containing the VCM coefficients for each order plus a *.IIH file which gives the total number of coefficients in the files and describes their ordering. For TIM2 the maximum file size for a single order is 316MB. Note that throughout these operations only the file name suffix is changed, the first part of the file name remains unchanged and is given in Table 1 for each model.

Balmino Interface

The VCM computations described in this paper were performed using software, described in RD2 and RD3, which can be obtained from the GUT website. The first challenge faced by novice users is to convert the ascii VCM data into a format compatible with the Balmino software, which requires a full square matrix given as an unformatted sequential access file with one record corresponding to one row of the VCM. A small tool was written to perform this operation. The procedure is:

1. Read ascii files and write L-triangular matrix as unformatted binary; sequential access; 1 row = 1 record; single precision (DIR1: 35=>13Gb)
2. Generate square matrix as direct access file (shown schematically in Fig. 1):
    1. Create blank direct access file
    2. Determine max block size within memory limits (user defined)
    3. Fill rectangular block from sequential file containing L-tri
    4. Read in rows of direct access file, append corresponding columns of rectangular block and write back to file from first row to last before new block
    5. Complete upper triangular part of rectangular block and write rows to direct access file.
    6. Repeat until complete (1GB ram = 7 loops for DIR1)
3. Convert direct access file to sequential access

In fact, the first two operations have been combined into a single step, so that we go in one step from the supplied ascii files to the direct access square matrix file. The process was validated using the simulated GOCE VCM supplied as part of the Balmino tools package. As supplied, the Balmino routines expect the VCM to be double precision. For this study the routines were modified to take single precision. With this change, the size of the VCMs are generally substantially reduced from the uncompressed ascii files (see Table 1), with the smallest file size being 8GB for the SPW1 model and the largest being 16GB for the TIM2 model. Although not implemented here, a further reduction in file size, by a factor of 2, should be possible by storing the VCMs in two byte integer (INT*2) form, and modifying the Balmino routines accordingly.

The Balmino routines require that the rows/columns of the VCM be ordered by increasing spherical harmonic order, and within this by increase spherical harmonic degree with the even (C) and odd (S) coefficients supplied as pairs. An additional complication for the user, as shown in Table 1, is that two ordering schemes are used within the HPF. For the direct models the odd and even coefficients are ordered as pairs (or interleaved) as required by the Balmino routines. However, for the TIM and SPW solutions they are not, and an extra step is required to reorder the coefficients. A further complication is that for the spacewise models variances/covariances are defined for the C00,C10,C11, and S11 terms, whereas this is not the case for the other models.

It is worth bearing in mind that while these issues may be trivial for experienced users of error covariance products, they are unwelcome complications for the novice/less experienced user of these products. However, to ease the use of the GOCE VCMs we have developed a small set of Fortran utilities to convert the ascii files into the form required by the Balmino routines. These will be made available as part of a future GUT package.

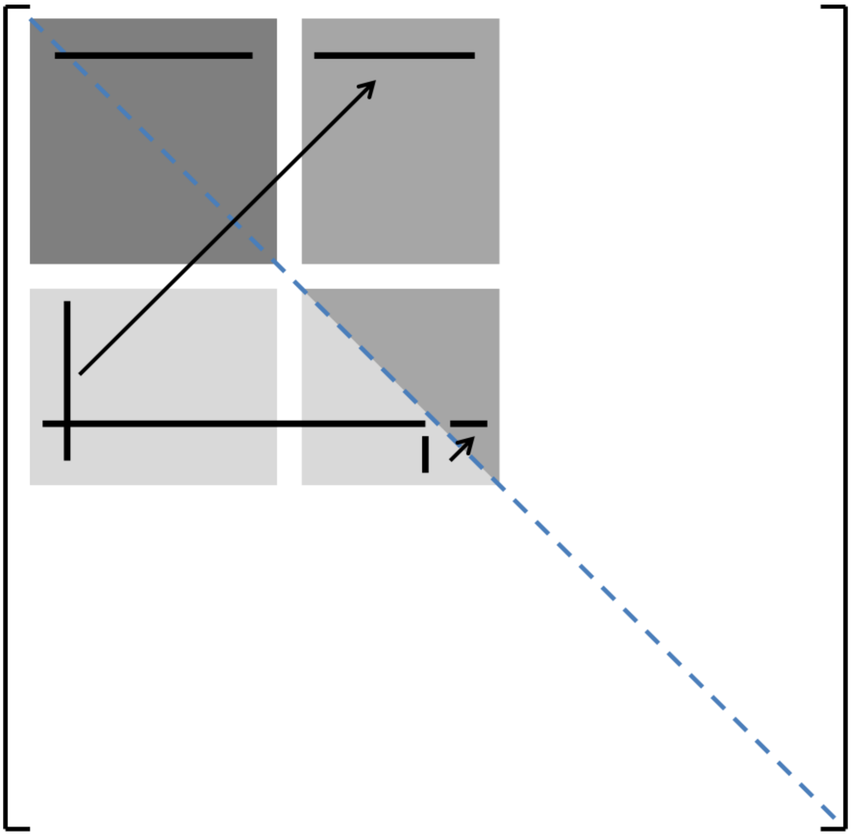

Figure 1: Schematic of the procedure for generating a full square variance covariance matrix suitable for use in the Balmino routines from the supplied ascii format.

2.2 Using the Balmino routines

The error calculations shown below were computed using the Balmino routines. Their use is described in detail in the documentation accompanying the Balmino package (RD3). Here we provide a brief discussion of their use from the perspective of a first time user as well as some comment on performance.

As already mentioned, the Balmino routines were modified to read the VCMs in single precision format. Apart from this a few further modifications were required to get the routines to run with our platform and compiler. These mainly concerned the format of read/write statements and also the formatting of the directing files in which the parameters of a calculation are specified. These initial stages were performed using the examples supplied as part of the Balmino package using the simulated GOCE VCM.

2.2.1 The error variance routine(covhsmp)

The geoid error maps shown below were computed using the Balmino covhsmp routine. A directory was created into which the Fortran program e_covhsmp.f90, validated against the supplied examples, was copied. With this code the parameter `lim`, which defines the maximum degree and order of the model, was changed from 201 to accommodate the maximum d/o of a particular model. This program was then complied to give an executable. Next the directing file was copied into the working directory from the supplied example and modified appropriately. The e_covhsmp routine requires that the name of the directing file be of the form covhsmp_dir_{VCM_NAME}, where VCM_NAME can be up to 15 characters in length. Below an example directing file for the e_covhsmp routine is shown (line numbers are given here for reference but do not appear in the direction file itself).

```
1.  GDIR240          (GOCE DIR) : name given to model = 15 first characters (max.)
2.  meanponc=1    0 : grid of mean values  ;  1 : grid of point values
3.  gm=0.39860044150000e+15,a=0.63781364600000e+07,uapl=0.29825765000000E+03,om=0.72920905111492E-04
4.  lmin=002  min. degree taken into account
5.  lsup=240   max. degree ...
6.  mmin=000 min. order ...
7.  msup=240 max. order ...
8.  m=-99,ldebp=000,lfinp=000  for specific orders (m=...) : min. and max. degree (end if m=-99)
9.  s0=+1.48547e+00             variance factor, will multiply the covariance matrix (read in e12.5)
10. kf=1           function type : 1=n(geoid),2=deltag(FA),3=dg=trr,4=d2T/dr2,5=dFA/dr,6=water eq.,0=other
11. kse=2          key for type of latitudes (1:geoc. , 2:ellip.)
12. h=0.0000000000  altitude (km): in effect according to function type: for kf =3,4, or 5 (read in f12.0)
13. unit=0         iunit for lat./lon. steps   (0:degree  , 1:minute)
14. fimin=-89.50,fimax=+89.50,dfi=+01.00,xlmin=+000.50,xlmax=+359.50,dxl=+01.00  grid limits (deg.)
15.  f0=000000000.00    factor depending of function type (effective only if kf = 0)    , read in f12.0
16. kfilter=00,dfilter=300000.00,psi0=5.000,fract0=0.500 filter parameters (no filtering if kfilter=0)
17. l1=002,l2=240,lstp=00 step by step cumulated errors from deg. l1 to l2, by step lstp (if =0 : l1 to l2)
18. 0    end of file (for PC)
```

Note that VCM_NAME is given in the first line of the directing file and this must be consistent with the name of the file, so in this case the directing file name is covhsmp_dir_GDIR240, and the name of the file containing the VCM has the form matcov_{VCM_NAME} (e.g. matcov_GDIR240 in this case). Either this file or a link to this file with the matcov_{VCM_NAME} name must be in the working directory from which the routine is executed. Once these components are in place the e_covhsmp routine can be executed. Upon execution the user is asked to enter VCM_NAME at the command line. The routine will then run to completion provided VCM_NAME is consistent across all instances just discussed, and provided the result file named grid_err_{VCM_NAME} does not already exist within the directory, such as might be the case if the routine has already been executed if only partially. Additionally the file covhsmp_out_{VCM_NAME} contains run time messages as to the progress of the routine.

Assuming the user is interested in computing geoid errors, apart from the first line discussed above, the most important lines of the directing file – i.e. those they are most likely to wish to alter – are:

- Lines 5 and 7, which should be changed to reflect the degree and order to which the gravity model under consideration is defined. In the example these are 240 to reflect the maximum d/o of the direct models.
- Line 14, which defines the grid on which the error is computed. In the example a global 1x1 degree grid is defined from 89.5S to 89.5N and 0.5-359.5E.

Somewhat more involved, line 17 can be altered to calculate the accumulated errors over some range of wavelengths, and, more involved still, line 16 can be altered to determine the effect of some standard filters on the error field. Finally, line 10 can be modified so that the errors of a derived quantity other than the geoid can be calculated.

To compute the error field associated with a TIM2 geoid truncated at the maximum d/o of 250, on our average PC took less than 100 minutes. For the other models defined to a lower d/o the calculation was correspondingly faster. And, a calculation to d/o=50 took only a few minutes.

For a calculation of accumulated errors to a specified d/o the output (grid_err_{VCM_NAME}) is given as formatted ascii, with one row corresponding to a constant latitude and with rows arranged from north to south. Preceding this is a one row header given the degree range over which the errors are calculated.

2.2.2 The error variance-covariance routine (covhs2p)

The GOCE geoid error covariance functions described below were computed using the Balmino covhs2p routine. Although quite a different calculation, the steps involved in successfully running the routine are just as described for the covhsmp routine. As before three files are required: The Fortran program, this time e_covhs2p.f90, which required similar modifications to read/write statements and the `lim` parameter; a directing file – covhs2p_dir_{VCM_NAME}, which required some minor modification to the formatting of the parameters; and, of course, the VCM file or link to it, named as before. For the analysis described below in Section 4 error covariance functions were computed in a 40x40 degree window at every point on a global grid. The directing file for this calculation with a direct solution is shown below:

```
1.  GDIR240             (GOCE DIR model) : name given to model = 15 first characters (max.)
2.  typgrid=0     0 : direct access     1 : sequential  (binary files)
3.  meanponc=1     0 : grid of (pseudo) mean values  ;  1 : grid of point values
4.  gm=0.39860044150000e+15,a=0.63781364600000e+07,uapl=0.29825765000000E+03,om=0.72920905111492E-04
5.  lmin=002  min. degree taken into account
6.  lsup=240   max. degree ...
7.  mmin=000 min. order ...
8.  msup=240 max. order ...
9.  m=-99,l_beg=000,l_end=000  for specific orders (m=...) : min. and max. degree (end if m=-99)
10. s0=+1.00000e+00        variance factor, will multiply the covariance matrix (read in e12.5)
11. kf=1          function type : 1=n(geoid),2=deltag(FA),3=dg=trr,4=d2T/dr2,5=dFA/dr,6=water eq.,0=other
12. kse=2          key for type of latitudes (1:geoc. , 2:ellip.)
13. h=+0.000000000  altitude (m): in effect according to function type (if kf=3, 4 or 5), read in f12.0
14. iunit=0        iunit for lat./lon. steps   (0:degree  , 1:minute)
15. fimin=-89.50,fimax=+89.50,dfi=+01.00,xlmin=+000.50,xlmax=+359.50,dxl=+01.00  grid limits (deg.)
16. H=lath=020,K=lonk=020   window size : half-height, halh-width (in number of grid points)
17. f0=1.0000000000 factor depending on function type (effective or not) , read in f12.0
18. kfilter=00,dfilter=300000.00,psi0=5.000,fract0=0.500 filter parameters (no filtering if kfilter=0)
19. l1=001,l2=240   computation for degree between l1 and l2 (eventually: reduction of cov. matrix)
20. dpsi=01.000000  stepsize (in degree) for tables of covariance functions) , read in f9.0
21. kverif=0    key for verification by "brute force" at a few points (if cov. matrix fits in core), 0: no
22. interp_ex=1             key for testing the interpolation procedure (if DA file), 0: no; 1:yes, for pair below
23. zi_lat=+40.50,zi_lon=+000.50,v_lat=+48.50,v_lon=+003.50  pair of points (1 in Z ; 2 in W [1]) for interp.
24. end of file (for PC)
```

Again, assuming the user is interested in computing geoid error covariances the most important lines of the directing file – i.e. those they are most likely to wish to alter – are:

- Line 1, which must be VCM_NAME
- Lines 6 and 8, which should be changed to reflect the degree and order to which the gravity model under consideration is defined. In the example these are 240 to reflect the maximum d/o of the direct models.
- Line 15, which defines the grid over which the error covariance functions are to computed (the outer window). In the example a global 1x1 degree grid is defined from 89.5S to 89.5N and 0.5-359.5E.
- Line 16, which defines the zonal and meridional half widths of the window in which the error covariance relative to the central point is determined. The resolution of this inner window is the same as for the outer window.

Somewhat more involved, line 19 can be altered to calculate the accumulated errors covariances over some range of wavelengths, and, more involved still, line 18 can be altered to determine the effect of some standard filters on the error covariance functions. Finally line 11 can be modified so that the errors of a derived quantity other than the geoid can be calculated. Further details can be found in the user guide accompanying the Balmino routines.

For this calculation, the computation time on our typical PC for the TIM2 model was under 1 day. Thus, we see that the despite the large VCMs the error calculations are unlikely to be prohibitively expensive for most users, with the greatest barrier perhaps being disk space, particularly if the maximum degree and order of the GOCE models increases much beyond its present limit of 250.

3 Geoid errors

One of the first questions a user who has calculated a GOCE geoid is likely to ask is ``what are the magnitude of the errors on the geoid estimate?". Because this will depend on the degree and order to which the geoid has been calculated – errors grow with increasing d/o – it is not possible to provide a single error map. Availability of the error variance covariance information, together with the Balmino covhsmp routine, allows the user to calculate an error map to the required degree and order and on the same grid as the geoid.

The theoretical description of the error propagation performed by the covhsmp routine to obtain the geoid error field is as follows: Let the gridded geoid be given by

$$N(\emptyset, \lambda) = Y^T X,$$

where ϕ is longitude and λ is geocentric latitude and

$$X = \{C_{lm}; S_{lm}\}_{l,m}$$

are the spherical harmonic coefficients of degree l and order m of the earth gravity model (GOCE level 2 products EGM_GOC_2_), and

$$Y = \{f_{lm} P_{lm}(\sin\phi)\cos m\lambda\,; f_{lm} P_{lm}(\sin\phi)\sin m\lambda\}_{l,m}$$

are the usual spherical harmonic functions with

$$f_{lm} = \frac{GM}{r\gamma}\left(\frac{R}{r}\right)^l$$

where GM is Earth's gravitational mass constant, R is the Earth's mean radius, γ is normal gravity at the computation point and r is radial distance. Then the corresponding error variance field is given by:

$$\sigma_N^2(\phi, \lambda) = Y^T \Gamma Y,$$

where Γ is the variance-covariance matrix (GOCE level 2 product EGM_GVC_2_) with ordering consistent with Y.

GOCE MDTs (left columns) and associated error fields (right columns) derived from the six GOCE models so far released are shown in Figure 2 (d/o=50), Figure 3 (d/o=100), Figure 4 (d/o=150), Figure 5 (d/o=200), Figure 6 (d/o=224), and Figure 7 (d/o=240). As error magnitudes depend primarily on latitude, zonal mean errors for all of the models, and for a GRACE model for comparison, are shown in Figure 8. MDTs are computed by the spectral method to reduce omission error as far as possible. Apart from this no additional filtering (e.g. Gaussian smoothing) has been applied. The mean sea surface used was the CLSMSS01. Note the errors maps only account for geoid commission error. The MDTs are shown just to give the reader an impression of the relative size of the errors and will not be discussed in detail. Suffices to say, it is clear that even at d/o=50 most of the MDT is present and adding further terms only changes the finer details. On the other hand the errors grow substantially between d/o=50 and d/o=240. Clearly therefore there is likely to be a point where the inclusion of additional spherical harmonic terms will increase MDT errors more than it reduces them.

In general, geoid errors decrease with latitude to some latitude beyond which they jump sharply. In the discussion of error magnitudes below, errors poleward of this point will be ignored. At d/o=50, the DIR2 model has the largest errors, reaching a peak of about 2.5 cm at the equator and a minimum of 1.5 cm at 80 degrees. This is about 1 cm greater than the first direct model, showing the impact the additional a priori constraint had on that solution. The errors of the first timewise model are very similar to those of DIR1, but for TIM1 the minimum point is reached at 60 degrees from the equator. For the second timewise release the additional 6 months of GOCE observations have reduced the errors by just under 0.5 cm. At d/o=50 the spacewise solutions have the lowest errors of just under 1 cm. For comparison we see that the GRACE errors are about an order of magnitude smaller than this. This is as expected, as the GRACE mission is better able to measure the longer wavelengths of the Earth’s gravity field. One notable difference between the two spacewise solutions is that the errors in SPW2 grow much more rapidly with latitude than the errors in SPW2. This is particularly the case at d/o=50, but is also true, although to a lesser degree, for higher truncations.

At d/o=100, the DIR2 model again has the largest errors, with an equatorial maximum of just over 4 cm, about 1.5 cm greater than the DIR1 geoid. The SPW2 model has the smallest errors at low latitudes, with a maximum of 1.2 cm, about 1.5 cm less than the first release. All of the first generation models have similar zonal mean errors at this truncation, but for the second generation models they have a greater range: 4.2 cm at the equator for DIR2 compared with about 1 cm for SPW2. At d/o=150, the relative ordering of the models has been just about preserved, with the first generation models lying between the DIR2 model, for which the peak errors at 5.5 cm are greatest, and the TIM2 and SPW2 models, for which the errors at 2.8 cm (peak) are the smallest. The widening gap between releases 1 and 2 of the timewise and spacewise models as the truncation is increased shows that the impact of the additional GOCE observations grows with decreasing spatial scale. However, in per cent terms the improvements remains about constant at around 40-60%. At d/o=150 the GRACE errors are now larger than those from the GOCE models, showing how GOCE is better able to measure the shorter wavelengths of the Earth’s gravity field. The zonal variations are greatest for the first generation models, a reflection of the fact that ground tracks of the satellite become more densely packed towards higher latitudes. In the second release the ground track gaps have been filled in resulting in a more zonally homogenous error field, particularly at lower latitudes.

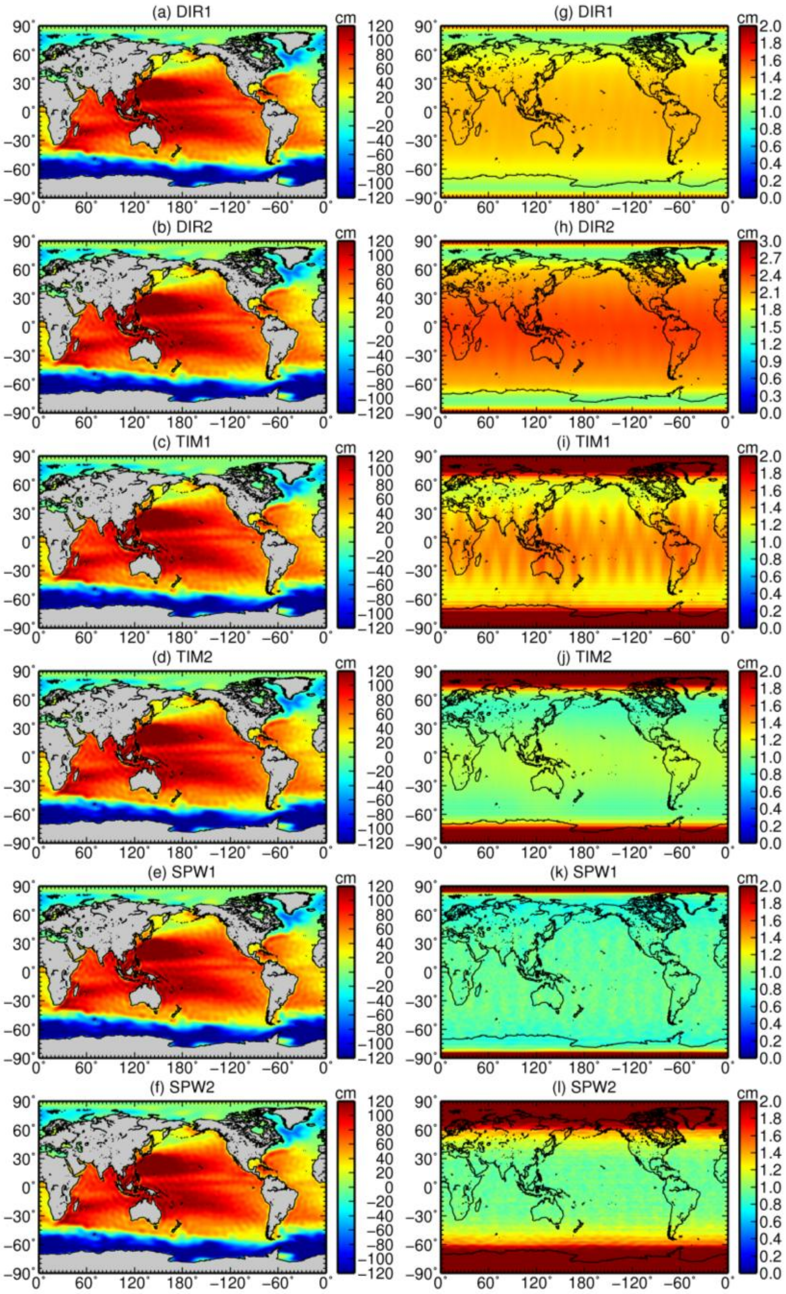

Figure 2: (a-e) MDTs derived from the GOCE gravity models by the spectral approach, with truncation at d/o=50. (f-j)The corresponding geoid error maps.

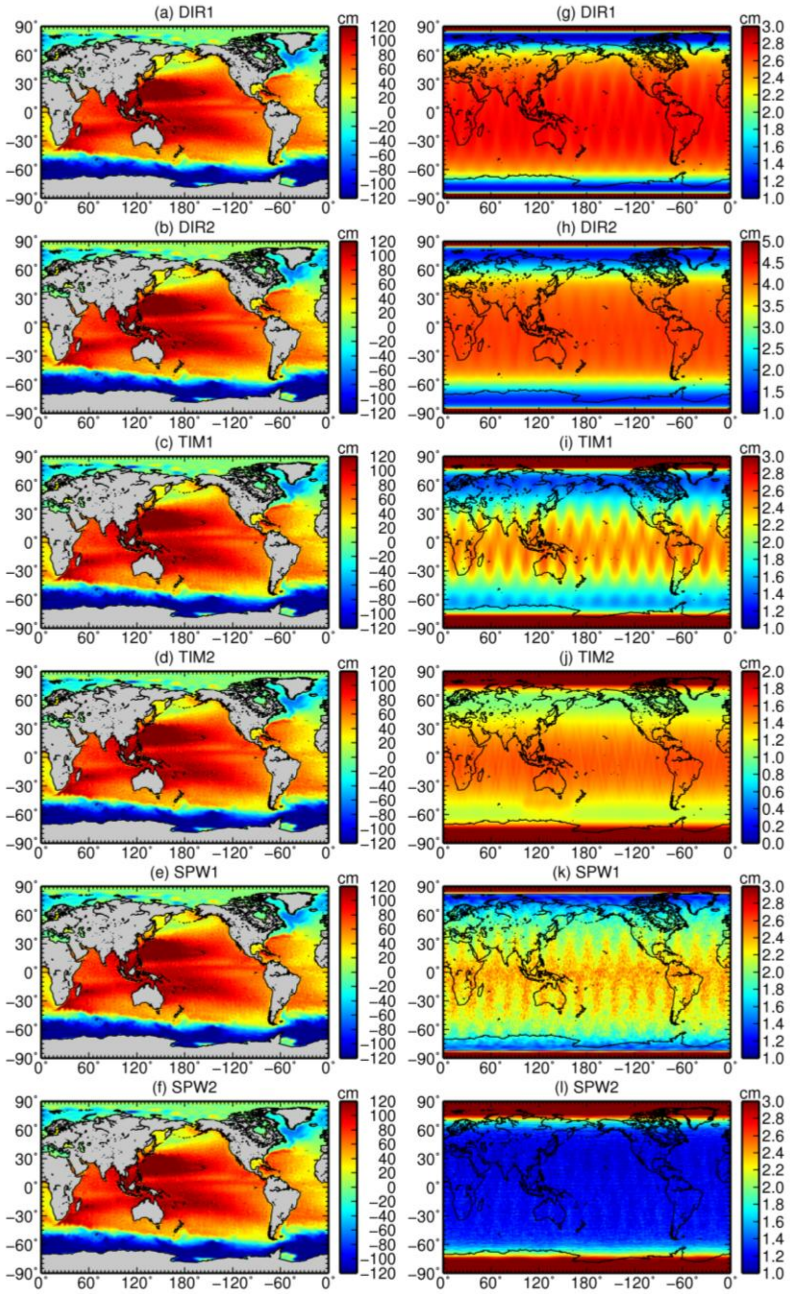

Figure 3: (a-e) MDTs derived from the GOCE gravity models by the spectral approach, with truncation at d/o=100. (f-j)The corresponding geoid error maps.

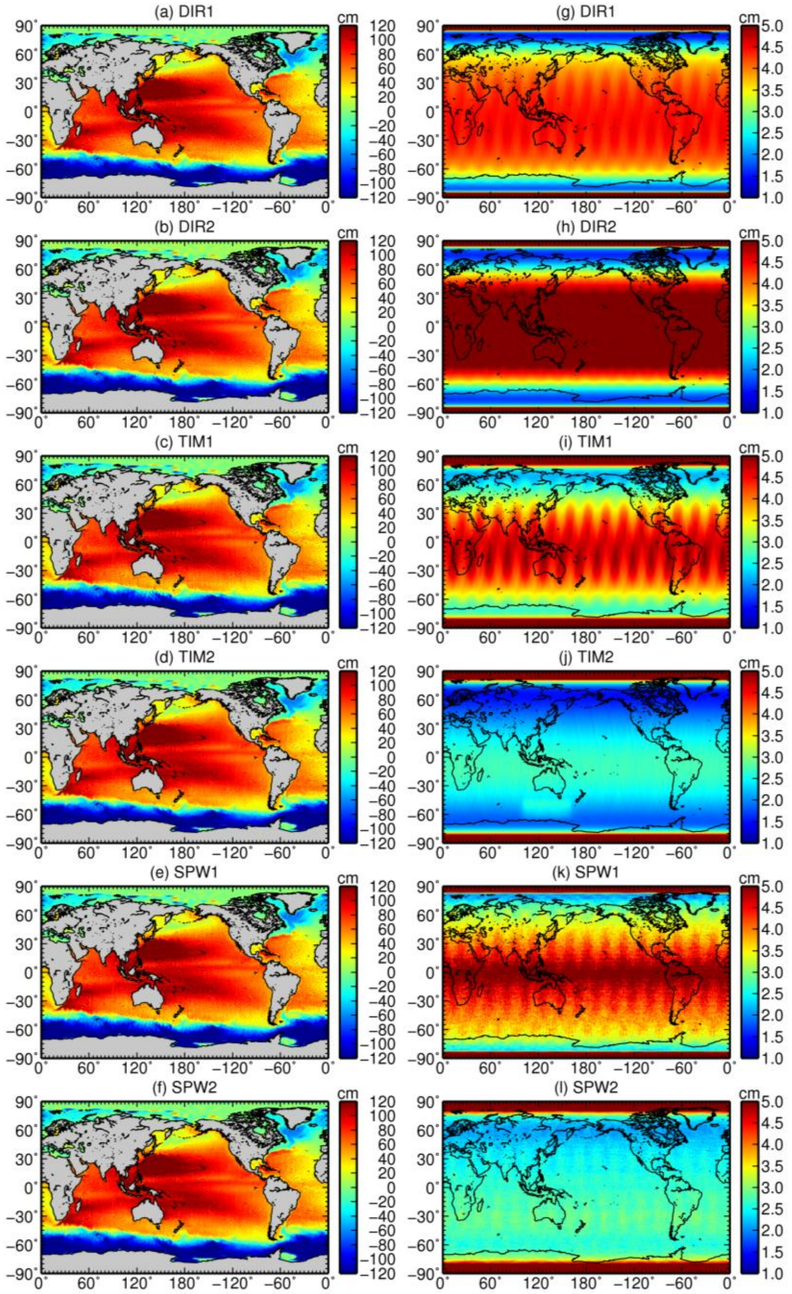

Figure 4: (a-e) MDTs derived from the GOCE gravity models by the spectral approach, with truncation at d/o=150. (f-j)The corresponding geoid error maps.

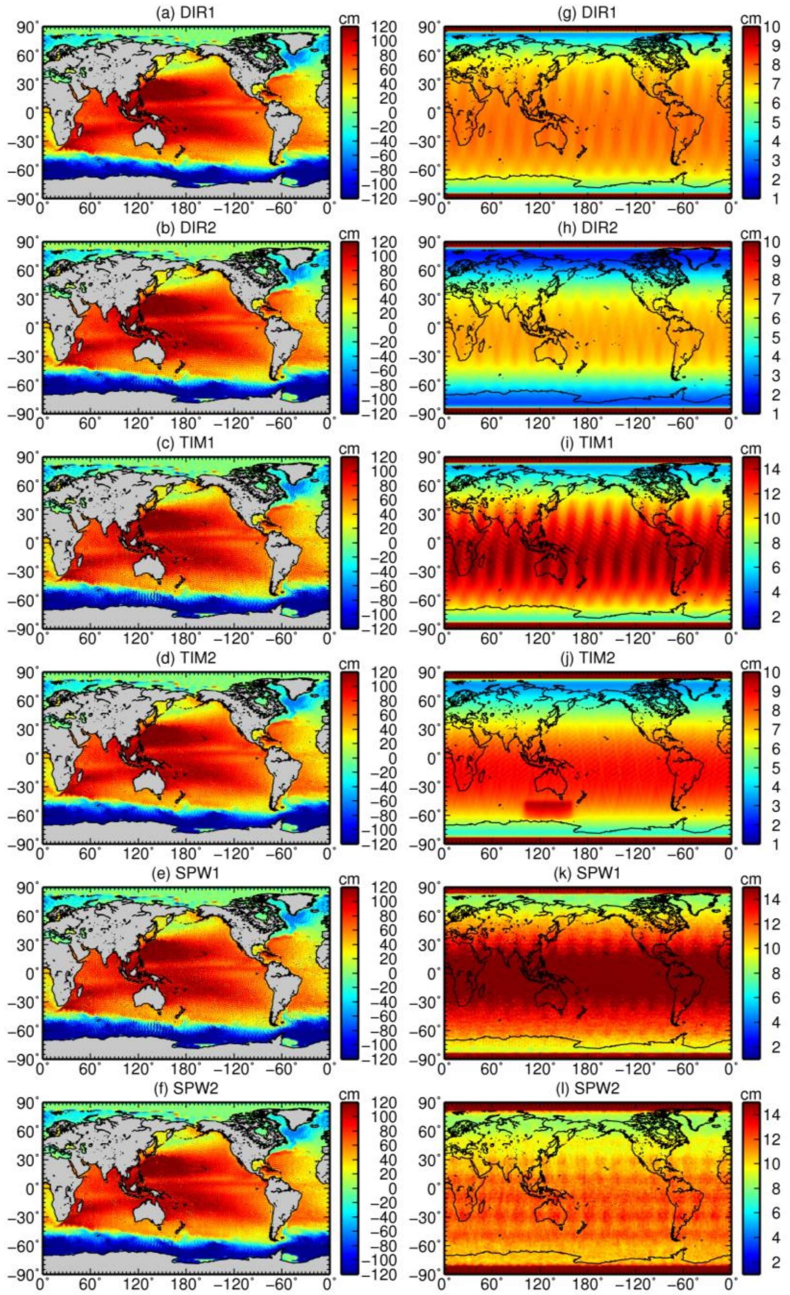

Figure 5: (a-e) MDTs derived from the GOCE gravity models by the spectral approach, with truncation at d/o=200. (f-j)The corresponding geoid error maps.

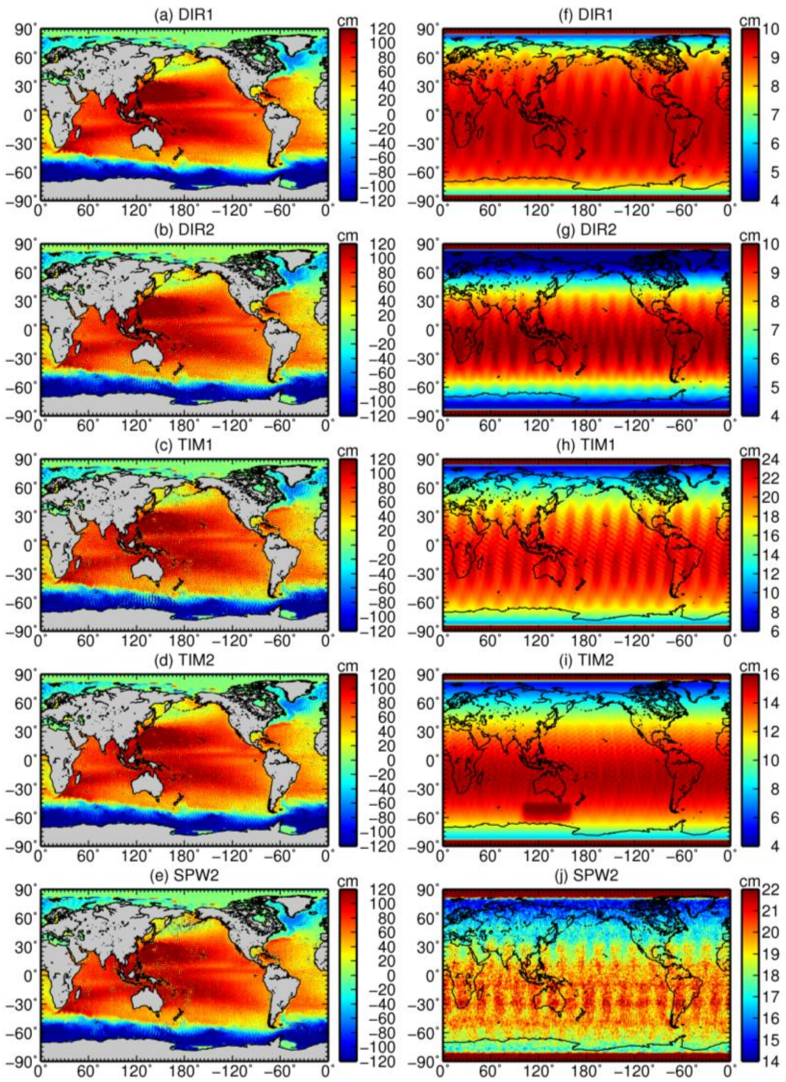

Figure 6: (a-e) MDTs derived from the GOCE gravity models by the spectral approach, with truncation at d/o=224. (f-j)The corresponding geoid error maps.

At d/o=200, the SPW1 model has the greatest errors ranging from 18 cm at the equator to 8-9 cm at 80 degrees from the equator. Next is the TIM1 model with errors ranging from just over 14 cm at low latitudes to 6-7 cm at 80 degrees from the equator. The additional 6 months of GOCE observations reduces these errors by about 5 cm near the equator and about 2 cm at high latitudes. At d/o=200, the spacewise model is the worst performing second generation solution. The shape of the zonal mean errors of SPW2 are now more similar to the other models, compared with SPW1. However, whereas the other solutions have smooth curves, for SPW2 the zonal mean error curve is bumpy, which most likely reflects the different way the errors have been derived for this model (i.e. a Monte Carlo simulation).

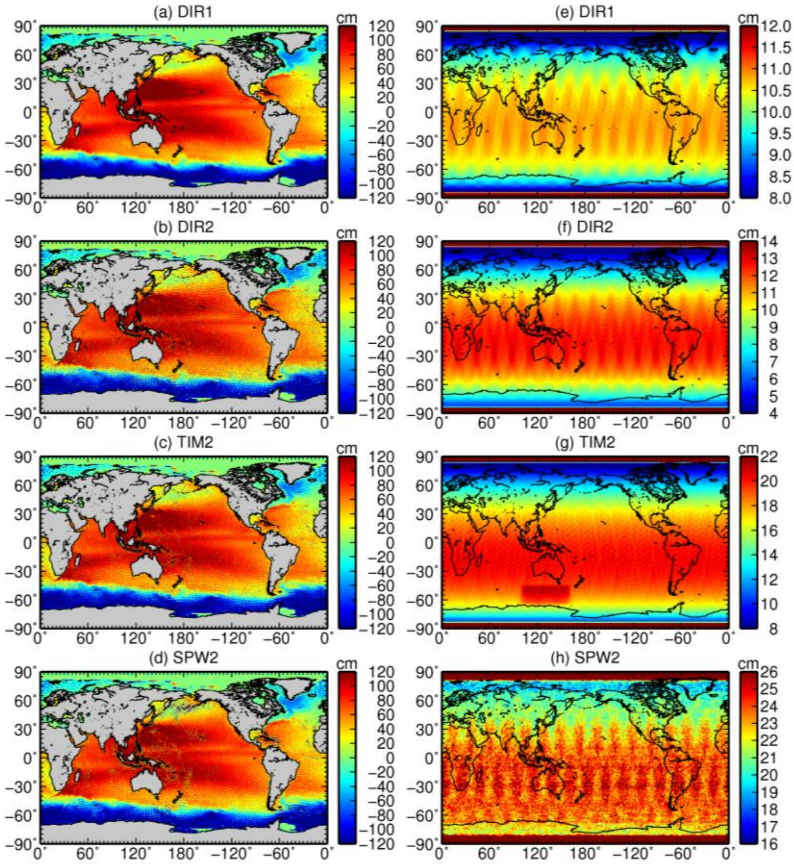

Figure 7: (a-e) MDTs derived from the GOCE gravity models by the spectral approach, with truncation at d/o=240. (f-j)The corresponding geoid error maps.

Between d/o=150 and d/o=200 the errors of the timewise solutions grow much more rapidly than do those from the direct models, particularly the second generation direct model, such that at d/o=200 the errors of the direct models are similar to those of the second timewise model. This change continues such that at d/o=240 the errors of the TIM2 model at 20 cm peak are about 7 cm larger than those of the DIR2 model. The reasons for this are unclear. Note that at d/o=240, the equatorial errors of DIR1 are still less than the DIR2 model, but overall the errors of DIR1 and DIR2 are quite similar. This shows that the a priori constraint used in DIR1 has an impact on the errors at least equal to that of the additional GOCE data. Quite why the errors of DIR2 should be so much less than those of TIM2, it not obvious, but it does show how dependent error magnitude estimates are on the solution method. From d/o=200 to d/o=240, the second spacewise solution remains the worst performing model, with peak zonal mean errors at d/o=240 of 24 cm, even larger than for TIM2 at d/o=250. It is interesting to note though that this model also shows the zonal asymmetry seen in the other models.

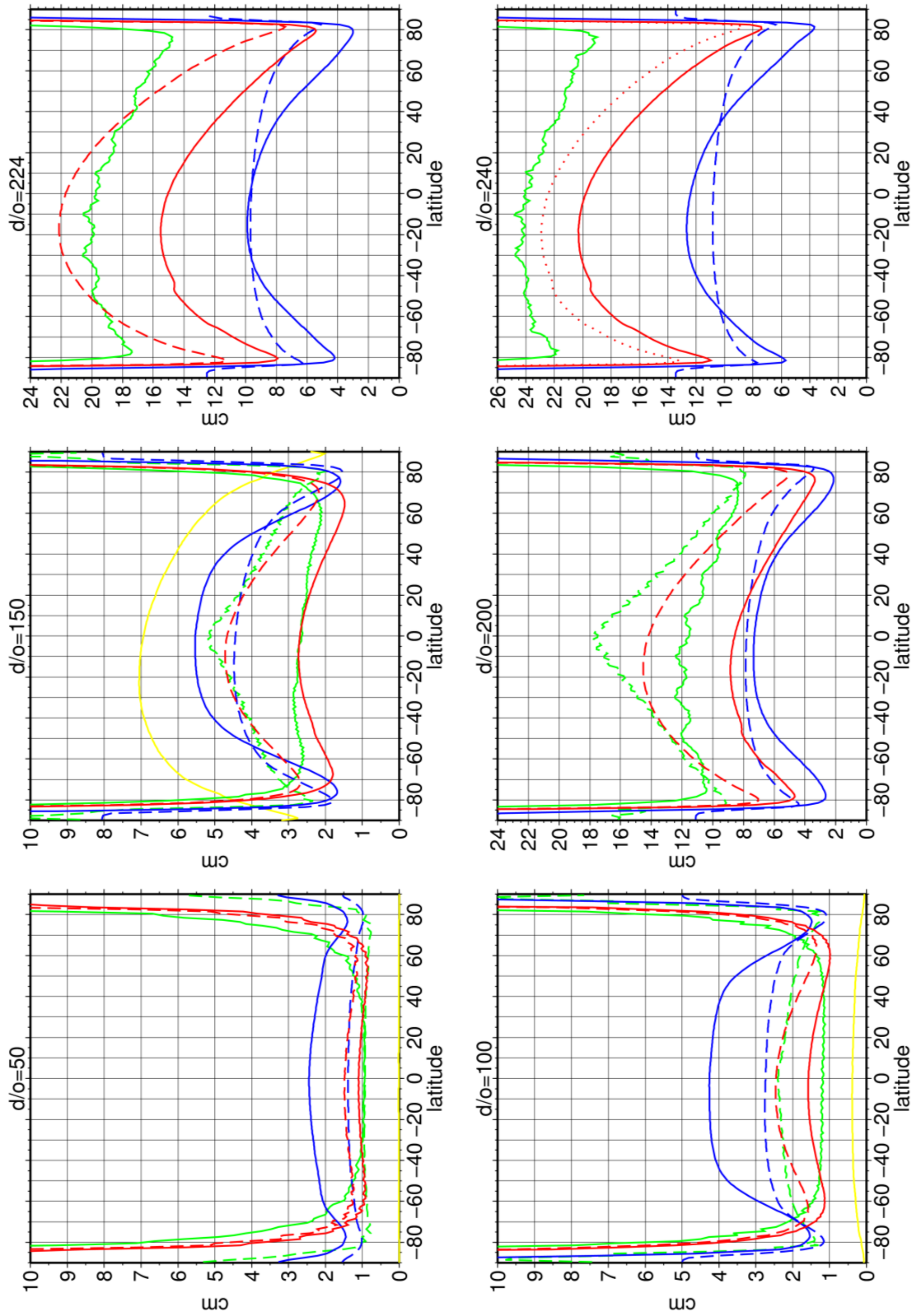

Figure 8: Zonal mean errors for the GOCE geoids: DIR models (blue); TIM models (red); SPW model (green). First generation models are given by the dashed curves. The red dotted curve in the lower right panel is for the TIM2 model at d/o=250. For reference errors for the GRACE EIGEN-GL04S1model are also given to d/o=150 (yellow).

4 Geoid error covariances

A more abstract notion than error variance (the diagonal elements of a variance-covariance matrix) is error covariance (the off-diagonal elements). In simple terms, the error covariance shows the degree to which errors at two points are related. For any point, it is possible using the GOCE error variance covariance information, together with the Balmino covhs2p routine, to calculate a discrete error covariance function, which shows how the error at that point is related to the errors at surrounding points. With covhs2p it is possible to specify a grid over which error covariance functions will be calculated for each point (the outer-zone) and the boundaries to which the error covariance function for each point will be calculated (the inner zone). In theoretical terms, the routine covhs2p calculates an error covariance map:

$$\Lambda_{(\theta_0,\lambda_0)}(\theta,\lambda) = Y^T_{(\theta,\lambda)}\Gamma Y_{(\theta_0,\lambda_0)}$$

for each point θ_0, λ_0 within the inner window, with $Y_{(\alpha,\beta)}$ signifying the evaluation of Y as defined in section 3 at the location α,β.

In this section the properties of the GOCE geoid error covariances are examined. Assuming the geoid is the largest source of errors in a geodetic MDT these errors can also be considered as applying to geodetic MDTs computed from GOCE EGMs. Error covariances do not include geoid omission error. However, computing a geodetic MDT using the spectral approach reduces such errors. The examination of error variance covariances is arranged according to increasing truncation degree and order. Truncations examined are d/o=50, 100, 150, 200, for which all six models are defined, and d/o=224 for which both direct and timewise solutions and the second spacewise solution are defined, and d/o=240 for which both direct solutions and the second timewise and spacewise solutions are defined.

4.1 Spatial homogeneity

The expectation was that the error characteristics of the GOCE gravity models would vary primarily with latitude. The discussion of the previous section shows that this is generally true of the error variance. To test this in respect of the error covariances, zonal mean error covariance functions were computed at each latitude from the 360 individual ECFs at a given latitude. This was done for each of the six models at each truncation d/o=50, 100, 150, 200, 224, 240 (where possible). (These will be shown in the next sub-section.) To establish the zonal homogeneity of the geoid models the skill of the zonal mean ECF at a particular latitude in accounting for the spatial variance in the actual ECFs at that latitude was calculated, where skill is defined as

$$S = 100 \times \left(1.0 - \frac{\langle f - f' \rangle}{\langle f \rangle}\right),$$

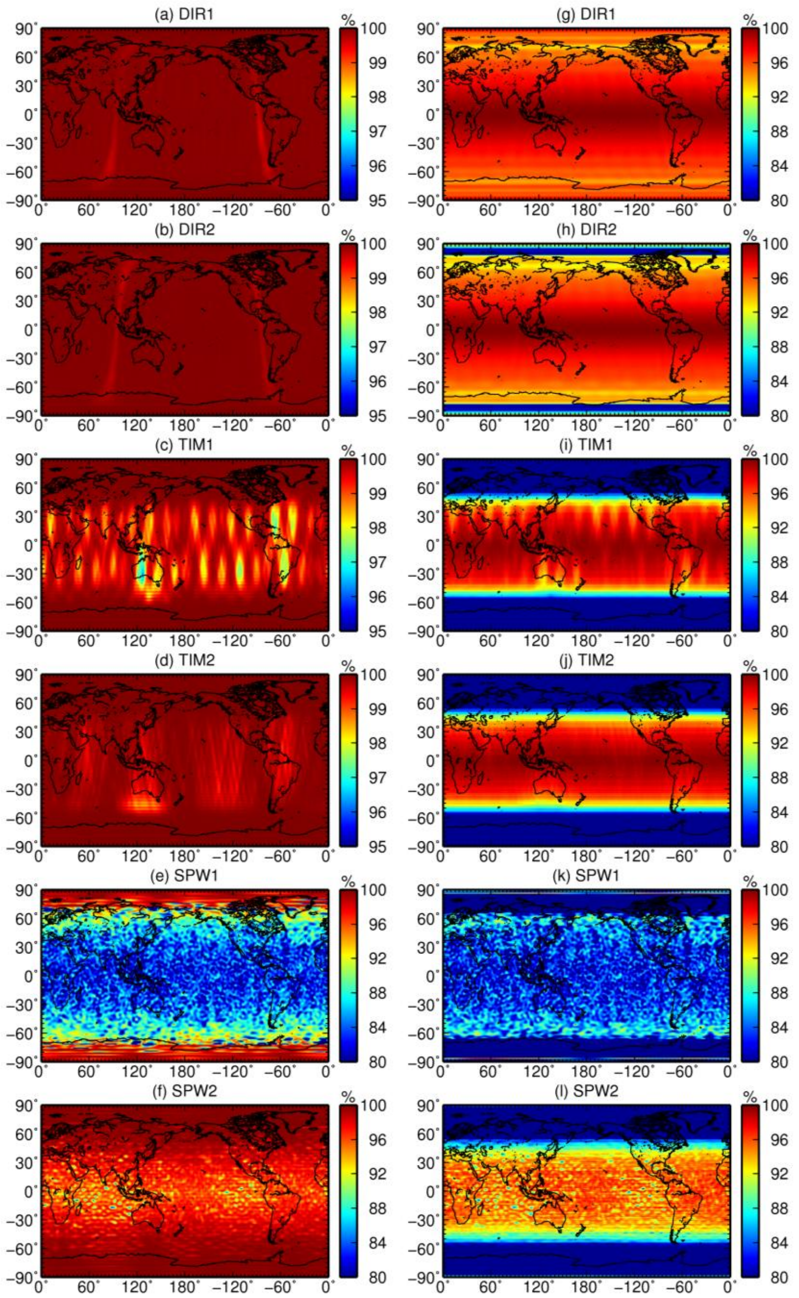

Figure 9: (a-e) Skill of the zonal mean error covariance function for each latitude in accounting for the actual error covariance functions at the same latitude, with truncation at d/o=50.(f-j)Repeating the left column but for each latitude using the mean of the north and south hemisphere zonal mean functions.

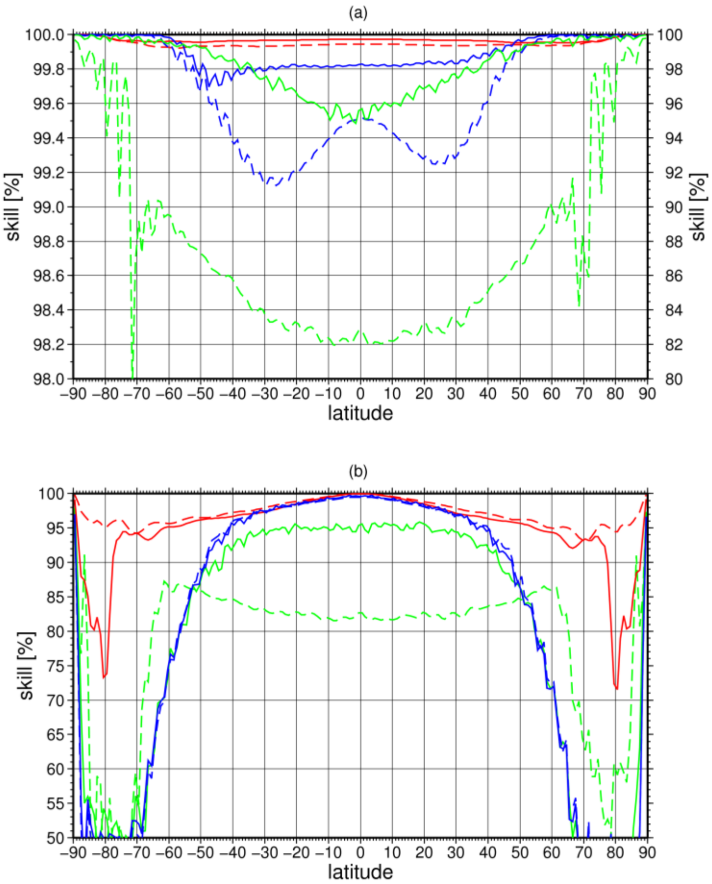

Figure 10: (a) The zonal mean skill of the zonal mean error covariance function for each latitude in accounting for the actual error covariance functions at the same latitude, with truncation at d/o=50 (b) Repeating (a) but for each latitude using the mean of the north and south hemisphere zonal mean functions. The colours are as follows: direct (DIR) models (red); timewise (TIM) models (blue); spacewise (SPW) models (green). Dashed curves correspond to first generation models. Note that in the upper panel the spacewise zonal mean profiles are plotted on a different scale to the other models as given by the right hand y axis.

The results of this skill analysis for the six models are shown in the left hand columns of Figure 9 (d/o=50), Figure 11 (d/o=100), Figure 13 (d/o=150), Figure 15 (d/o=200), Figure 17 (d/o=224) and Figure 19 (d/o=240). The results are further summarised by zonal mean skill scores in the top panels of Figure 10 (d/o=50), Figure 12 (d/o=100), Figure 14 (d/o=150), Figure 16 (d/o=200), Figure 18 (d/o=224) and Figure 20 (d/o=240). For both of the direct (DIR) solutions the skill of the zonal mean ECF is close to 100% for all latitudes and for all geoid truncations. The zonal mean skill score is never less than 99.8%. The lowest skill occurs along an orbital path between 120-60W and about 30S. But even here the skill is still greater that 98%. It can be concluded therefore that for the direct solutions for any given latitude or truncation the ECFs are very similar and are well characterised by a mean ECF, or indeed by any one of the actual ECFs at that latitude.

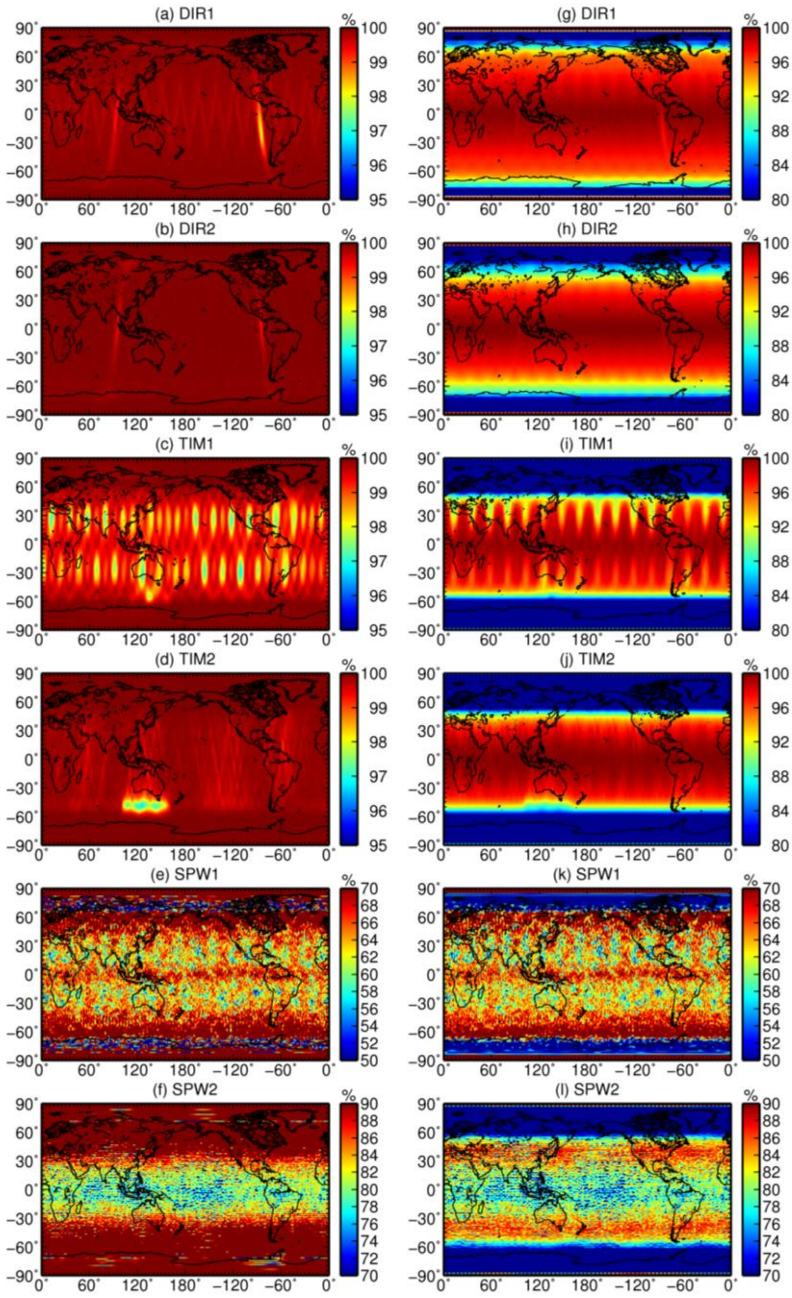

Figure 11: (a-e) Skill of the zonal mean error covariance function in accounting for the actual error covariance function at each latitude, with truncation at d/o=100.(f-j)Repeating the left column but for each latitude using the mean of the north and south hemisphere zonal mean functions.

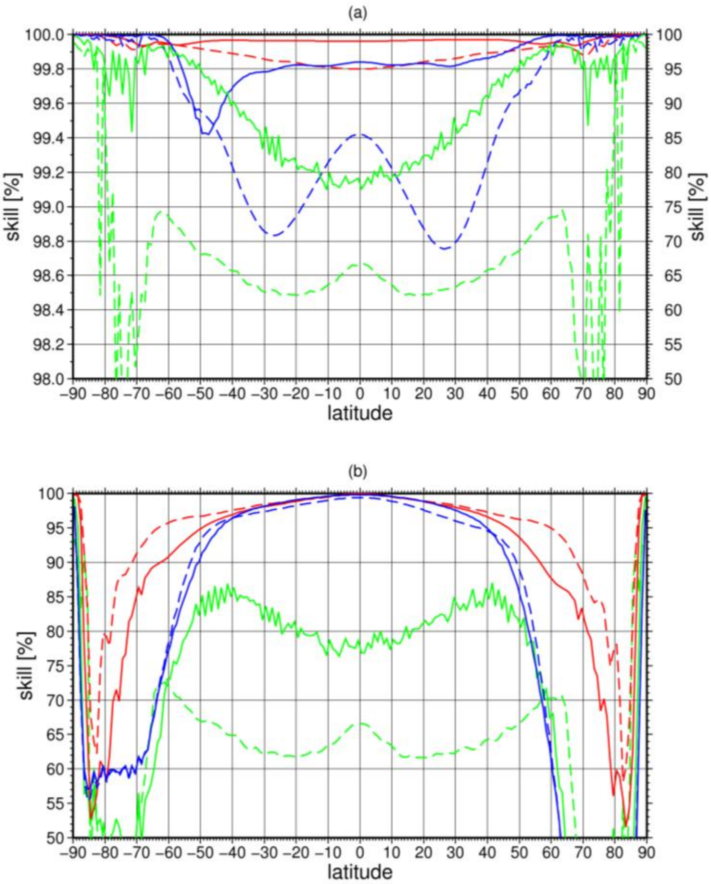

Figure 12: (a) The zonal mean skill of the zonal mean error covariance function for each latitude in accounting for the actual error covariance functions at the same latitude, with truncation at d/o=100 (b) Repeating (a) but for each latitude using the mean of the north and south hemisphere zonal mean functions. The colours are as follows: direct (DIR) models (red); timewise (TIM) models (blue); spacewise (SPW) models (green). Dashed curves correspond to first generation models. Note that in the upper panel the spacewise zonal mean profiles are plotted on a different scale to the other models as given by the right hand y axis.

For the first timewise solution (TIM1) there is somewhat greater longitudinal variation in the ECFs particularly at mid-latitudes. From the error variance maps it can be seen that this arises primarily from variations in the magnitudes rather than the form of the ECFs, which in turn is related to the orbital configurations of the satellite. The variations are greatest at the lowest truncations. However, even at d/o 50 all skill scores are above 97% and lowest zonal mean vale is 98.8% for d/o=100 at about 25N. Compared with TIM1, the second generation timewise solution (TIM2) is, in general, more zonally homogenous. An exception to this is the anomalous block to the south of Australia described earlier which skews the zonal mean ECFs for latitudes between 60-50S, a biasing strongest for truncation at d/o=200. Even with this problem the mean ECF for these latitudes still accounts for more 97% of the variance in the actual ECFs, except within the anomalous region itself, where skill scores fall as low as 85%. Yet, even this is still a reasonable skill score.

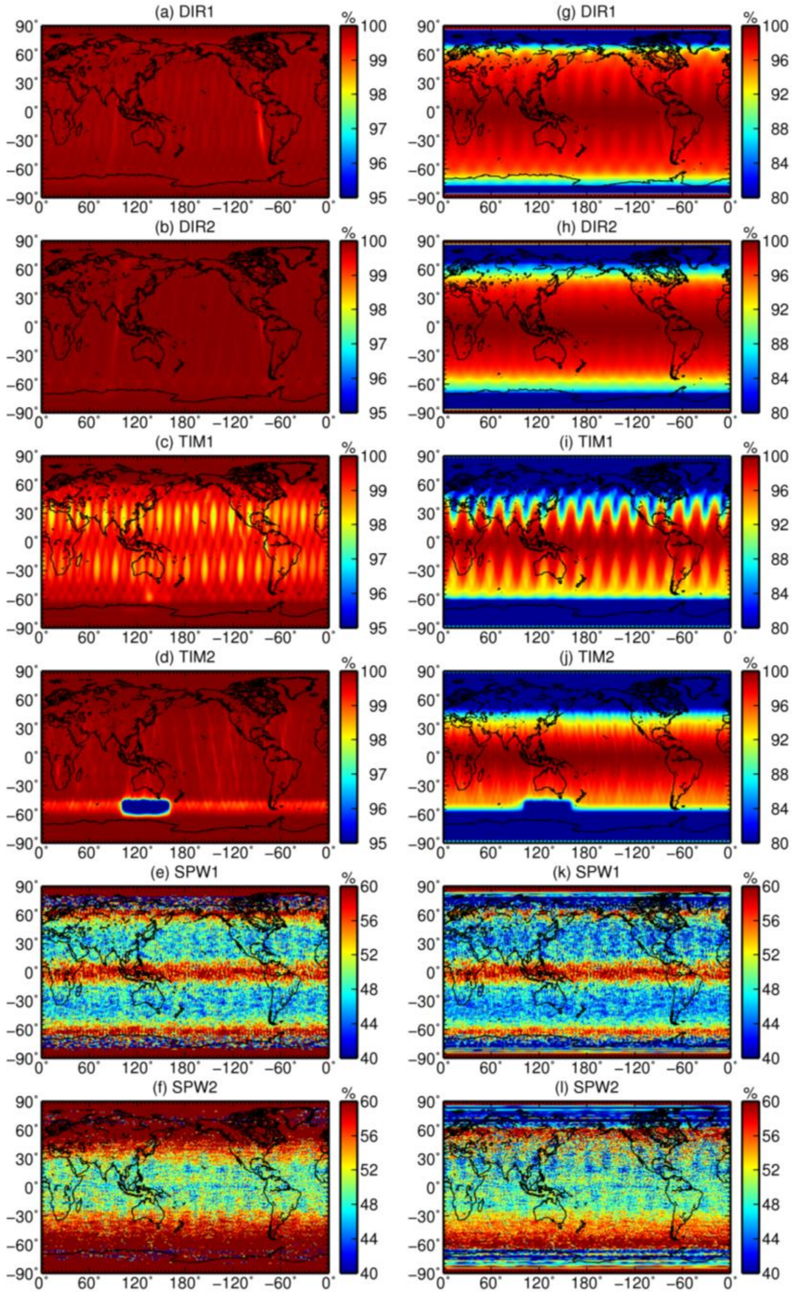

Figure 13: (a-e) Skill of the zonal mean error covariance function in accounting for the actual error covariance function at each latitude, with truncation at d/o=150.(f-j)Repeating the left column but for each latitude using the mean of the north and south hemisphere zonal mean functions.

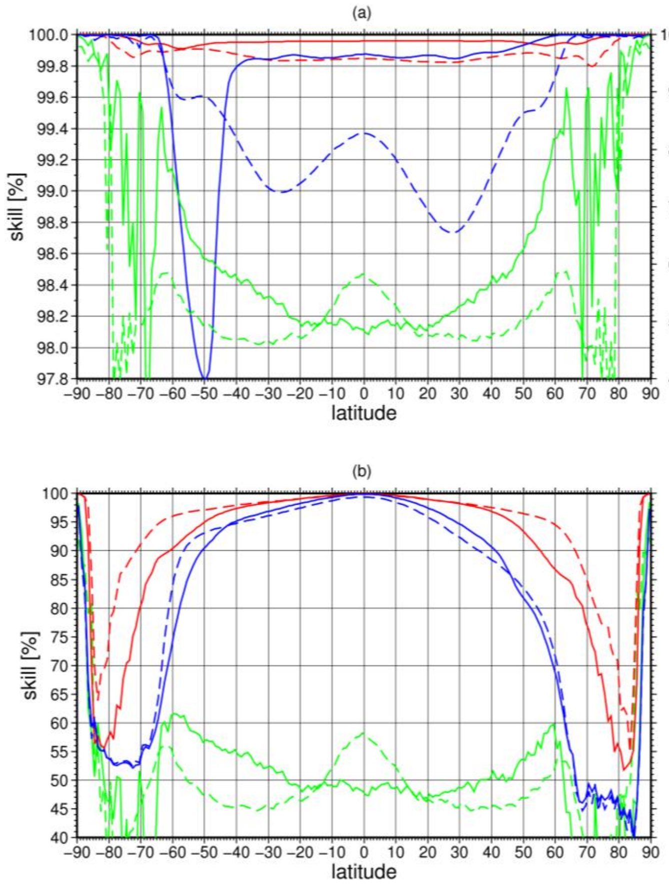

Figure 14: (a) The zonal mean skill of the zonal mean error covariance function for each latitude in accounting for the actual error covariance functions at the same latitude, with truncation at d/o=150 (b) Repeating (a) but for each latitude using the mean of the north and south hemisphere zonal mean functions. The colours are as follows: direct (DIR) models (red); timewise (TIM) models (blue); spacewise (SPW) models (green). Dashed curves correspond to first generation models. Note that in the upper panel the spacewise zonal mean profiles are plotted on a different scale to the other models as given by the right hand y axis.

The first spacewise solution (SPW1) is the least zonally consistent of the GOCE gravity models. It is also the model that shows the greatest variation in skill scores with latitude, and with truncation d/o. For truncation at d/o=50 skill of the zonal mean ECF ranges from a minimum of around 80% at the equator to a maximum greater than 90% poleward of 60 degrees. At d/o=100 the skill ranges from a minimum of about 60% at 20S and 20N, to a maximum of about 75% at 60S and 60N. In both hemispheres beyond 60 degrees the skill drops down to less than 50% before peaking at near 100% in the polar gap regions, where the error covariance is in any case not well defined. For truncations at d/o=150 and 200 a similar pattern is seen, but with mid-latitude minima now falling to approximately 45%. Therefore, in contrast to the other GOCE solutions, the error covariances of the SPW1 model cannot be adequately represented by either a zonal mean ECF or by an ECF at any individual longitude. For truncations up to d/o=100 the second spacewise solution is somewhat more zonally homogenous than SPW1. However, for high truncations this difference between the two solutions disappears and both models are much less zonally homogenous than the direct or timewise solutions.

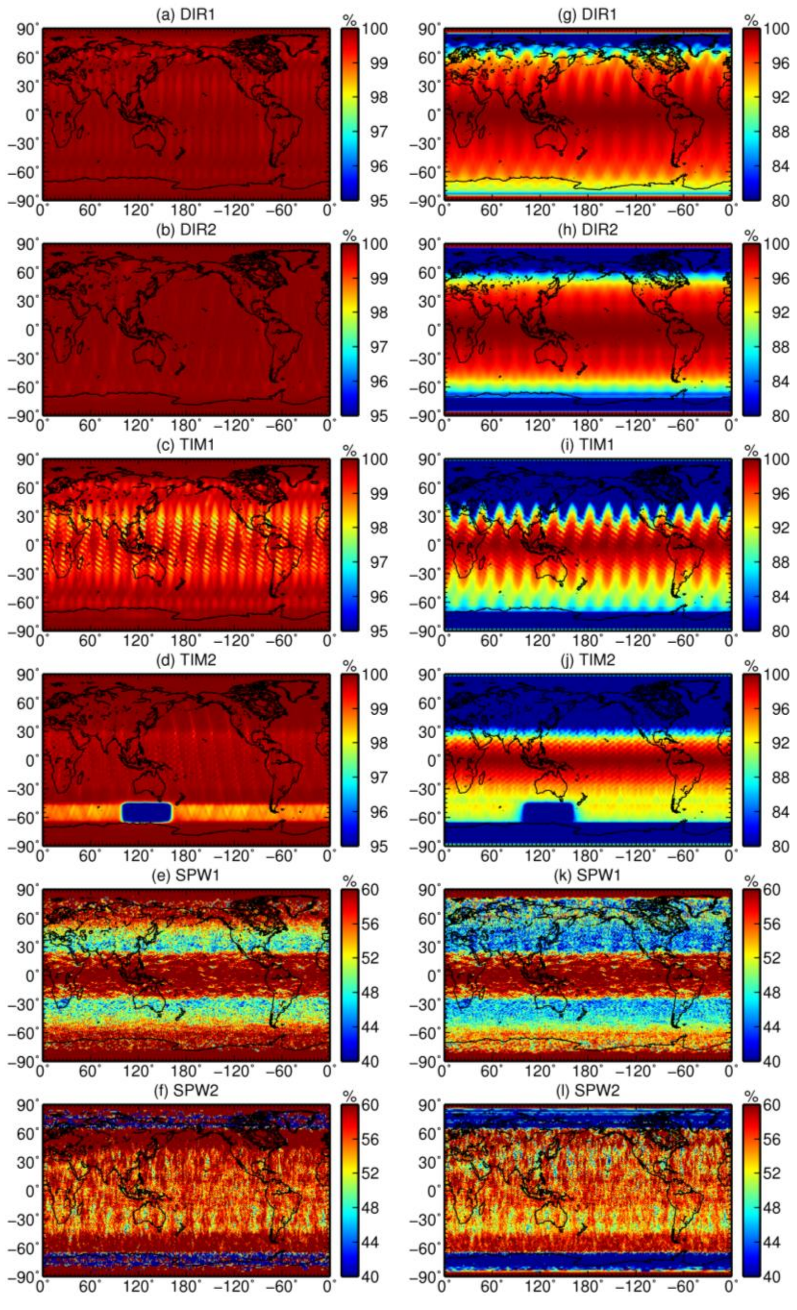

Figure 15: (a-e) Skill of the zonal mean error covariance function in accounting for the actual error covariance function at each latitude, with truncation at d/o=200.(f-j)Repeating the left column but for each latitude using the mean of the north and south hemisphere zonal mean functions.

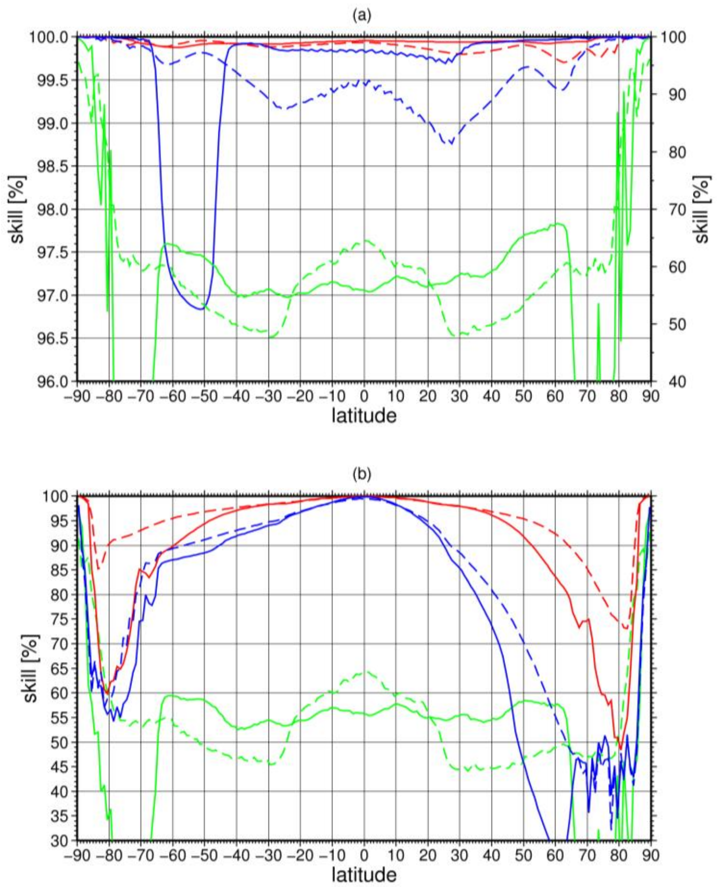

Figure 16: (a) The zonal mean skill of the zonal mean error covariance function for each latitude in accounting for the actual error covariance functions at the same latitude, with truncation at d/o=200 (b) Repeating (a) but for each latitude using the mean of the north and south hemisphere zonal mean functions. The colours are as follows: direct (DIR) models (red); timewise (TIM) models (blue); spacewise (SPW) models (green). Dashed curves correspond to first generation models. Note that in the upper panel the spacewise zonal mean profiles are plotted on a different scale to the other models as given by the right hand y axis.

Finally, the degree to which GOCE geoid error characteristics are symmetric with respect the equator is considered. To assess this the zonal mean ECFs described above are "folded" about the equator to give one mean ECF for each latitude magnitude (e.g. a single ECF for latitudes 20S and 20N is formed by computing the average of the zonal mean ECFs for 20S and 20N). The skill of these mean-mean ECFs in accounting for the actual ECFs at the corresponding latitudes is then computed as before. These results are shown in the right hand columns of Figures 9, 11, 13, 15, 17 and 19 and the bottom panels of Figures 10, 12, 14, 16, 18, and 20. The results show that for all models and across all truncations there is an hemispheric asymmetry that grows with latitude. However, the models vary with regard to the degree of this asymmetry. The DIR1 model is the most symmetric. At d/o=50 the skill for this model is never less than 95%. As the truncation degree is increased the degree of asymmetry increases, as reflected in equatorward shift in the north and south latitudes at which the zonal mean skill falls below 90%. For d/o=100 and 150, this is at about 70S and 65N. For higher truncations the degree of asymmetry again decreases, such that at d/o=240 the skill remains above 90% over almost the entire latitudinal range.

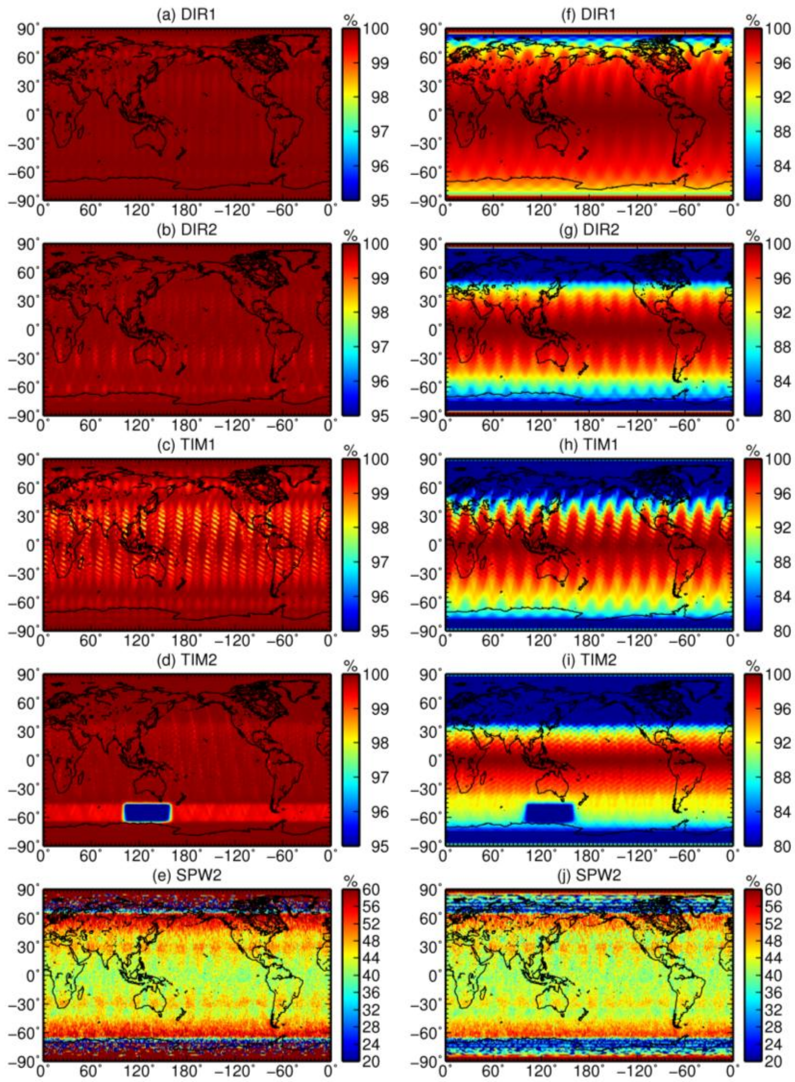

Figure 17: (a-e) Skill of the zonal mean error covariance function in accounting for the actual error covariance function at each latitude, with truncation at d/o=224.(f-j)Repeating the left column but for each latitude using the mean of the north and south hemisphere zonal mean functions.

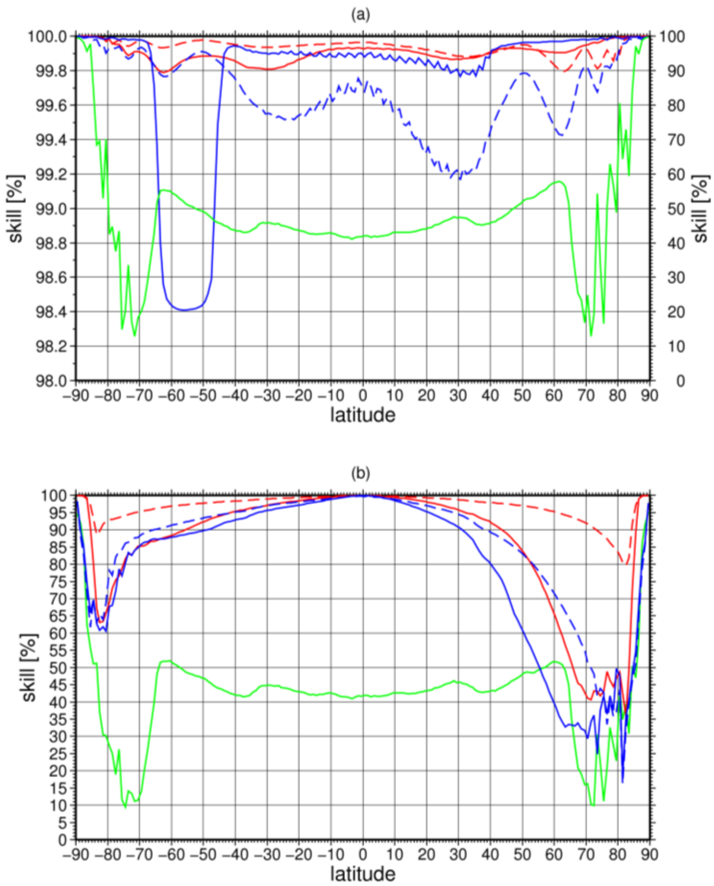

Figure 18: (a) The zonal mean skill of the zonal mean error covariance function for each latitude in accounting for the actual error covariance functions at the same latitude, with truncation at d/o=224 (b) Repeating (a) but for each latitude using the mean of the north and south hemisphere zonal mean functions. The colours are as follows: direct (DIR) models (red); timewise (TIM) models (blue); spacewise (SPW) models (green). Dashed curves correspond to first generation models. . Note that in the upper panel the spacewise zonal mean profile is plotted on a different scale to the other models as given by the right hand y axis.

The DIR2 model is somewhat more asymmetric than DIR1, with the skill falling to below 90% 10 to 20 degrees closer to the equator than DIR1. The timewise models are similar with respect to their degree of asymmetry, with both being more asymmetrical than DIR2, especially at higher latitudes. Again the degree of asymmetry grows with increasing degree and order. Interestingly, while beyond d/o=150 the DIR1 model becomes more symmetrical, at this point, with respect to the asymmetry, the DIR2 model becomes much more similar to the timewise models. All these models continue to decrease in symmetry. At d/o=240, the skill for the DIR2 and TIM2 models falling below 90% at about 55S and 40N. For these models the drop in skill is much greater in the Northern Hemisphere than it is in the Southern Hemisphere. This indicates that the mean-mean ECFs are being skewed towards the southern hemisphere ECFs, due to the larger errors in this hemisphere. For this test, the skill scores for the spacewise models are similar the earlier results for the "unfolded" cases, and the growth of asymmetry with latitude similar to the timewise models.

In conclusion then, while a zonal mean ECF is adequate to represent the error characteristics of a model at a particular latitude, the degree of hemispheric asymmetry is such that we cannot in general obtain a further economy by making the ECF a function of distance from the equator only. (In fact, it is likely that much of this asymmetry results from an hemispheric asymmetry in the magnitude of the error variances. This should be investigated further.)

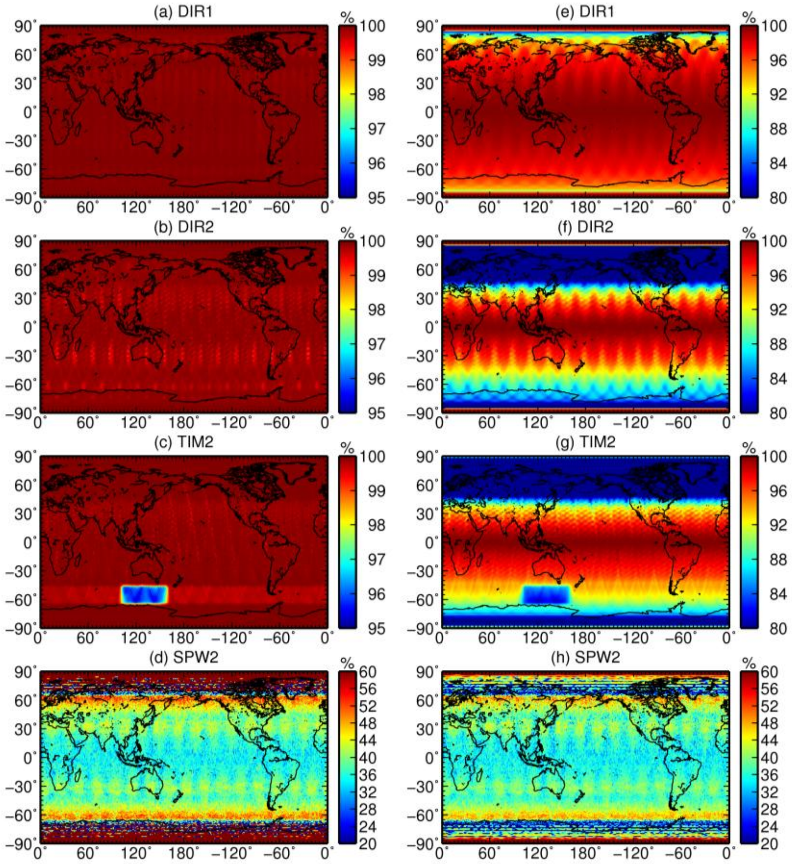

Figure 19: (a-e) Skill of the zonal mean error covariance function in accounting for the actual error covariance function at each latitude, with truncation at d/o=240.(f-j)Repeating the left column but for each latitude using the mean of the north and south hemisphere zonal mean functions.

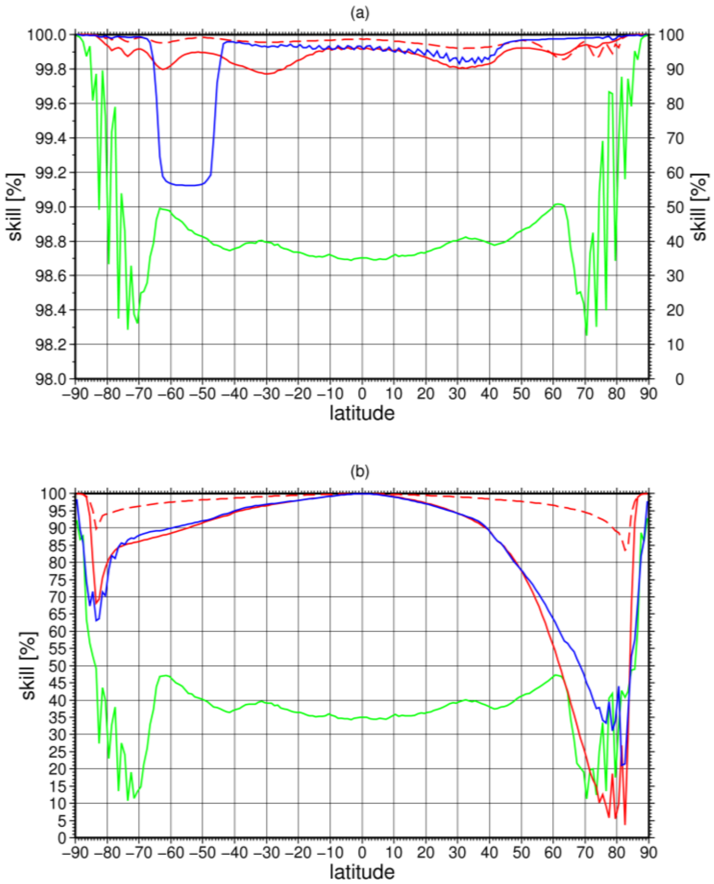

Figure 20: (a) The zonal mean skill of the zonal mean error covariance function for each latitude in accounting for the actual error covariance functions at the same latitude, with truncation at d/o=240 (b) Repeating (a) but for each latitude using the mean of the north and south hemisphere zonal mean functions. The colours are as follows: direct (DIR) models (red); timewise (TIM) models (blue); spacewise (SPW) models (green). Dashed curves correspond to first generation models. Note that in the upper panel the spacewise zonal mean profile is plotted on a different scale to the other models as given by the right hand y axis.

4.2 Zonal mean covariance functions

In the previous section the zonally similarity of the error covariance functions was established. In this section the spatial forms of these zonal mean ECFs are examined for the latitudes between 80S and 80N in 20 degree intervals. The normalised maps (scaled by 10 for convenience) are shown in Figure 21 (d/o=50), Figure 23 (d/o=100), Figure 25 (d/o=150), Figure 27 (d/o=200), Figure 29 (d/o=224) and Figure 31 (d/o=240). To give a clearer picture of the relative magnitudes of the peaks and troughs within the ECFs, zonal and meridional cross sections through the 2 dimensional error covariance maps are provided in Figure 22 (d/o=50), Figure 24 (d/o=100), Figure 26 (d/o=150), Figure 28 (d/o=200), Figure 30 (d/o=224) and Figure 32 (d/o=240).

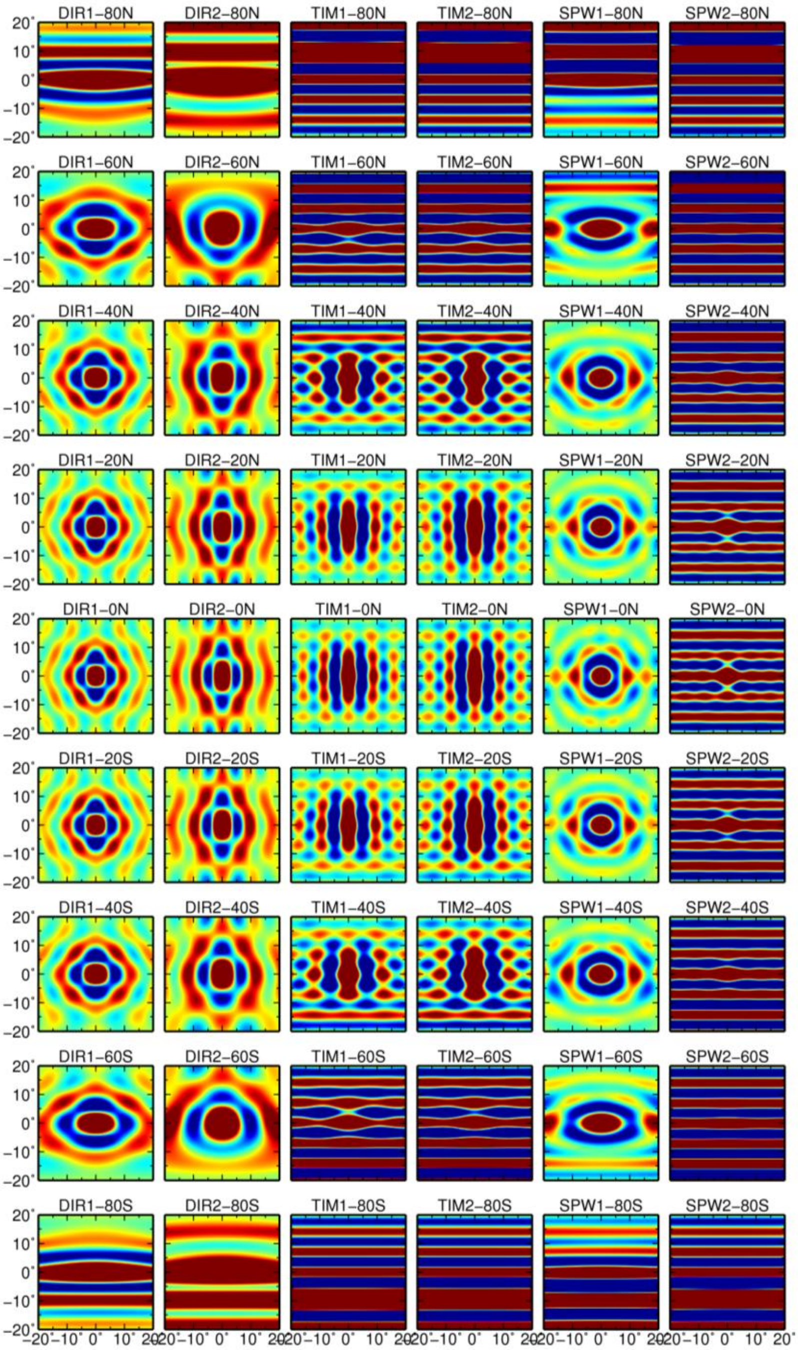

Figure 21: Zonal mean geoid error covariance functions over a range of latitudes for each of the GOCE models, with truncation at d/o=50.

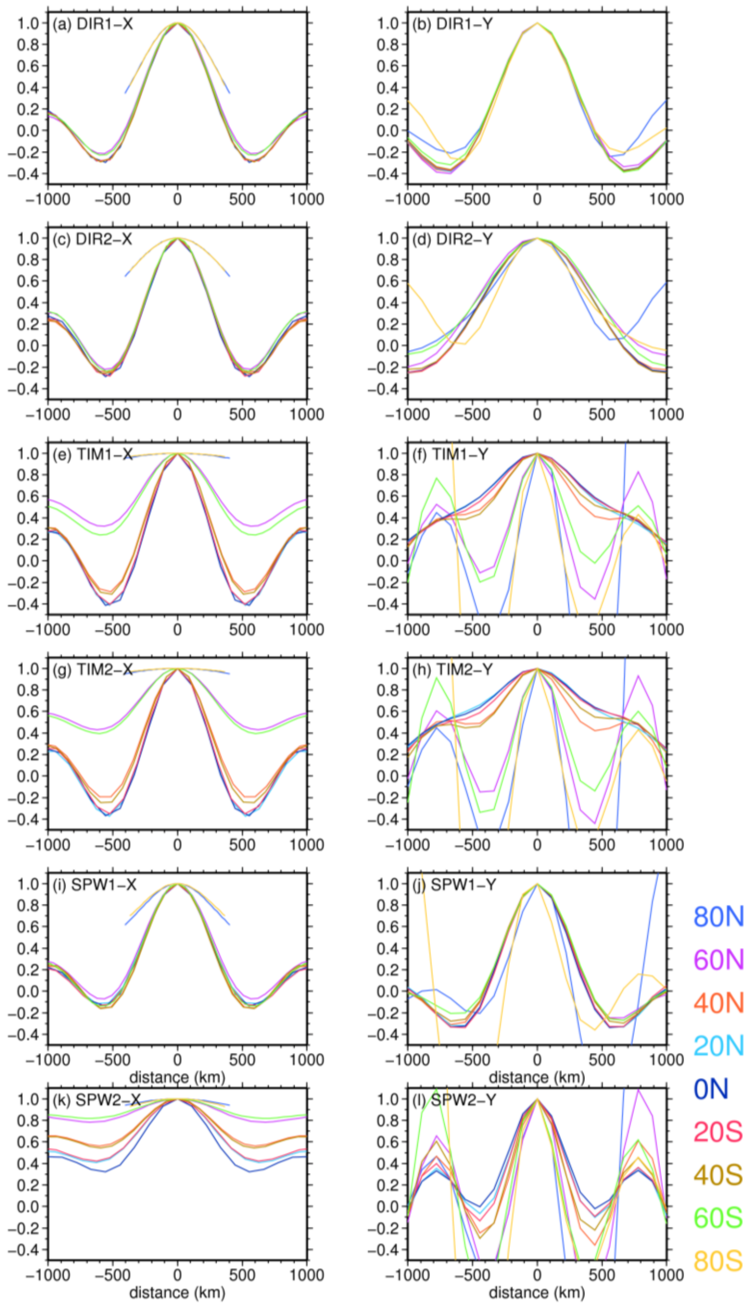

Figure 22: Zonal (left) and meridional (right) cross-sections through the d/o=50 zonal mean geoid error covariance functions shown in Figure 21.

The first consistent feature to note is that the spatial form of the ECFs depends strongly on the solution method. Even though the second timewise solution (TIM2) uses 8 months of data compared with the first timewise solution (TIM1) which uses just 2 months of observations, the form of the ECFs from both solutions are almost identical, and this remains true for all latitudes and for all truncations. This shows that increasing the observations changes the magnitude of the error variances, but it does not change the error covariance structure; the latter depends on the method used. This visual impression of the near identity of the error

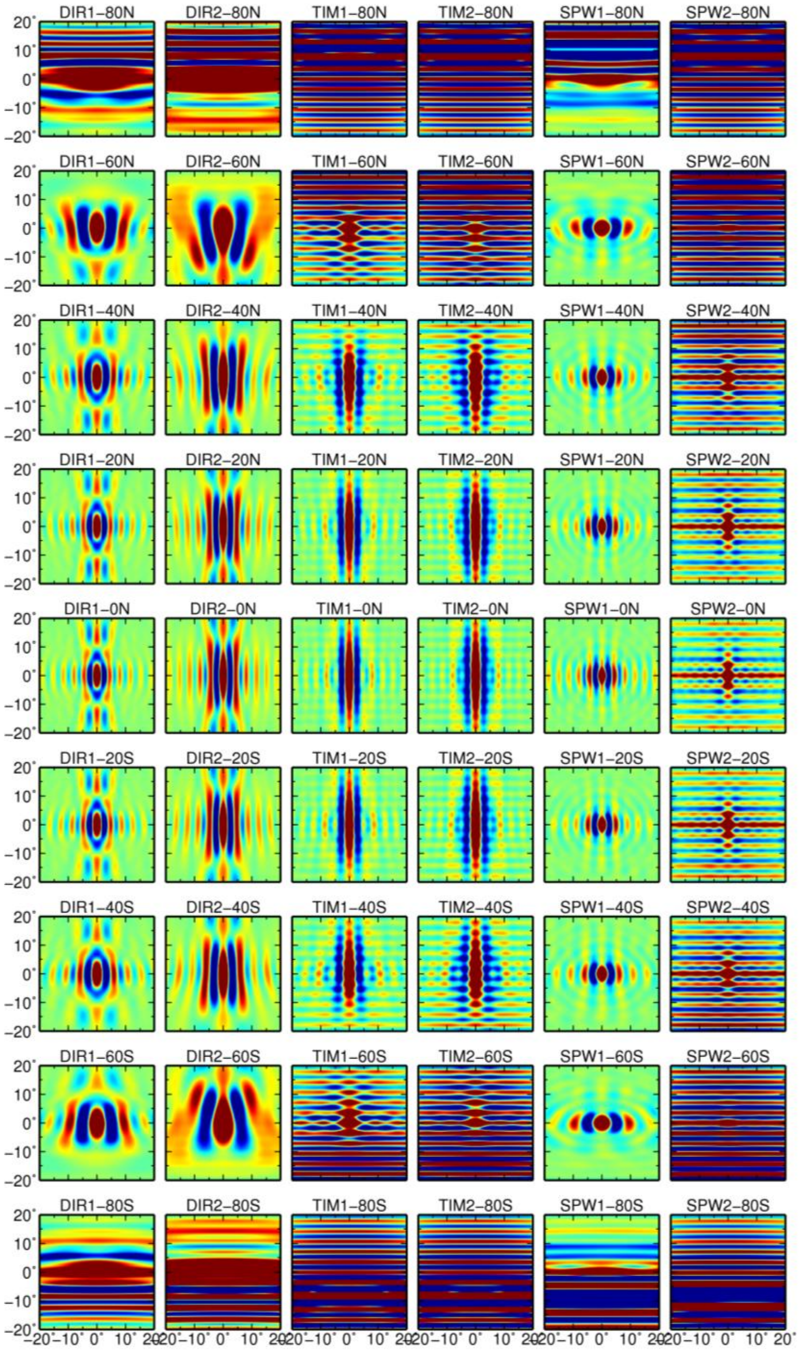

Figure 23: Zonal mean geoid error covariance functions over a range of latitudes for each of the GOCE models, with truncation at d/o=100.

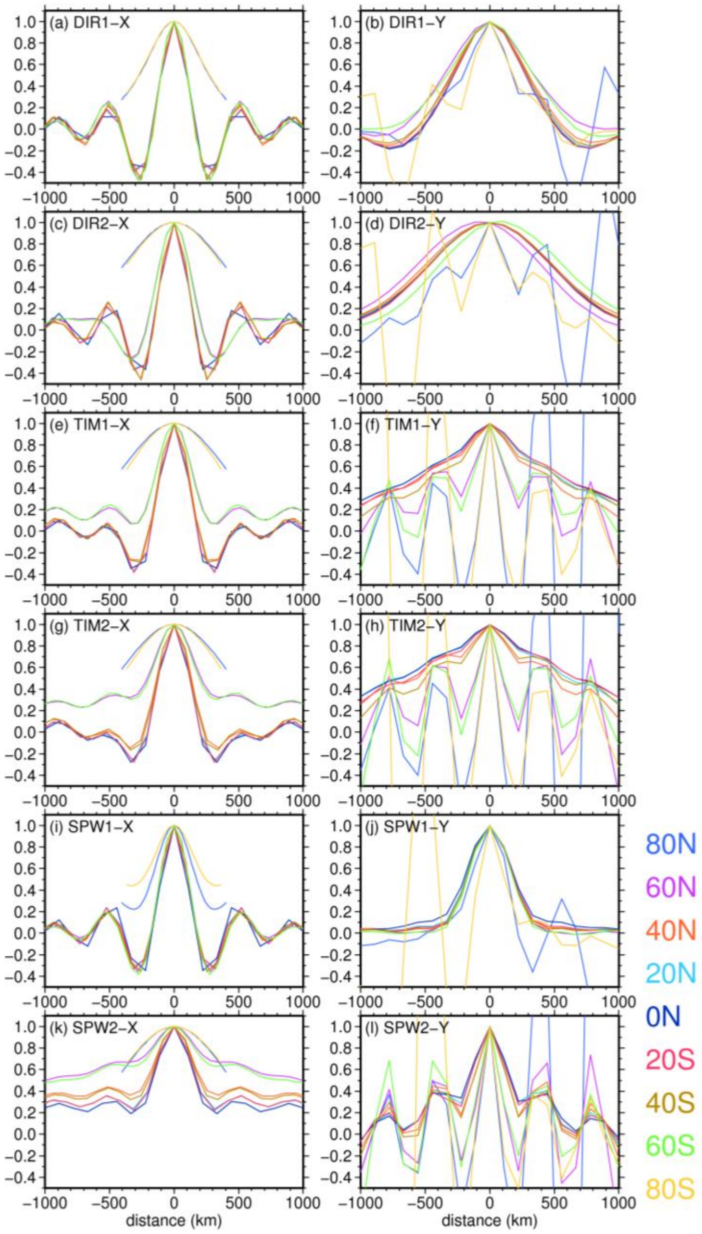

Figure 24: Zonal (left) and meridional (right) cross-sections through the d/o=100 zonal mean geoid error covariance functions shown in Figure23.

covariance structure for the two timewise models is confirmed globally in panel (h) of Figure 33 (d/o=50), Figure 35 (d/o=100), Figure 37 (d/o=150) and Figure 39 (d/o=200) and in panel (f) of Figure 41 (d/o=224; the maximum d/o of TIM1). It is also confirmed for the zonal mean patterns displayed in Figure 34 (d/o=50), Figure 36 (d/o=100), Figure 38 (d/o=150), Figure 40 (d/o=200) and Figure 42 (d/o=224). (Therefore, for the remainder of this discussion we refer to the two models as one.) The two generations of the direct solution cannot be group in a similar fashion because DIR1 uses an a priori constraint as described earlier that was not used in the second model. Thus they effective can be considered as distinct methods. For low d/o truncations the two spacewise methods have very different form, which suggests either some change in the solution method, or, contrary to what the similarity between TIM1 and TIM2 suggests, that extra data can impact of the error covariance form.

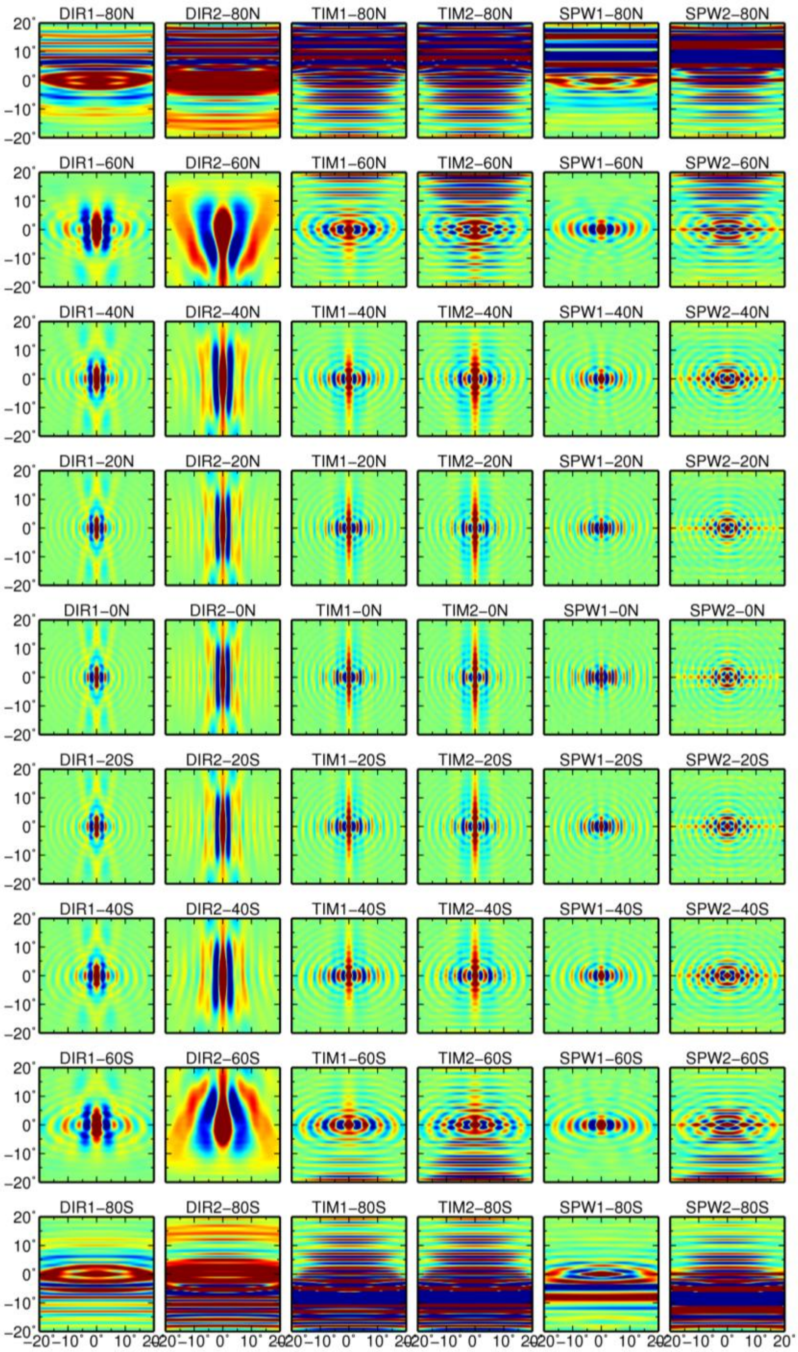

Figure 25: Zonal mean geoid error covariance functions over a range of latitudes for each of the GOCE models, with truncation at d/o=150.

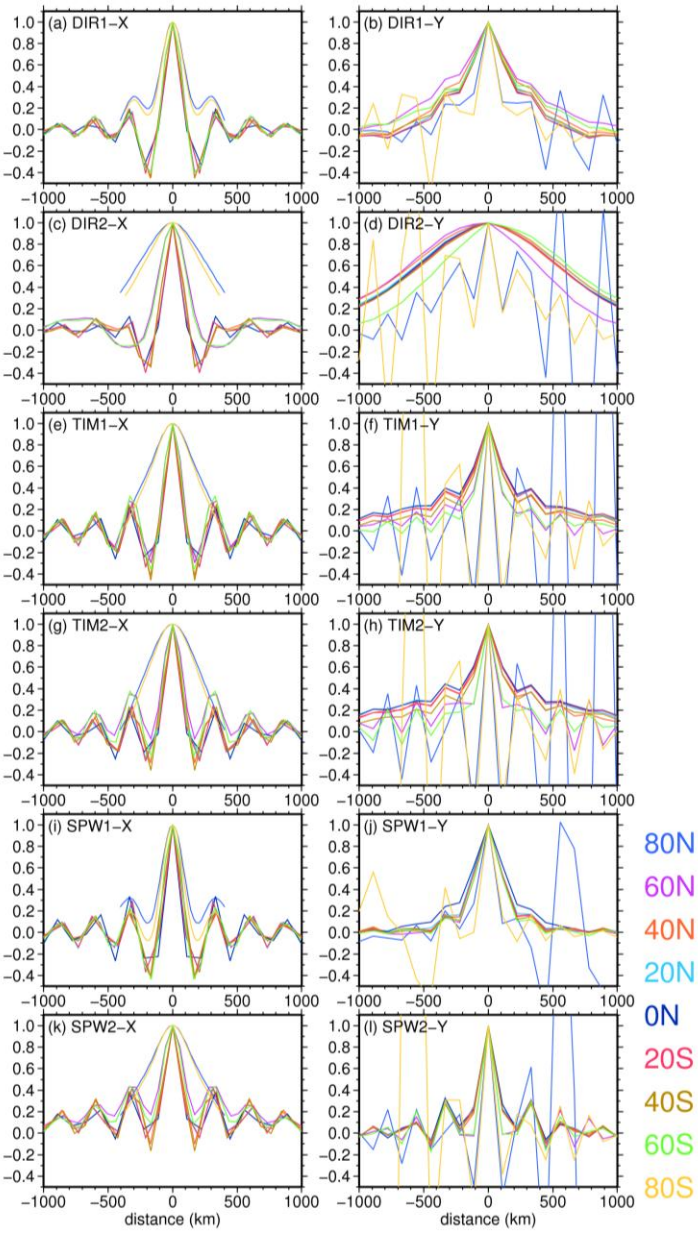

Figure 26: Zonal (left) and meridional (right) cross-sections through the d/o=150 zonal mean geoid error covariance functions shown in Figure 25.

Concentrating first of the error covariance structure of the timewise solutions with truncation at d/o=50 it is clear that the patterns are quite symmetric about the equator. Thus further indicating the previously described hemispheric asymmetry comes mainly from the magnitude of the errors (the variance) rather than from the covariance. This is, in fact, true for all of the models for all truncations. At the equator the covariance pattern is primarily one of decaying meridional stripes, with weaker zonal stripes intersecting to give the observed gridded effect. A clear impression of how these stripes decay in the zonal and meridional directions can be obtained from panels e and g (zonal) and panels f and h (meridional) of Figure 34. The meridional striping of the pattern presents itself as the much slower decay of the y component of the ECF compared with that of the x component. Moving towards higher latitudes the amplitude of the zonal stripes increases until at 60N(S) they dominate the form of the ECFs.

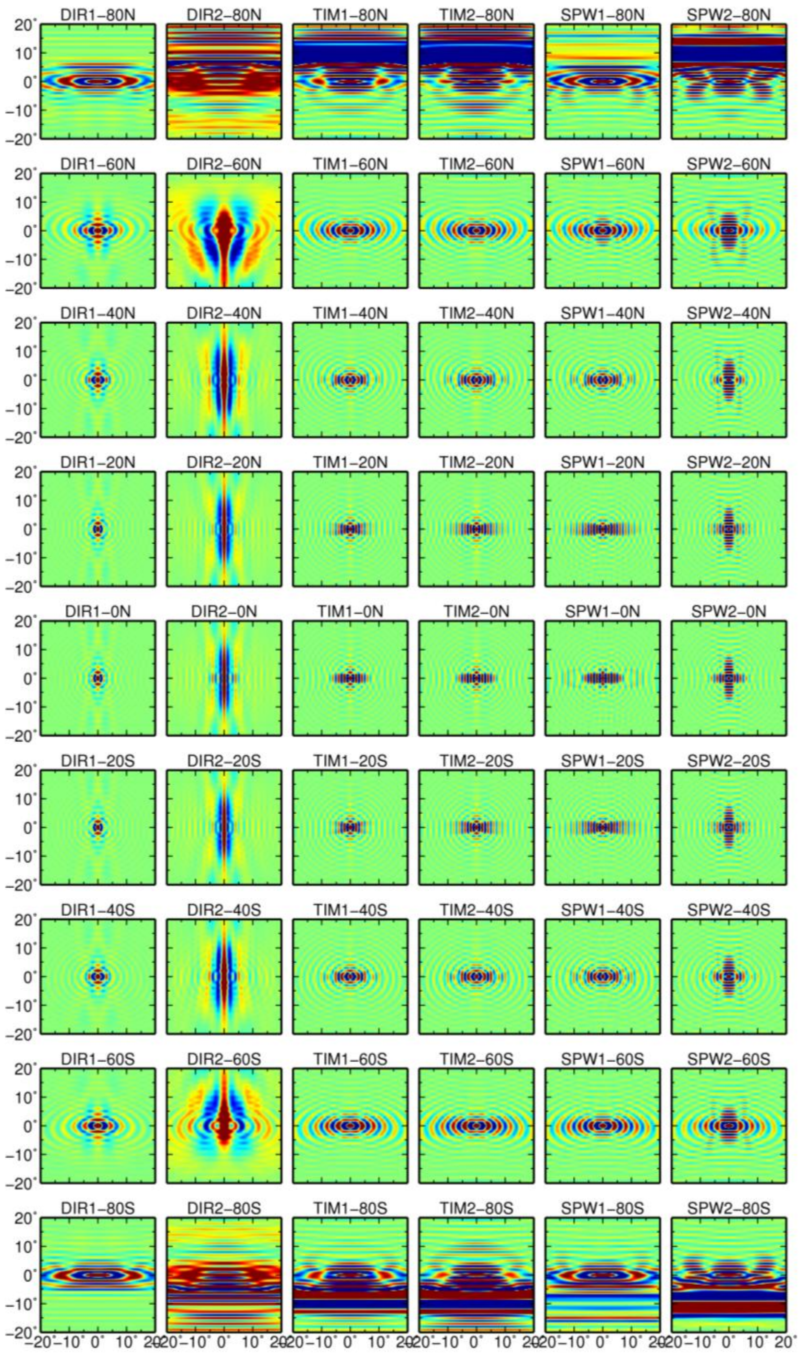

Figure 27: Zonal mean geoid error covariance functions over a range of latitudes for each of the GOCE models, with truncation at d/o=200.

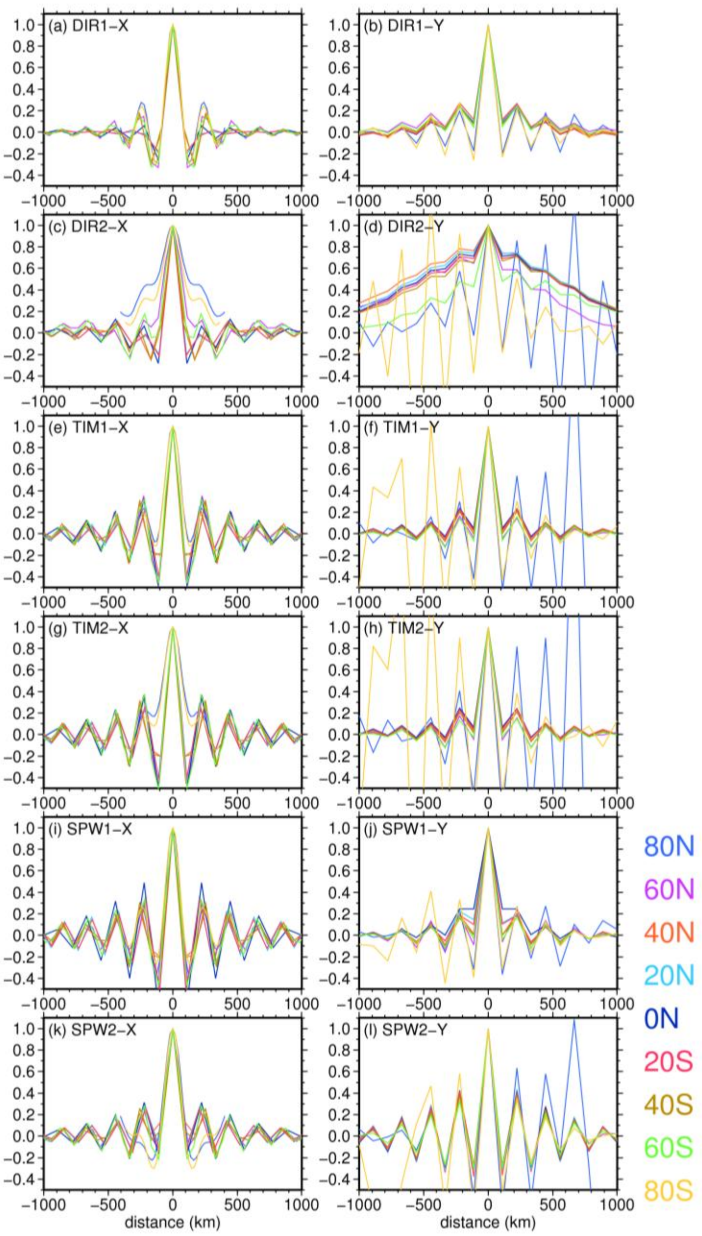

Figure 28: Zonal (left) and meridional (right) cross-sections through the d/o=200 zonal mean geoid error covariance functions shown in Figure 27.

The growth of the zonal stripes is also clear in the meridional cross sections. Given the presentation as a function of degree in the Figures showing the ECF maps, it is not easy to judge the similarity of the ECFs between different latitudes. This, however, can be done in the cross section plots where the independent variable is distance. From these plots we see that the zonal mean ECFs of the timewise models at d/o=50 are very similar within at least 40 degrees of the equator. Between 40 and 60 degrees from the equator the zonal stripes increase rapidly in magnitude leading to a quite different form for the ECFs. Some hemispheric asymmetry in terms of form is also now apparent, with greater zonal oscillations in the Northern Hemisphere. These zonal stripes are most likely related to the polar gap problem.

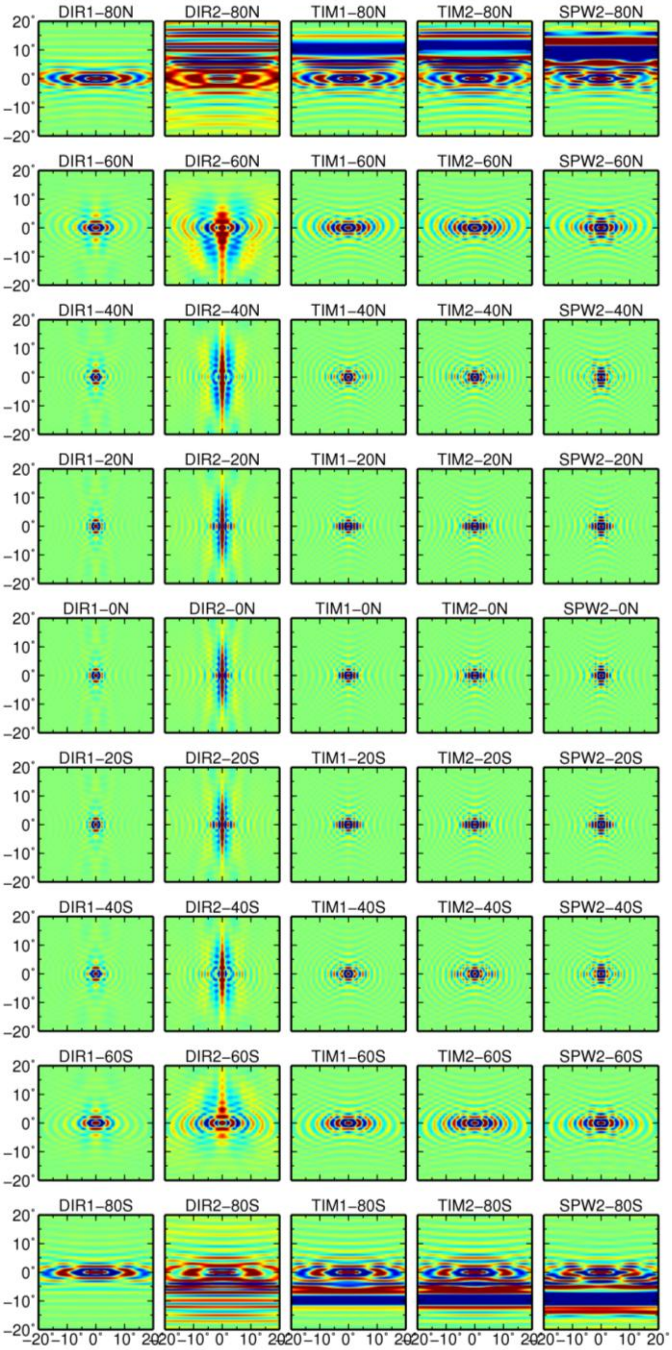

Figure 29: Zonal mean geoid error covariance functions over a range of latitudes for each of the GOCE models, with truncation at d/o=224.

Moving to higher truncation values the form of the timewise ECFs change. The zonal strippiness decreases, and the meridional stripes become narrower and reduced in amplitude. At d/o=200 and higher, the zonal strippiness of the TIM ECFs has all but disappeared except at the highest latitudes. Comparison of the zonal and meridional cross-sections of the timewise ECFs at d/o=200 and above reveals that the ECFs within 60 degrees of the equator have become symmetrical with regard the zonal and meridional directions, that is, they are largely rotationally symmetric, except that the oscillatory decay in the zonal direction is somewhat less than for the meridional direction. It is also clear that within 60 degrees of the equator for truncations of 200 and greater the timewise ECFs have very similar form.

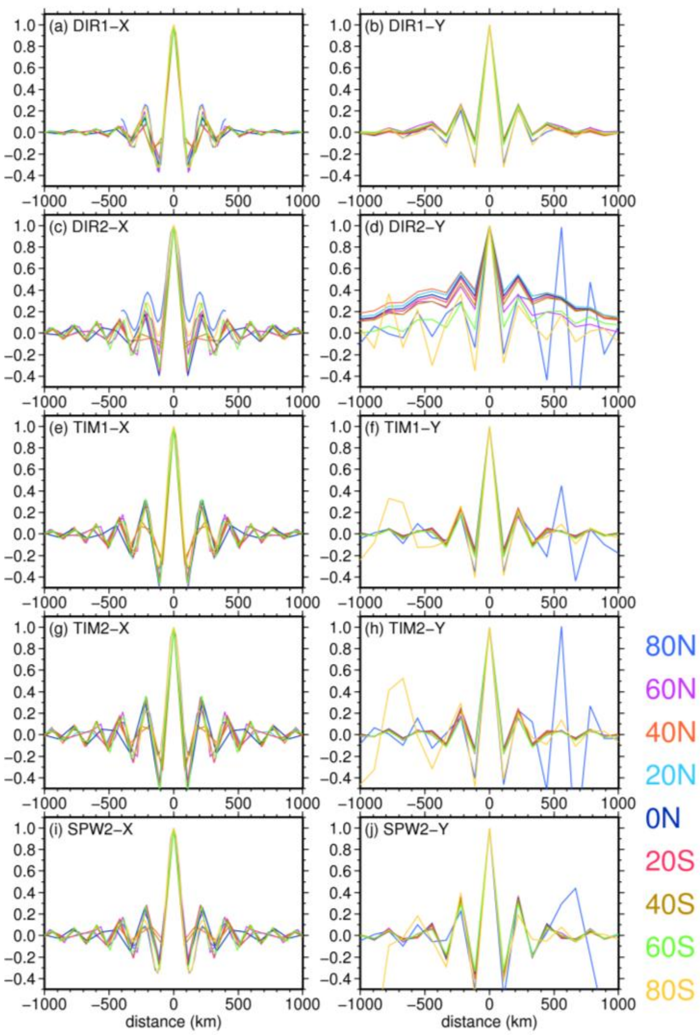

Figure 30: Zonal (left) and meridional (right) cross-sections through the d/o=224 zonal mean geoid error covariance functions shown in Figure 29.

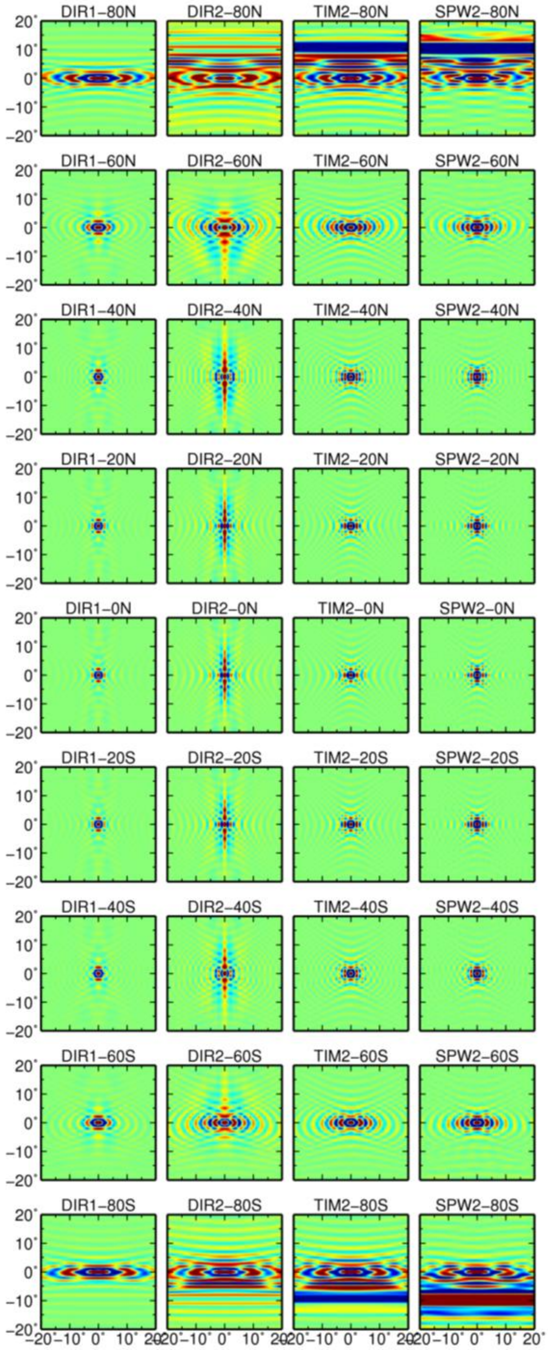

Figure 31: Zonal mean geoid error covariance functions over a range of latitudes for each of the GOCE models, with truncation at d/o=240.

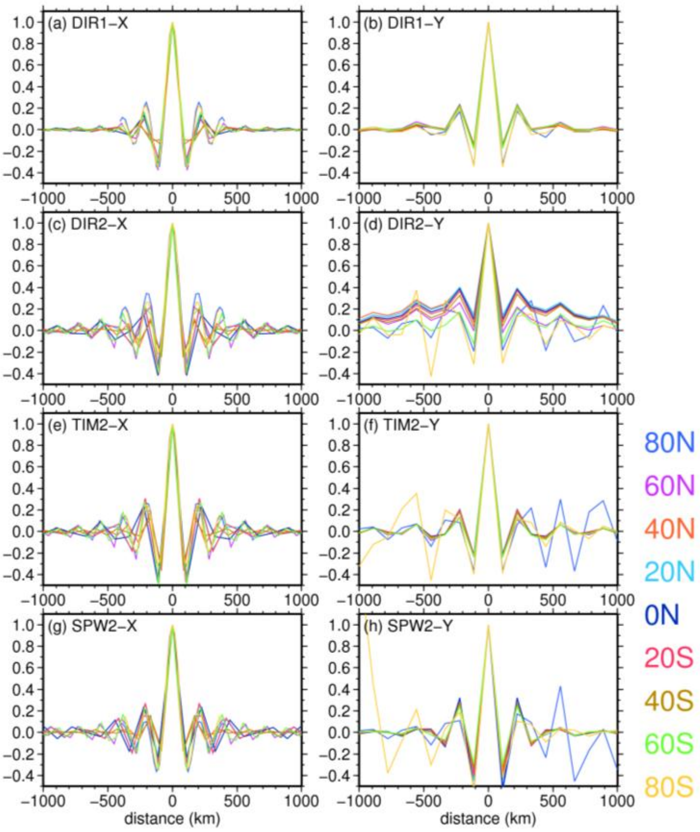

Figure 32: Zonal (left) and meridional (right) cross-sections through the d/o=240 zonal mean geoid error covariance functions shown in Figure 31.

At d/o=50 the first direct solution has a largely rotationally symmetric pattern, apart from at the highest latitudes, and from the zonal cross-sections plots the ECFs do not change much with latitude within 80 degrees of the equator. For d/o=100 and d/o=150 some of the error covariance patterns become somewhat elongated in the meridional sense . This is particularly clear in the cross section plots. From d/o=200 onward the DIR1 ECFs return to a more rotationally symmetric form and the patterns become tightly focused around the central point, with only marginal correlation in the errors at surrounding points. At d/o=50 the ECFs of the second direct solution are similar to those of the first model, but with meridional length scales somewhat greater, as is clear from the cross section plots. As for the DIR1 model for d/o=100 and d/o=150 the ECFs patterns become more meridionally elongated. However, unlike the DIR1 model and the TIM models, the DIR2 ECFs do not return to a largely rotationally symmetric form at d/o=200 and above. This asymmetry between the zonal and meridional length scales is clear in the cross section plots. Also greater differences between the ECFs and different latitudes are seen, as is a greater asymmetry between the north and south hemispheres. Looking for instance at the cross section plots at d/o=200 (Figure 28) one can see that in this respect the DIR2 model is similar to the TIM1 and TIM2 models. The asymmetry and strong oscillations at 80N and 80S seen in these models is not seen in the DIR1 or SPW1 models. Since these latter models employ an a priori constraint, whereas the others do not, this shows the impact such a constraint has on the solutions at high latitudes, even at high degree and orders. This perhaps explains why the zonal mean ECFs of the first spacewise model are quite similar over all latitudes and truncations to those of the DIR model. The main difference being a somewhat slower decay of the zonal oscillations and slightly less meridional elongation. This likely reflects differences in the solution procedures.

At d/o=50, the ECFs of the SPW2 model are very unlike those of the other models, including SPW1. The zonal strippiness seen in the timewise models at high latitudes persists even at the equator in SPW2, although as Figure 22 shows the amplitude of the oscillations does decrease somewhat with latitude. The picture at d/o=100 is similar, but a meridional central stripe is now visible. At d/o=150 the SPW2 ECFs are rather more rotationally symmetric than the SPW1 ECFs, but then at d/o=200 meridional oscillations along the central axis are more pronounced. Beyond d/o=200, the SPW2 ECFs are similar to those of the timewise model.

4.3 Model inter-comparisons

In the previous section, similarities between the ECFs of the various models were noted. In this section the degree of similarity is quantified by calculating the spatial correlation between the ECFs. This is done globally for actual ECFs in Figure 33 (d/o=50), Figure 35 (d/o=100), Figure 37 (d/o=150), Figure 39 (d/o=200), Figure 41 (d/o=224), and Figure 43 (d/o=240). Correlations as a function of latitude are also calculated for the zonal mean ECFs discussed in the previous section. These are shown in Figure 34 (d/o=50), Figure 36 (d/o=100), Figure 38 (d/o=150), Figure 40 (d/o=200), Figure 42 (d/o=224), and Figure 44 (d/o=240).

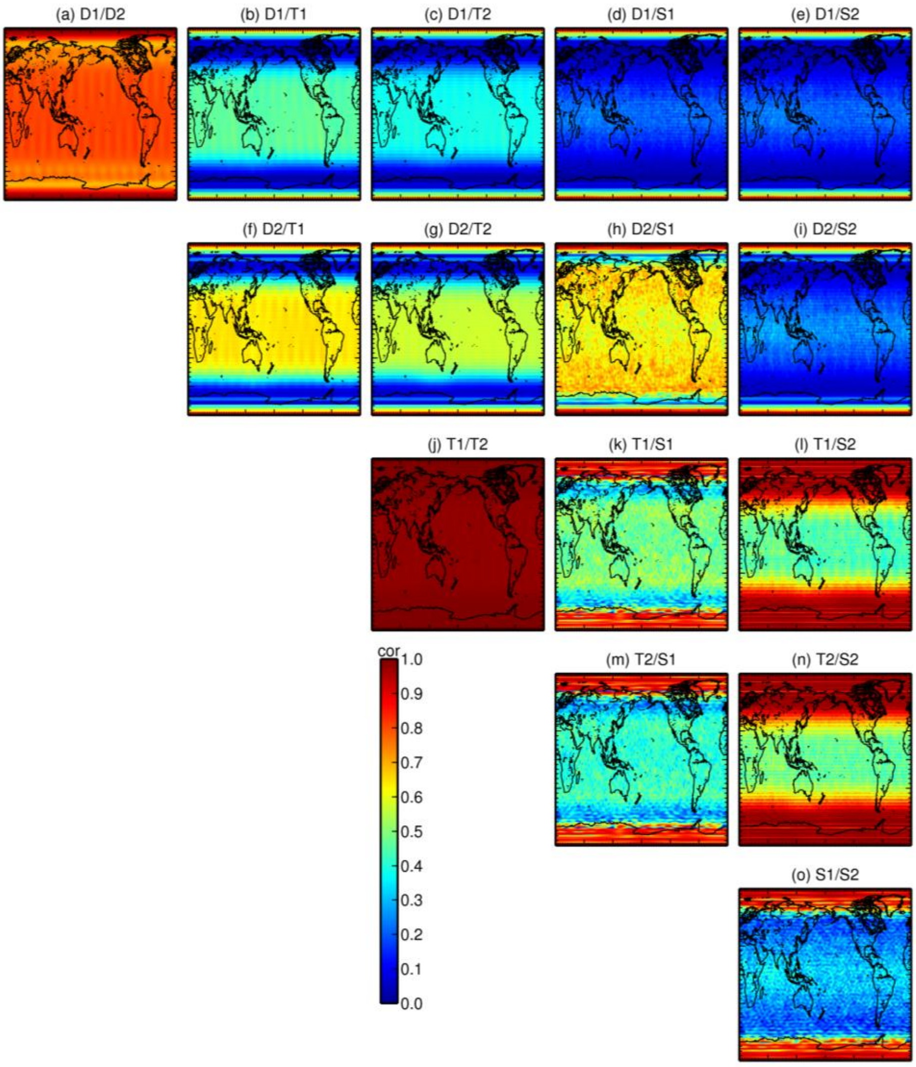

Figure 33: The correlation at each point on a global grid between each pair of error covariance functions at that point, with truncation at d/o=50.

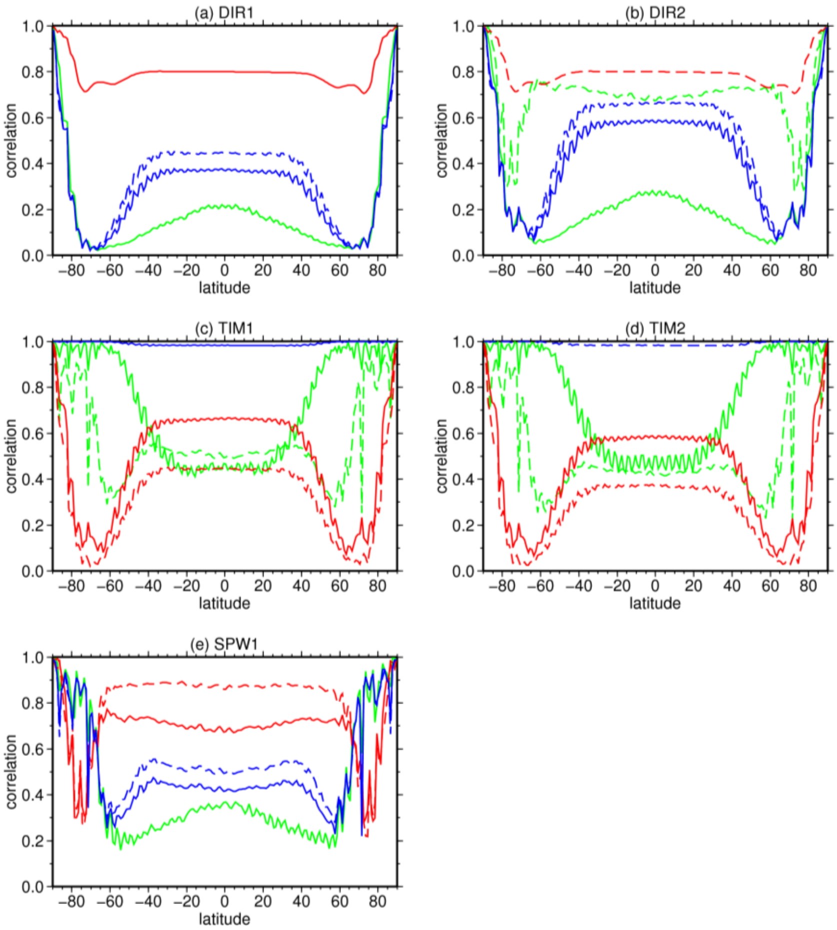

Figure 34: The correlation at each latitude between each pair of zonal mean error covariance functions at that latitude for truncation at d/o=50. The colours are as follows: direct (DIR) models (red); timewise (TIM) models (blue); spacewise (SPW) models (green). Dashed curves correspond to first generation models.

This correlation analysis confirms the earlier visual impression of the similarity between the two timewise models. This shows that while extra data decreases the error magnitudes, it does not change much the spatial form of the ECFs. The poorest agreement between the two models is seen near 60S and 60N, where the correlation drops to about 0.9. This suggests that the additional data has some impact on how the polar gap influences the form of the ECFs. Such a close correlation is not found between the first and second generations of the direct models. This shows that the additional constraint of the a priori model used in the first solution does have a substantial impact on the form of the ECFs. This is seen in both the global and zonal mean comparisons. In fact, for truncations greater than d/o=100, the DIR2 model is the least similar to the DIR1 model. At d/o=50 the DIR2 model is much more similar to the DIR1 model than either of the timewise models. However, at all but the highest latitudes – latitudes greater than 60 degrees – the ECFs of the first spacewise model are closer to those of the DIR1 model, although the difference is not great. Yet as the truncation d/o is increased from 50 to 200, the degree of similarity between the ECFs of the DIR1 and DIR2 models decreases, until for the zonal mean ECFs at d/o=200 the correlation between DIR1 and DIR2 is less than 0.6. At the same time as the truncation is increased, the similarity between the ECFs of DIR1 and those of the timewise model increases, such that at d/o=200 the zonal mean ECFs are correlated at around 0.8 within 50 degrees of the equator. At higher latitudes the correlations are much lower. For the global analysis, as the d/o is increased from 50 to 200 the correlation between the DIR1 model and the SPW1 model decreases, but not by a great deal, within 60 degrees of the equator, while, for the zonal mean ECFs, the correlation between DIR1 and SPW1 remains constant. Poleward of 60 degrees the agreement between DIR1 and SPW1 increases between d/o=50 and d/o=200. Just the reverse is seen with regard to the relationship between the SPW1 model and the timewise models, with similarity growing with increasing d/o within 60 degrees of the equator but falling at higher latitudes. In fact, within 60 degrees of the equator the zonal mean ECFs of the SPW1, TIM1 and TIM2 models are essentially identical at theses latitudes at d/o=200, with the DIR1 model not far behind.

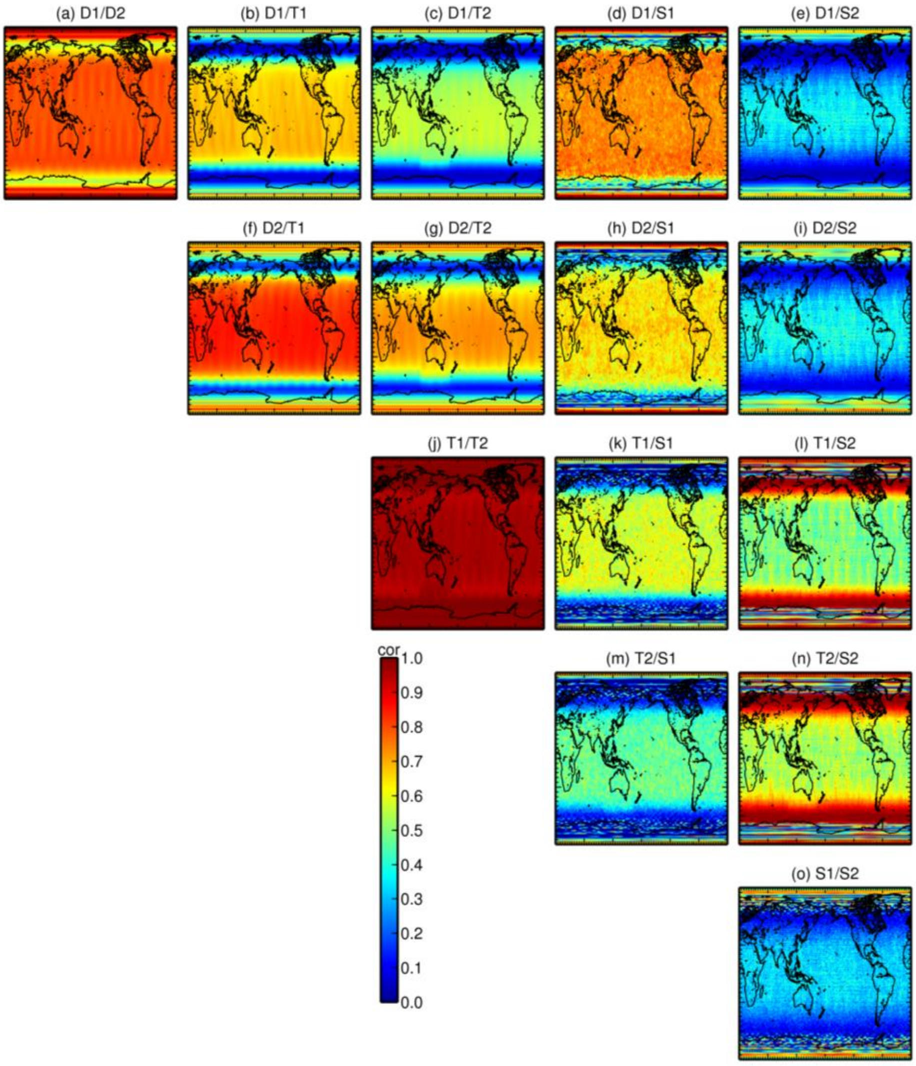

Figure 35: The correlation at each point on a global grid between each pair of error covariance functions at that point, with truncation at d/o=100.

Of all the solution methods, it is for the spacewise approach that the form of the EFCs has changed the most between generations, as reflected in the generally lower correlations globally. This is surprising given that it is the direct solution method, where the GRACE a priori constraint has been dropped, that would seem to have changed the most. Between d/o=50 and d/o=200 the two spacewise solutions become more similar, except at high latitudes where they diverge, but even at d/o=200 correlations are no more than about 0.6 globally or 0.8 for the zonal mean ECFs. Also, the second spacewise solution is less like the other models, than is the first spacewise solution, both globally and for the zonal mean ECFs.

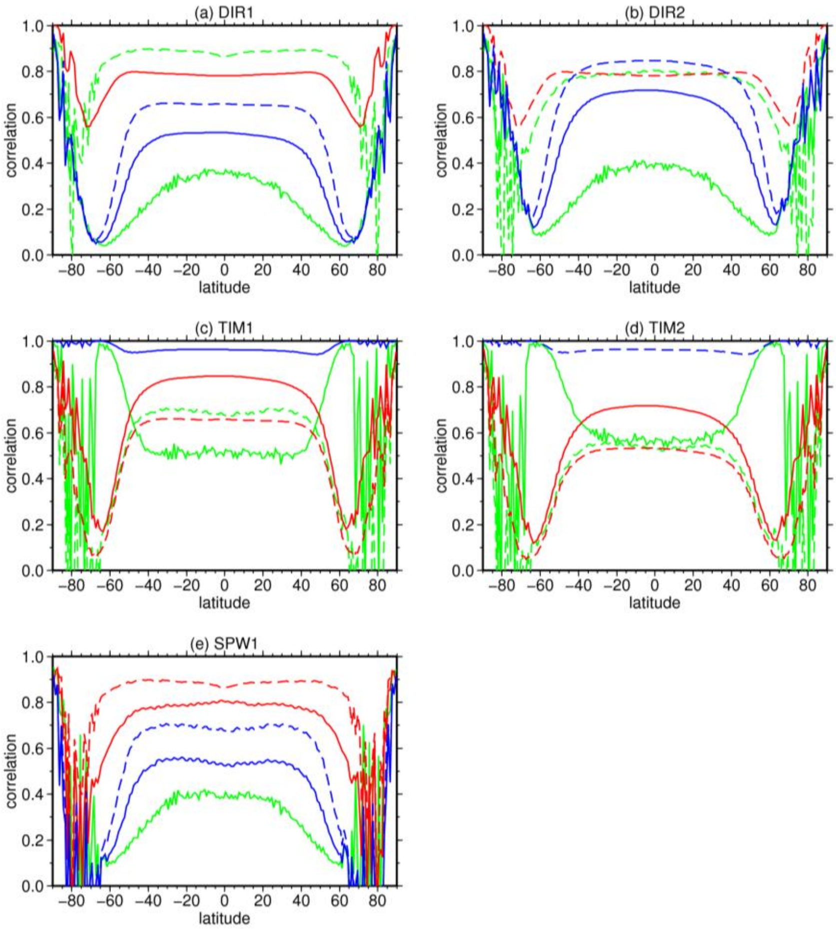

Figure 36: The correlation at each latitude between each pair of zonal mean error covariance functions at that latitude for truncation at d/o=100. The colours are as follows: direct (DIR) models (red); timewise (TIM) models (blue); spacewise (SPW) models (green). Dashed curves correspond to first generation models.

At d/o=224 (for which the first spacewise model is no longer defined) the DIR2 model starts to become more similar to the DIR1 model again and at d/o=240 the correlation between the zonal mean ECFs for the two models is around 0.8 except at 80N and 80S where it dips to 0.6. But the DIR2 model remains less similar to DIR1 than the timewise models which continue to become more like DIR1 except at the highest latitudes. This analysis therefore shows the DIR2 error characteristics to be quite different from the other models. This is because, as was seen above, while the other models become more rotationally symmetric with increasing degree, losing to a large extent any originally present meridional elongation of patterns, the ECFs of the DIR2 model keep their meridionally elongated form right up to d/o=240. Again the SPW2 model is the least like the other models, but is somewhat closer to the timewise models than the direct models, especially DIR2.

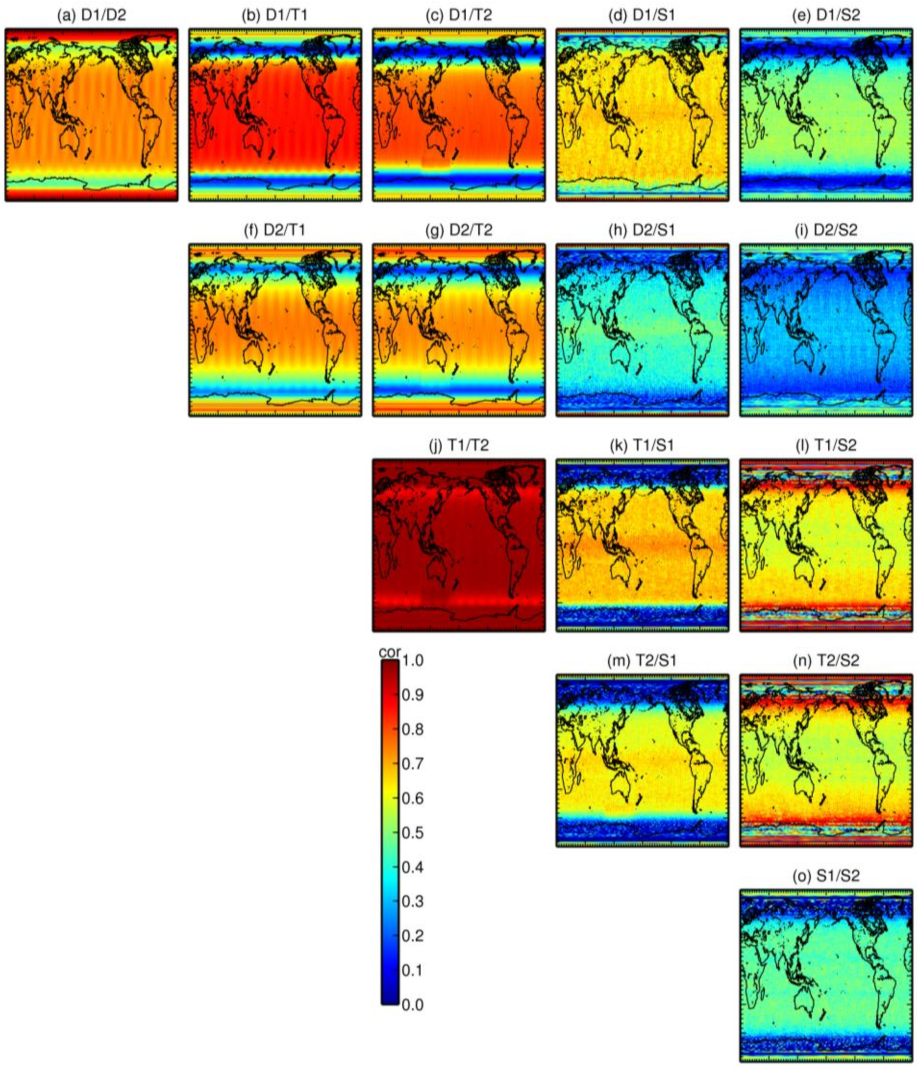

Figure 37: The correlation at each point on a global grid between each pair of error covariance functions at that point, with truncation at d/o=150.

However, at d/o=240 there is little to distinguish the DIR1, DIR2 and TIM2 models, except at the highest latitudes. One would imagine that this is because at high d/o truncations the ECFs are dominated by the larger amplitude errors in the higher degree and order terms that swamp the smaller, but larger scale errors in the lower degree and order terms. The length scales associated with this noise are obviously small and this is reflected in the similarity of the error length scales. However, this interpretation (made before the SPW2 model was available) is somewhat contradicted by the comparison with the SPW2 model, which shows that substantial differences in the form of the ECFs can remain even for the highest degrees. Nonetheless, the analysis shows that a single ECF will not be sufficient to fully characterise the error structure in a geoid or MDT. A way must be found of accounting for spatial scale.

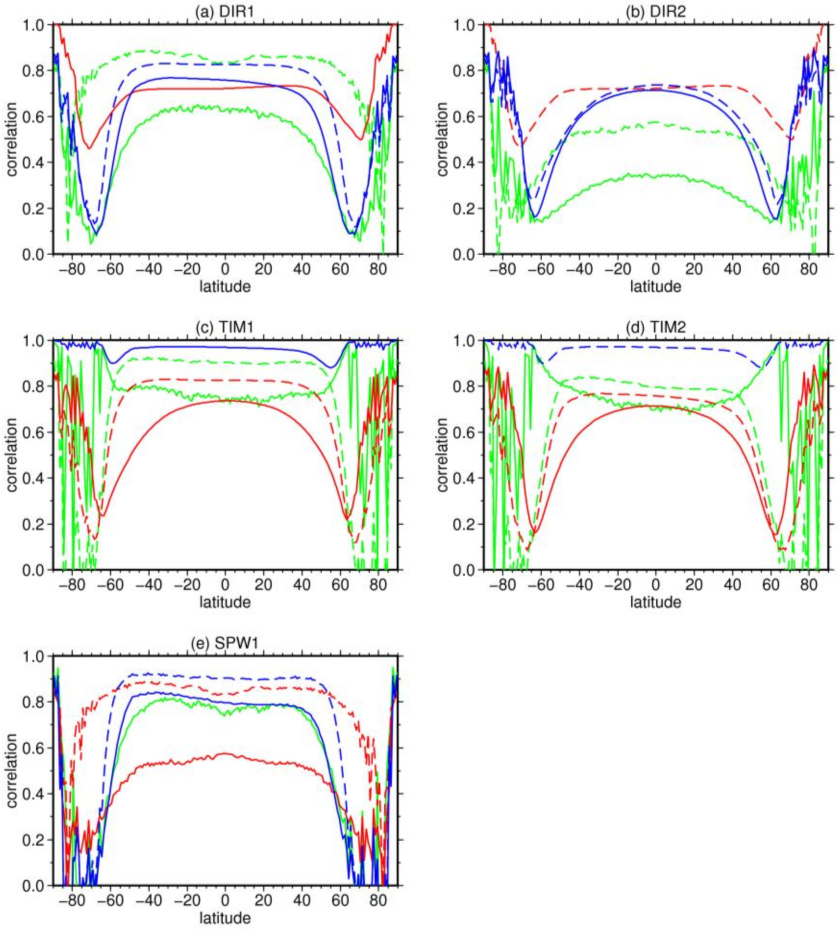

Figure 38: The correlation at each latitude between each pair of zonal mean error covariance functions at that latitude for truncation at d/o=150. The colours are as follows: direct (DIR) models (red); timewise (TIM) models (blue); spacewise (SPW) models (green). Dashed curves correspond to first generation models.

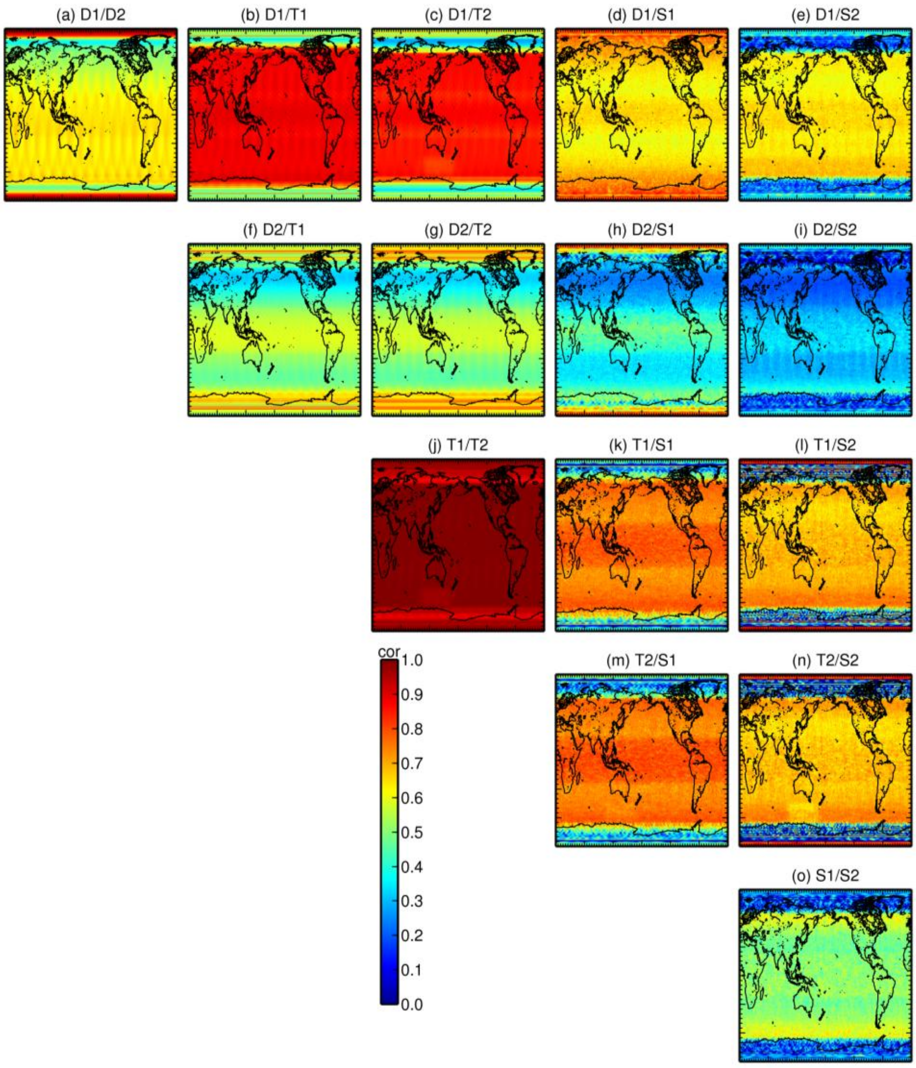

Figure 39: The correlation at each point on a global grid between each pair of error covariance functions at that point, with truncation at d/o=200.

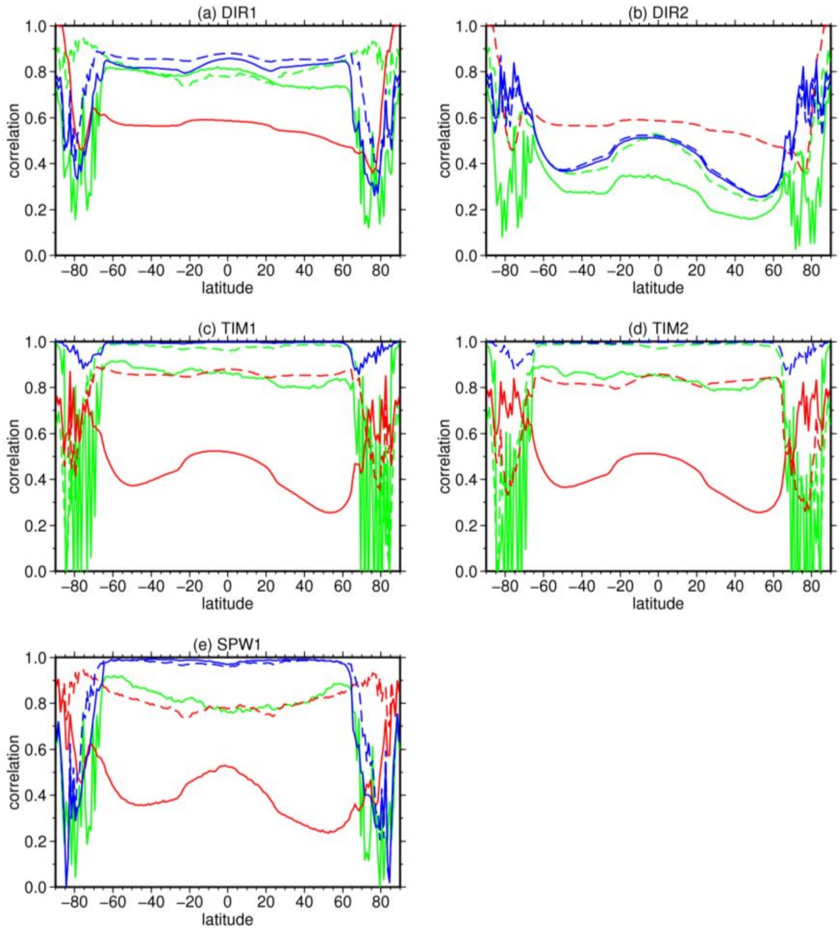

Figure 40: The correlation at each latitude between each pair of zonal mean error covariance functions at that latitude for truncation at d/o=200. The colours are as follows: direct (DIR) models (red); timewise (TIM) models (blue); spacewise (SPW) models (green). Dashed curves correspond to first generation models.

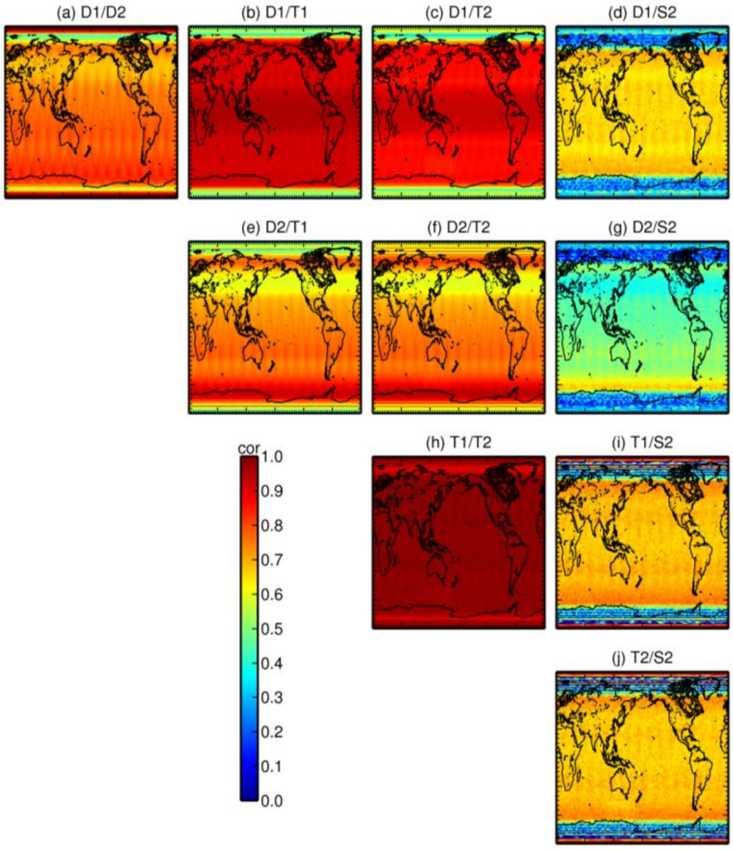

Figure 41: The correlation at each point on a global grid between each pair of error covariance functions at that point, with truncation at d/o=224.

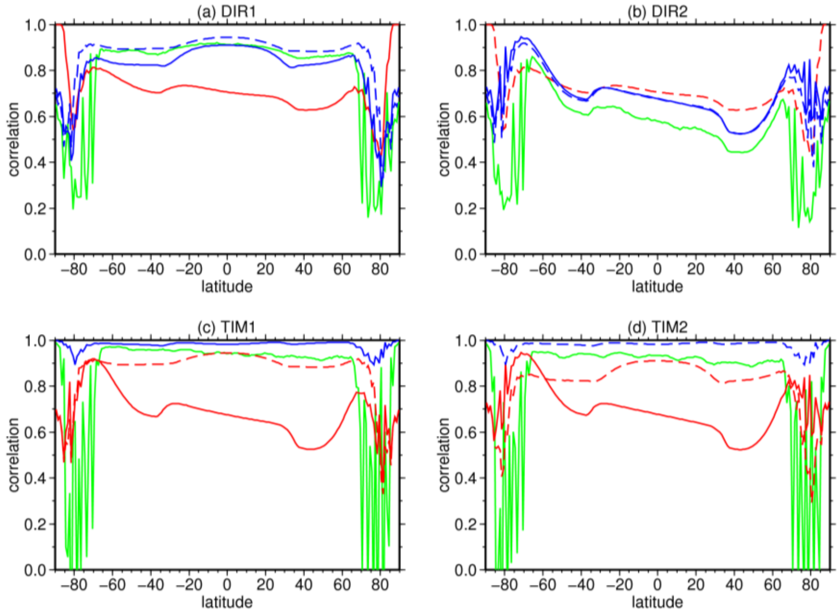

Figure 42: The correlation at each latitude between each pair of zonal mean error covariance functions at that latitude for truncation at d/o=224. The colours are as follows: direct (DIR) models (red); timewise (TIM) models (blue); spacewise (SPW) models (green). Dashed curves correspond to first generation models.

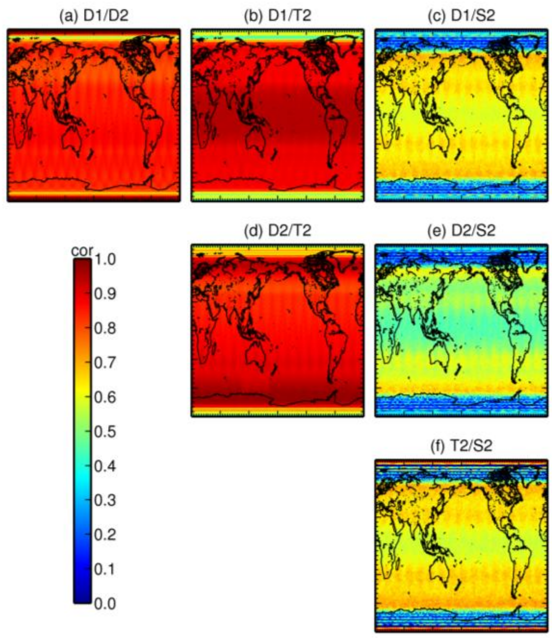

Figure 43: The correlation at each point on a global grid between each pair of error covariance functions at that point, with truncation at d/o=240.

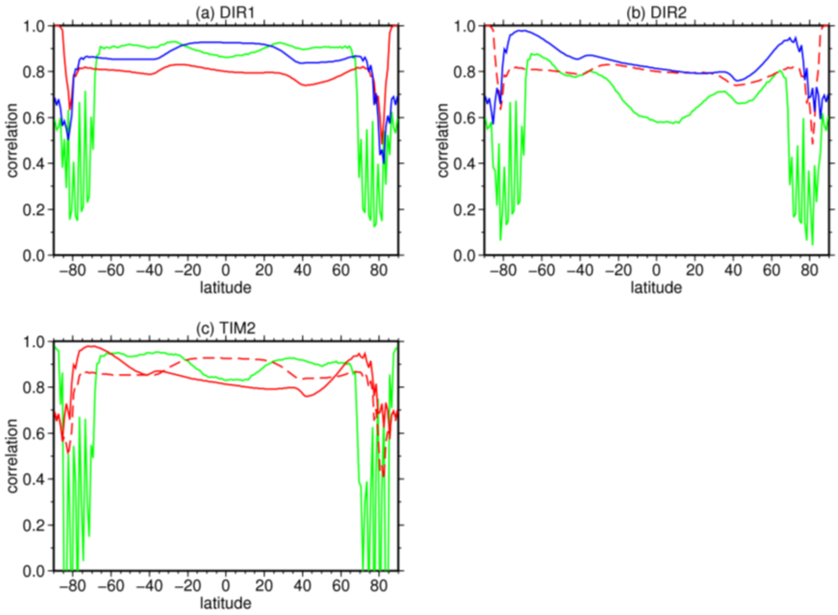

Figure 44: The correlation at each latitude between each pair of zonal mean error covariance functions at that latitude for truncation at d/o=240. The colours are as follows: direct (DIR) models (red); timewise (TIM) models (blue); spacewise (SPW) models (green). Dashed curves correspond to first generation models.

4.4 Correlation length scales

One important potential application of the GOCE geoid and error product is in the assimilation of a GOCE based MDT into an ocean model. In lieu of an ocean model data assimilation scheme directly using the full error variance-covariance matrix, a simpler approach is to characterise the error properties of the MDT in terms of an error magnitude, as shown in section 3 above, and a length scale, or scales, characterising the error structure. (For now we must assume that MDT errors results entirely from the geoid, since error covariance information for the mean sea surface is not available.) This approach is one presently being followed by the UK Met Office (see RD4).

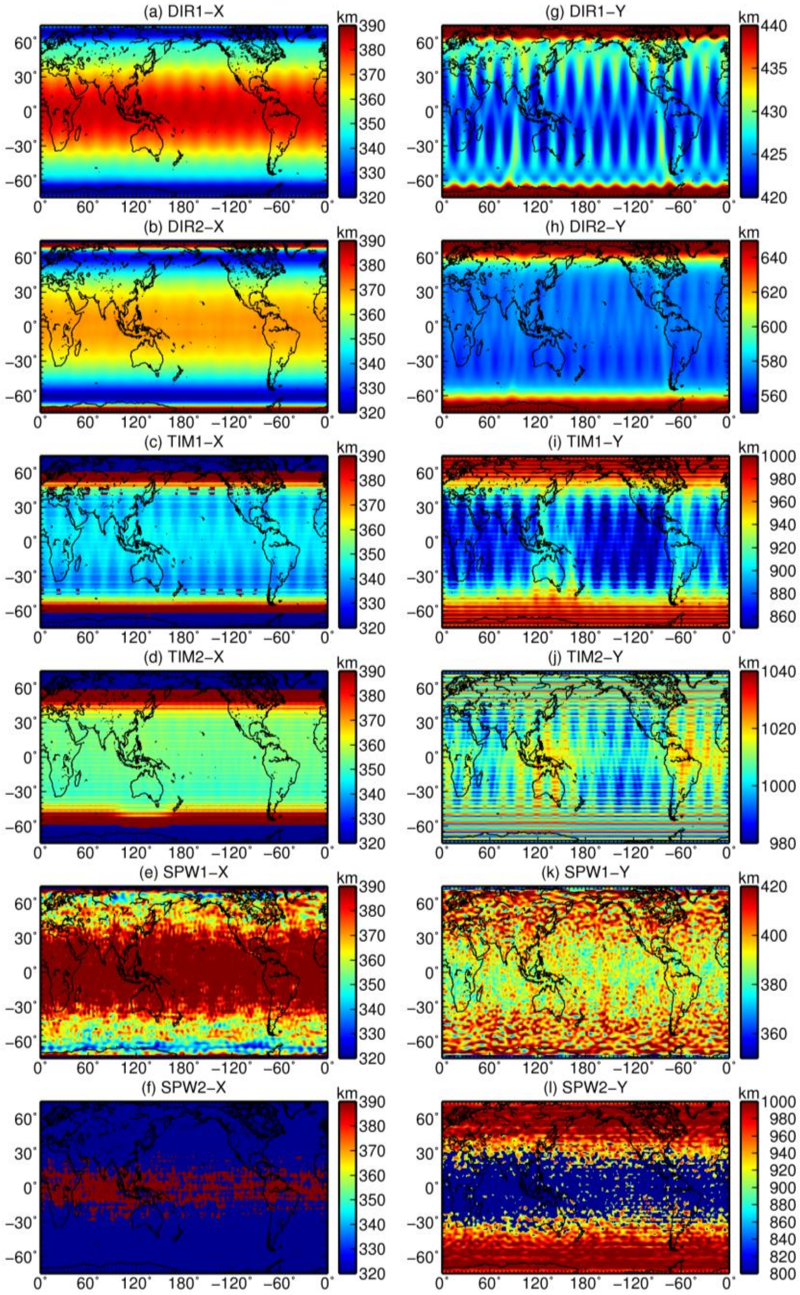

Figure 45: The zonal (left) and meridional (right) e-folding length scales of the geoid error covariance functions with truncation at d/o=50.

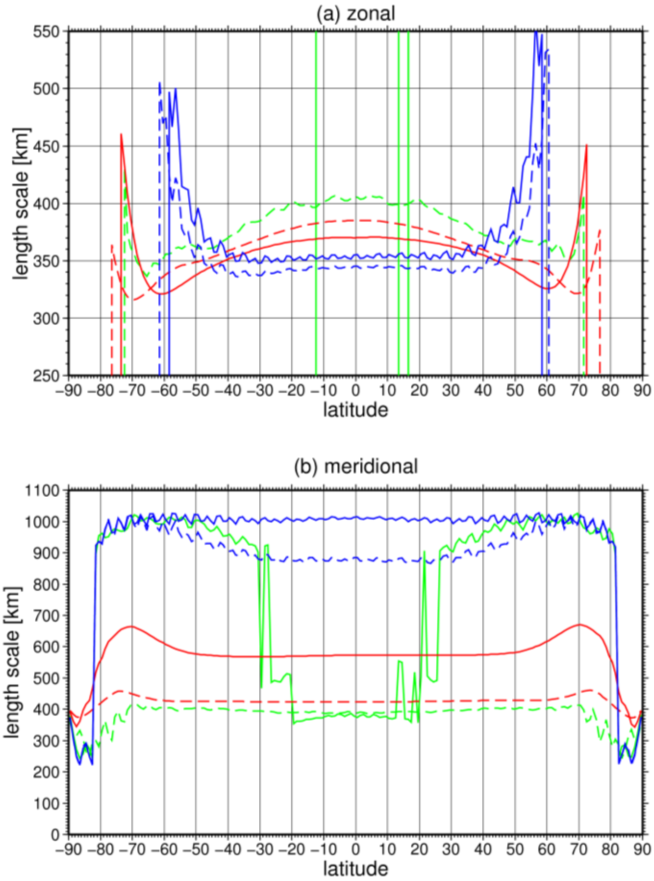

Figure 46: The zonal (a) and meridional (b) e-folding length scales of the zonal mean geoid error covariance functions with truncation at d/o=50. The colours are as follows: direct (DIR) models (red); timewise (TIM) models (blue); spacewise (SPW) models (green). Dashed curves correspond to first generation models.

A common characterisation of decorrelation length scale is the e-folding length, defined as the distance at which the covariance drops to e^{-1} of its value at the origin. If the ECFs were rotationally symmetric then it would be possible to define a single length scale. However, as shown above, this is not always the case for the GOCE models. The zonal and meridional length scales tend to be different, especially at lower degree and orders. With errors in the meridional (along track) direction tending to have greater length scales than those for the zonal (across track) direction. This anisotropy is related to the orbital configuration of the satellites, with errors tending to be more correlated along the meridional oriented track of the satellite. In this section, therefore the GOCE ECFs are characterised by zonal (x) and meridional (y) length scales, as defined by the zonal and meridional cross sections of the ECFs shown above (Figure 22 (d/o=50), Figure 24 (d/o=100), Figure 26 (d/o=150), Figure 28 (d/o=200), Figure 30 (d/o=224) and Figure 32 (d/o=240)).

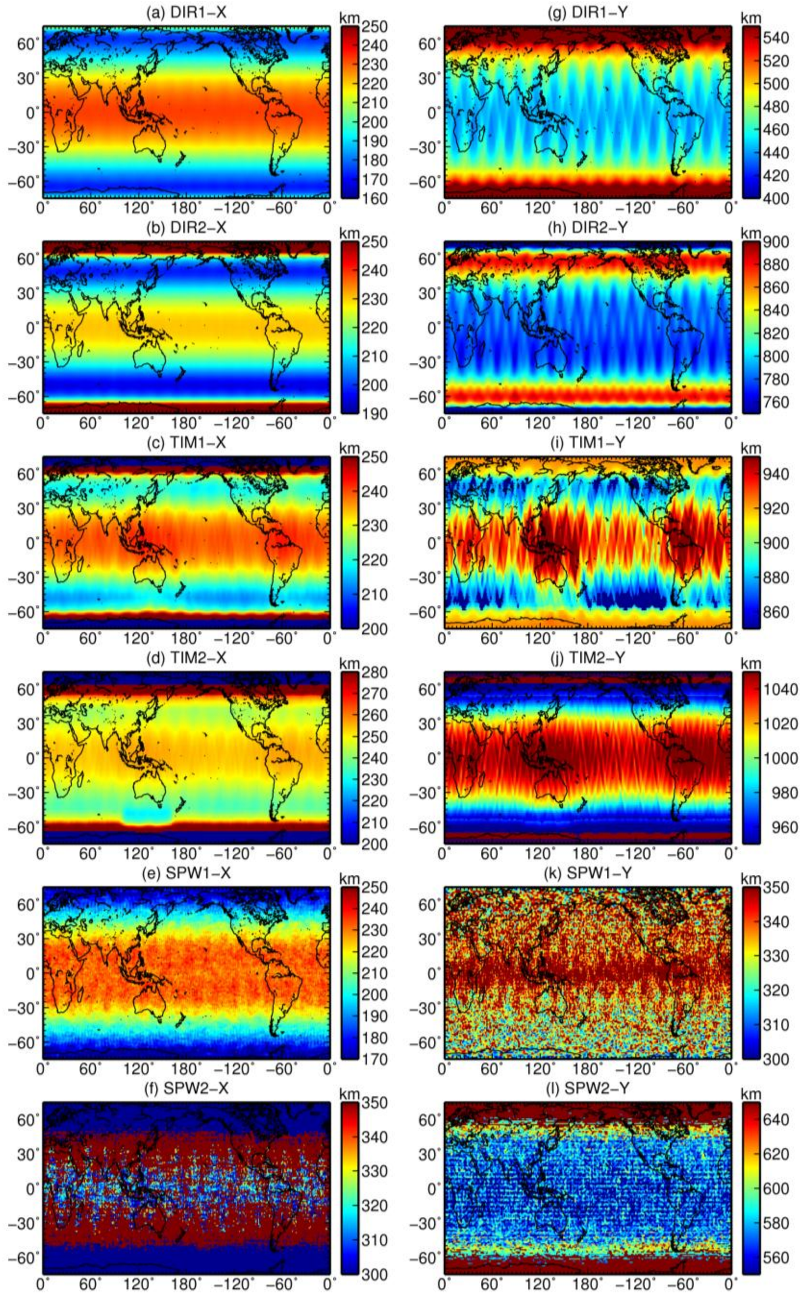

Figure 47: The zonal (left) and meridional (right) e-folding length scales of the geoid error covariance functions with truncation at d/o=100.

The x and y correlation length scales for the actual ECFs are shown in Figure 45 (d/o=50), Figure 47 (d/o=100), Figure 49 (d/o=150), Figure 51 (d/o=200), Figure 53 (d/o=224) and Figure 55 (d/o=240). For the zonal mean ECFs the length scales are shown in Figure 46 (d/o=50), Figure 48 (d/o=100), Figure 50 (d/o=150), Figure 52 (d/o=200), Figure 54 (d/o=224) and Figure 56 (d/o=240).

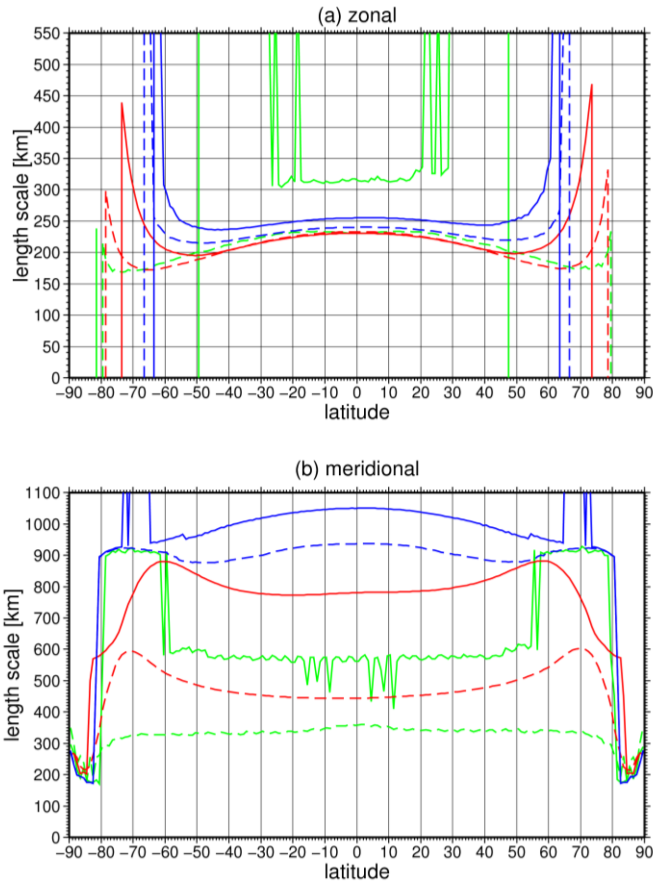

Figure 48: The zonal (a) and meridional (b) e-folding length scales of the zonal mean geoid error covariance functions with truncation at d/o=100. The colours are as follows: direct (DIR) models (red); timewise (TIM) models (blue); spacewise (SPW) models (green). Dashed curves correspond to first generation models.

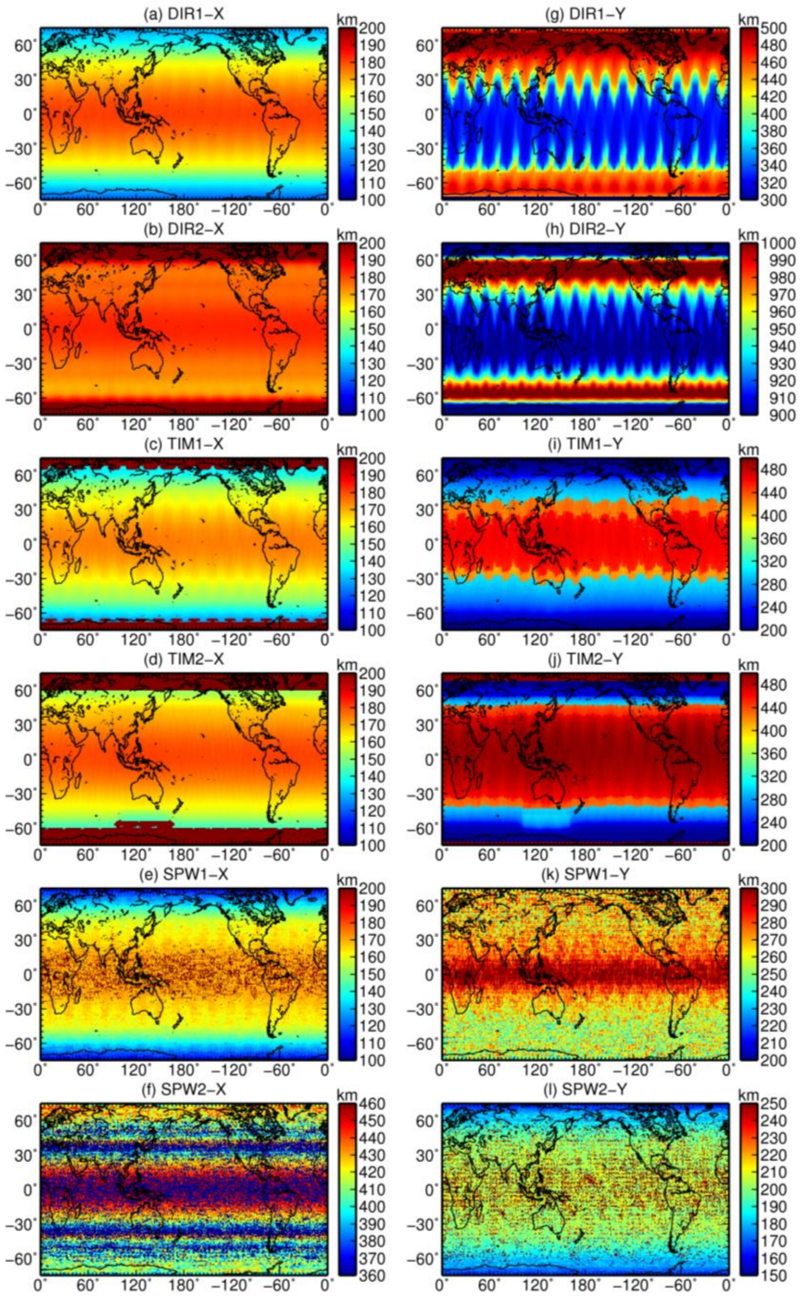

Figure 49: The zonal (left) and meridional (right) e-folding length scales of the geoid error covariance functions with truncation at d/o=150.

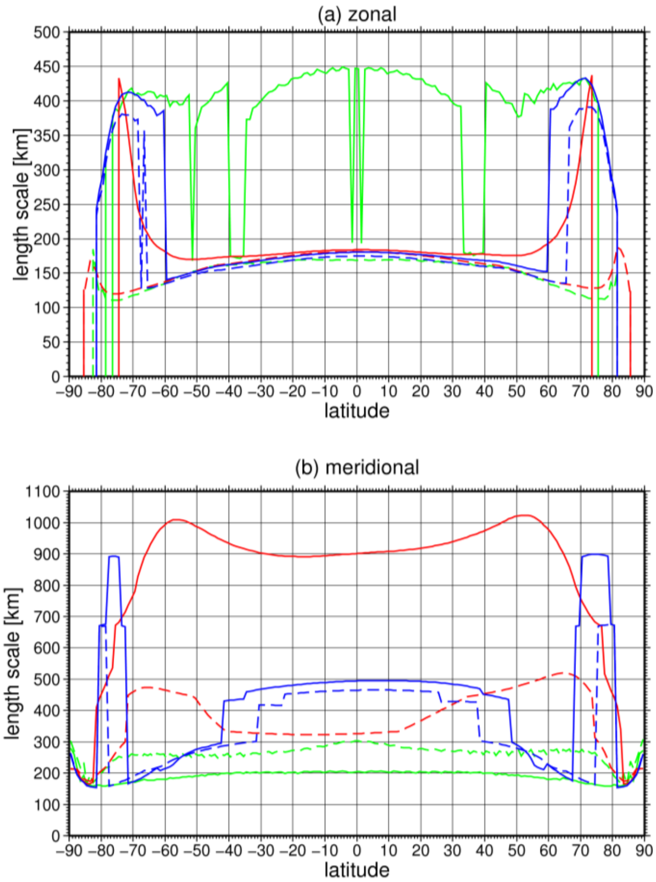

Figure 50: The zonal (a) and meridional (b) e-folding length scales of the zonal mean geoid error covariance functions with truncation at d/o=150. The colours are as follows: direct (DIR) models (red); timewise (TIM) models (blue); spacewise (SPW) models (green). Dashed curves correspond to first generation models.

Considering first the zonal length scales of the zonal mean ECFs, the overall tendency is for the models to converge as we move to higher truncations. The main difference being the latitude beyond which the length scale becomes undefined because it exceeds the width of the window in which the ECFs were computed (shown by the vertical lines in the figures). This is at about 60S(N) for the timewise models and 70-80S(N) for the direct models and the first spacewise model at d/o=50, but moves poleward for higher truncations. Excluding the high latitudes regions, where the zonal length is not well defined, the zonal length scale profiles as a function of latitude for the zonal mean ECFs general have a convex shape with a maximum at the equator. The greatest variation in the equatorial maximum is seen at d/o=50 where it varies between about 400 km for the first spacewise model to about 340 km for the timewise models, with the direct solutions mid way between this. At d/o=50 the strong zonal strippiness of the SPW2 solution means that the point at which the correlation falls bellow e^{-1}

lies beyond the window of the ECF calculation and so cannot be found. Excluding SPW2, at d/o=100 the range of the maximum is 200 to 250 km, while at d/o=150 the equatorial zonal length scales are similar at around 170 km. At d/o=100 and d/o=150, where they can be defined the zonal length scales of the SPW2 model are significantly greater than the other models. From d/o=200 onwards the zonal length scales of all the models, including SPW2, show a similar latitudinal dependence and all zonal length scales (except for SPW1) remain constant with increasing degree at close to 150 km at the equator.

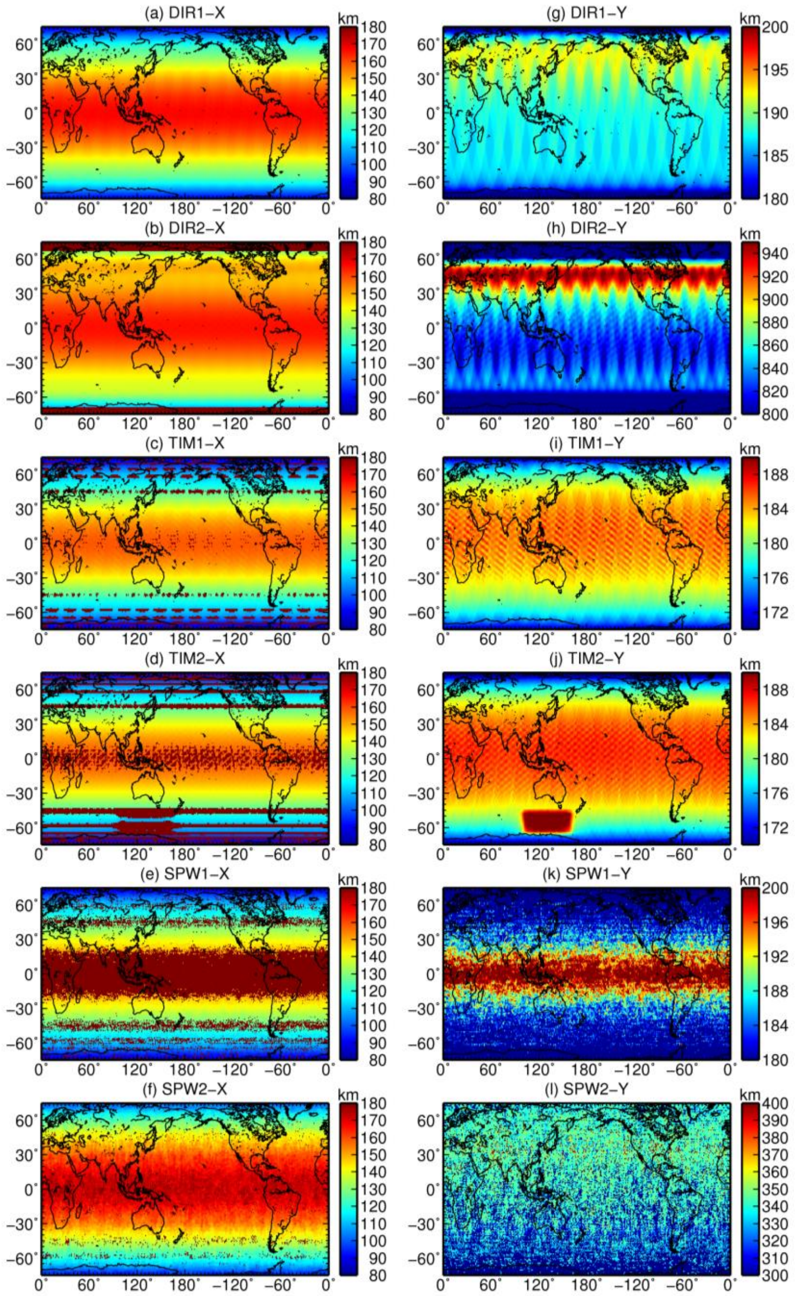

Figure 51: The zonal (left) and meridional (right) e-folding length scales of the geoid error covariance functions with truncation at d/o=200.

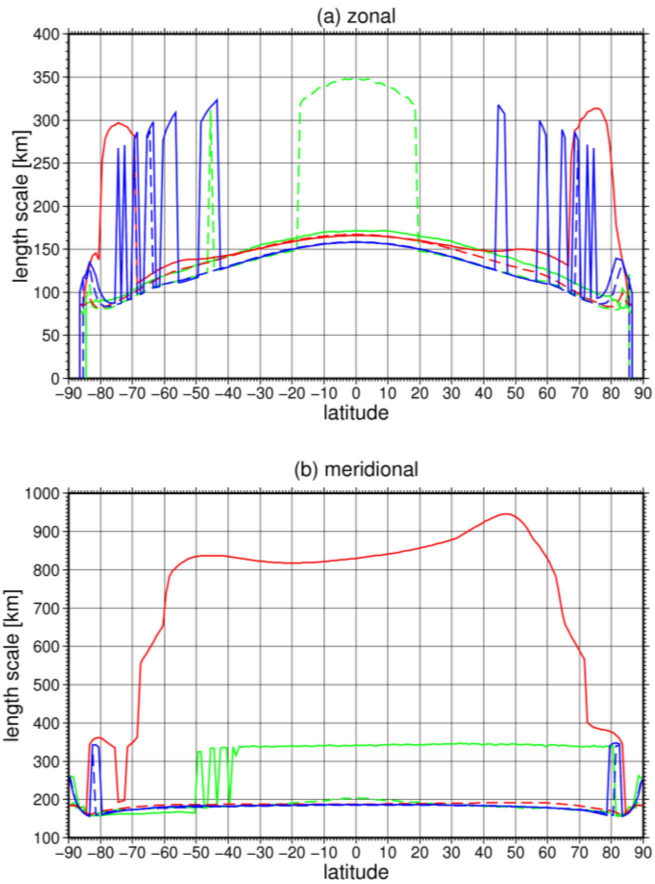

Figure 52: The zonal (a) and meridional (b) e-folding length scales of the zonal mean geoid error covariance functions with truncation at d/o=200. The colours are as follows: direct (DIR) models (red); timewise (TIM) models (blue); spacewise (SPW) models (green). Dashed curves correspond to first generation models.

The abrupt jump up in the zonal length scale for the first spacewise model at d/o=200 within 20 degrees of the equator, as well and similar spikes in the zonal scales for the other models at higher latitudes and at higher truncations reflects a limitation of the basic approach here of finding the e-folding length scale. As can be seen from inspection of the zonal and meridional cross-sections, the ECFs do not general show a smooth exponential decline especially at higher truncations. In fact, the ECFs tend to drop rapidly to below zero and then decay in an oscillatory fashion. The jumps in length scale occur when the secondary peak exceeds e^{-1}, and because the all the second peaks may be close to this threshold small variations in the amplitudes in the oscillations can produce large jumps in the length scale. The d/o=200 truncations are most affected by this problem because it is at this truncation that the amplitude of the secondary peak lies close to e^{-1}. (With hindsight a simple solution to this would be to define the length scale to be when the ECF *first* drops below e^{-1}, rather than when it *last* drops below e^{-1} as was done here. From inspection of the ECF cross section plots this would clearly produce smoother results. However, ideally a more sophisticated fitting approach would probably be best. This is presently under investigation but could not be completed with the deadline for this report.) This also demonstrates the difficulty of finding some simple form for the error covariance functions.

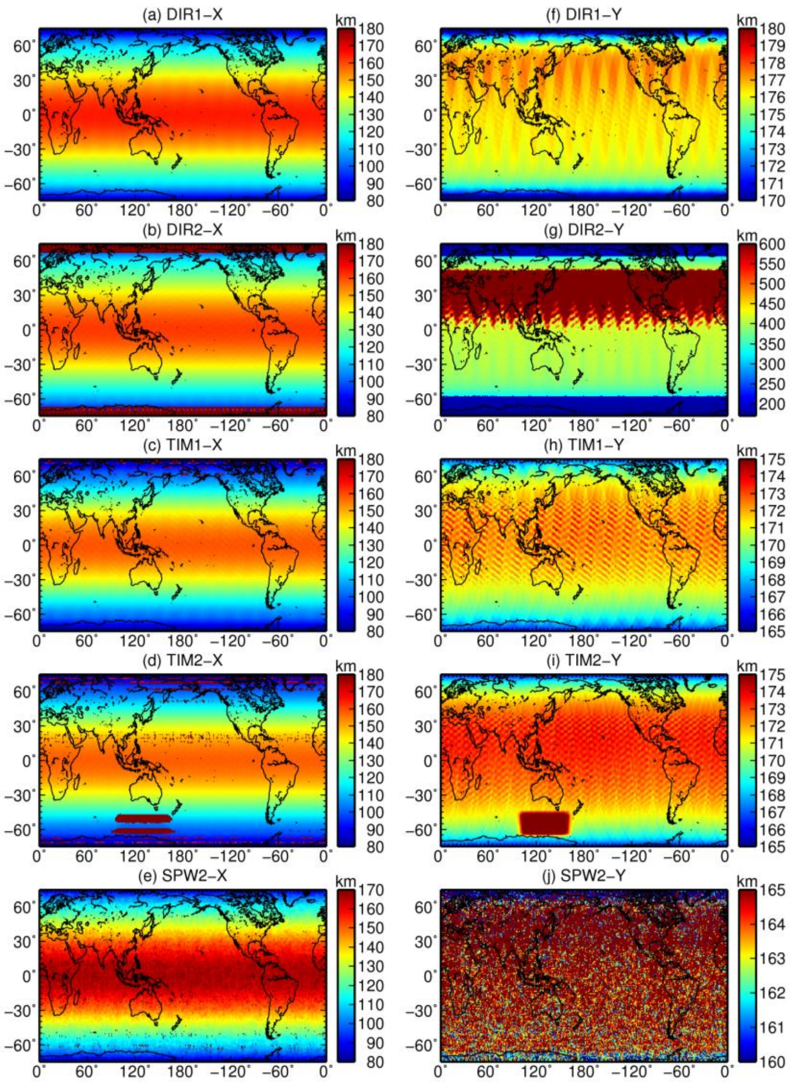

Figure 53: The zonal (left) and meridional (right) e-folding length scales of the geoid error covariance functions with truncation at d/o=224.

The zonal length scales computed globally for the actual ECFs largely follow what is found for the zonal mean ECFs. It is clear from these global maps how the length scale jumping issue does not affect the direct models to the same extent as the other models. It is also clear from the global plots that for the four models defined to d/o=240 the zonal length scales are quite similar, ranging from about 160 km at the equator to about 100 km at 70 degrees north and south.

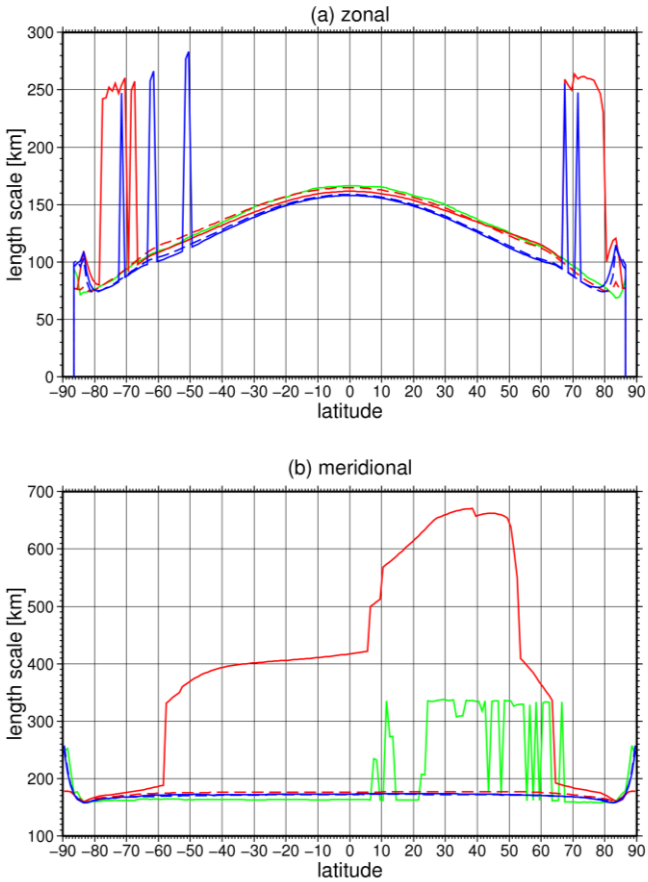

Figure 54: The zonal (a) and meridional (b) e-folding length scales of the zonal mean geoid error covariance functions with truncation at d/o=224. The colours are as follows: direct (DIR) models (red); timewise (TIM) models (blue); spacewise (SPW) models (green). Dashed curves correspond to first generation models.

It is true for all of the models that the meridional length scales for a given d/o are greater than the zonal length scales. Also for truncations up to d/o=150 there is a greater range of length scales between the models. At d/o=50, the meridional length scales from the DIR1 and SPW1 models are around 400 km (perhaps indicating the impact of an a priori constrain on the meridional length scale), while the timewise models are much greater at 870 to 1000 km. It is interesting that the additional data in the second release has lead to an increase in the meridional length scale, at lower latitudes. For the DIR2 model the meridional length scale is mid-way between these two extremes at around 570 km. SPW2 is similar to SPW1 within 20 degrees of the equator but then abruptly jumps to values closer to the timewise models. Note also that in comparison to the zonal length scales the meridional length scales are more constant with latitude. At d/o=100, except for SPW2, the ordering of the models in terms of meridional length scale has been preserved. For SPW1 the meridional lengths have been reduced to around 300 km, while for the timewise models they have changed little. However, for both the direct models, but particularly the DIR2 model, the meridional length scales have increased. This reflects the transition from a more rotationally symmetric form of the ECFs to a meridionally elongated form as observed above. SPW2 has a constant meridional length scale of just under 600 km between 60S and 50N. At d/o=150, with the exception of the DIR2 model, the meridional length scales of all the models, but most notable the timewise models, have decreased. The jumps in the length scales for the timewise model occur for a similar reason to the jump for the zonal scales. For the DIR2 the meridional length scales are now between 900 to 1000 km. For the timewise models the large drop in length scales reflects a transitions to a more rotationally symmetric form as seen above. At d/o=200 and beyond all of the models except DIR2 and to some extent SPW2 have very similar meridional length scales of around 180 km, similar the zonal length scales at these truncations.

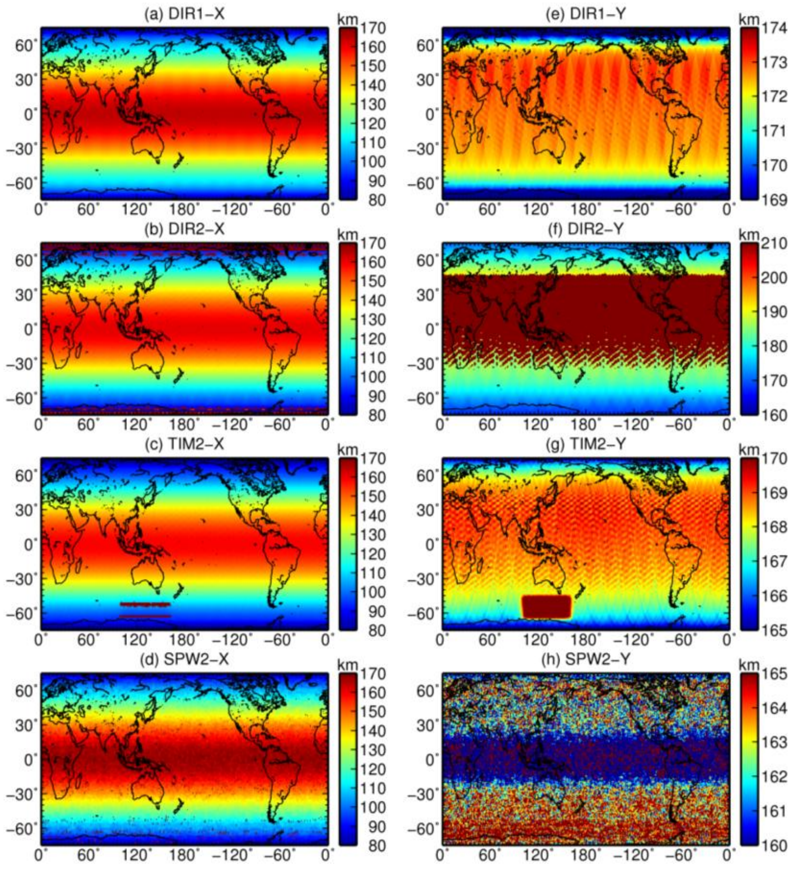

Figure 55: The zonal (left) and meridional (right) e-folding length scales of the geoid error covariance functions with truncation at d/o=240.

At d/o=200, in particular, the DIR2 model stands out from the other models in that the meridional length scales are much greater than for the other models. Inspection of the meridional cross sections for the zonal mean ECFs at d/o=200, shows that this difference arises because of the quite different form of the ECFs in the meridional direction for the DIR2 model, with the decay in the meridional direction being much slower than for the other models. For truncations greater than 200 the meridional profiles of the DIR2 start to become more similar to the other models. However, jumps in the meridional length scales arise because the amplitude of the first trough is close to e^{-1}. Again this show the limitation of the simple minded approach to defining a error correlation length scale taken here.

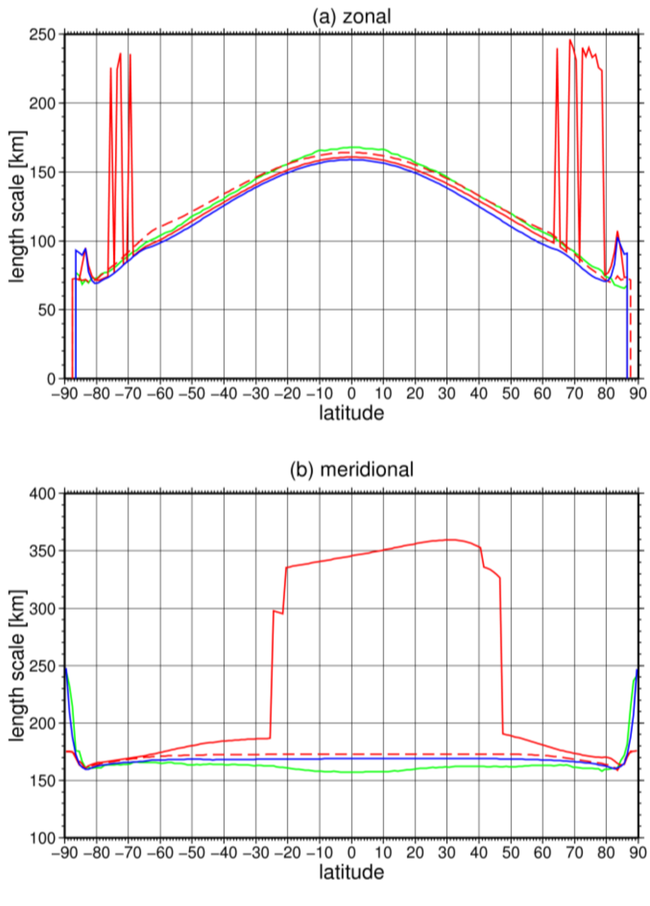

Figure 56: The zonal (a) and meridional (b) e-folding length scales of the zonal mean geoid error covariance functions with truncation at d/o=240. The colours are as follows: direct (DIR) models (red); timewise (TIM) models (blue); spacewise (SPW) models (green). Dashed curves correspond to first generation models.

5 Conclusions and recommendations

The availability of the full error variance-covariance matrices for the GOCE gravity field models is an important feature of the GOCE mission. Potentially, it will allow users to evaluate the accuracy of a geoid or mean dynamic topography (MDT) derived from the gravity field model at any particular location, design optimal filters to remove errors from the surfaces, and rigorously assimilate a geoid/MDT into ocean models, or otherwise combine the GOCE gravity field with other data. This report has presented an initial investigation into the error characteristics of the GOCE gravity field models as they are realised in the calculated geoid anomalies. This should be considered only a very preliminary investigation of the error characteristics of the GOCE EGMs, and a full physical interpretation of the results cannot, as yet, be given.

However, some general characteristics of the GOCE geoid error fields have emerged from the analysis conducted in this work package (WP3000). Error magnitudes depend primarily on latitude, and are nearly symmetrical about the equator. Errors are at a maximum at polar latitudes, but fall rapidly to the hemispheric minimum values just inside the polar gaps between 70-80N(S). Errors grow again and reach a local maximum near the equator. Relatively small zonal variations in errors resulting from the orbital path of the satellite are clear. Considering errors with truncation at d/o=200 (close to the highest common possible truncation), if the error estimates are to be taken at face value, then the second direct solution is the most accurate, with peak low latitude errors of about 7.5 cm and high latitude minimum errors of 2-3 cm. The errors for the second timewise model are around 2 cm greater. Comparing this with the first timewise solution, which differs only in the smaller number of observations used in the solution (2 months vs. 8 months), we see that the extra GOCE data has reduced the errors in the timewise solution by up to 6 cm or 40%. In contrast the errors of the two direct solutions are similar, showing the impact the GRACE a priori constraint used in the first solution, but not in the second, has on errors, even at short wavelengths. Of all the solutions the first spacewise solution is the worst but not by a great deal more than the first timewise solution, with peak errors of just under 18 cm right on the equator. For the timewise solutions a slight hemispheric asymmetry is clear with errors slightly greater in the southern hemisphere and peaking at around 15S. To a lesser extent this asymmetry is also seen in the other models.

For truncations below d/o=200, it was found that errors of the second timewise solution were the lowest and those of the second direct model the highest, with the difference being a factor of 2 at d/o=150 and more at lower d/o truncations. In contrast, for truncations beyond d/o=200, the errors are lower for the second direct solution than for the second timewise solution, with the difference growing to 8 cm – almost a factor of 2 at d/o=240. The obvious conclusion is that the timewise approach gives a better estimate of the longest wavelength terms of the gravity field, up to d/o=200, but for the shortest wavelengths between degree 200 and 240, the direct approach is superior. Comparing the timewise models across all truncations shows that the impact of the additional GOCE data is greatest in relative terms for the longer wavelengths, but the impact is generally between 40 and 50%. Comparing the error characteristics of the two direct models shows the error reduction due to the GRACE a priori is generally greater than the noise reduction from the additional GOCE data, with the difference in impact diminishing towards shorter wavelengths, and impacts becoming about equal beyond about degree 200.

The physical interpretation and significance of the error covariance is more challenging, and more work will be required to fully understand and exploit this information. The preliminary investigations presented here show that for all of the models and over all truncations, the error covariance function at any latitude can be closely approximated by the zonal mean ECF at that latitude. In terms of zonal and meridional cross sections, within about 60 degrees of the equator the form of the ECFs does not change much with latitude. The form of the ECFs seems to depend on the solution method. The ECFs of the two timewise models are essentially identical, and at low degree and order quite distinct from the other models. The ECFs of the two direct solutions are less similar, with the second model having a less rotationally symmetric pattern. Moving to higher d/o truncations, the ECFs of the various models converge on a similar rotationally symmetric pattern. The second direct solution, however, is an exception, maintaining its meridionally elongated pattern even at high degree and order. An attempt is made to characterise the ECFs in terms of zonal and meridional e-folding length scales, with the results generally confirming the preceding analysis.

Calculations were performed using the software developed by G. Balmino (RD2), which is provided in parallel with the GOCE User Toolbox (GUT). For the authors, the biggest initial challenge was putting the error variance covariance information as supplied by ESA into the form required by the Balmino routines. This was complicated by the fact that the format in which the error covariance information is supplied is not standardised across the models. The main difference being that some models the coefficients for a given order m are supplied as even and odd pairs C_{lm} and S_{lm} as required by the Balmino routines, whereas for other models the ordering is given in block format with all odd coefficients following all the even coefficients. Although relatively straightforward to address, it would seems sensible to remove this additional burden on the user by standardising the ordering scheme.

Another barrier to the use of the error information is that files containing the error information are large which may present a problem for some users. Obviously, all other things being equal, the sizes of the files are governed by the d/o to which the gravity model is defined. However, the primary governing factor for file size and the reason for the large differences between files is the number of decimal place to which the coefficients are defined. For the timewise models this is 16 decimal places, leading to a download file size for the second timewise model of 20GB and an uncompressed file size for the tarball containing the coefficients of 52GB. The large download file size may pose a problem for some users, while those that can download it may struggle to find sufficient disk space to uncompress and store the files. In contrast, however, the spacewise models are given to only three decimal places, resulting in much smaller file sizes. This suggests that the size of timewise and direct models (10 decimal places) are unnecessarily large and their size could be much reduced. It would seem wise to use a consistent number format with the lowest number of decimal places for all models. This would prevent the unnecessary download of GB and consumption of disk space, making the errors products more accessible.

Having written the required interfaces to convert the ESA supplied error information into the format required by the Balmino routines, these will now be made available to the user community in a future release of GUT. Looking further ahead, these small conversions routines could, without too much effort, be fully integrated into the toolbox. Thus providing a convenient entry point for those wishing to explore the error characteristics of the GOCE gravity models. This would, however, involve the defining of a new data type within the GUT framework. To fully integrate all of the error calculation functionality of the Balmino routines in the GUT toolbox, would likely require substantial recoding effort, and so they will likely remain, for now at least, as standalone tools. If there were the resources to develop the error handling capabilities of the toolbox further, then the most useful, and perhaps feasible, next step would be to include the ability to calculate error fields on an arbitrary grid or set of points and to an arbitrary degree and order. The ability to easily calculate the error field for a given geoid or similar product would be a valuable addition to the toolbox. On the other hand, it is likely that the GOCE error covariance information will only be of limited specialist interest, outside the realm of interest of most toolbox users. Therefore, the incorporation of this functionality into to the toolbox should be considered of much lower priority.

As stated in the original work package description, an aim of the work package was to look for fast approximations to the error variance/covariance. We have not been successful in finding such approximations. If they do exist their discovery will require further research effort. However we find the error propagation calculations with this software to be reasonably quick on a standard PC. For instance, calculating a global error map on a 1x1 degree grid for a geoid truncated at d/o=250 took less than 100 minutes. Similarly, the computation of the error covariance map in a 40x40 degree window, took no more than a few minutes per point. This may obviate the need to find fast approximations.

On the basis of the experience gained during the completion of WP3000 the following recommendations are made to the HPF (given in order of decreasing importance):

- Supply error variance-covariance matrix with a standard ordering scheme. Ideally the interleaved scheme required by Balmino routines.
- Supply error variance-covariance matrix with a standard number format, with only the numbers only given to minimum required precision to reduce size of files that the user must download, store and handle.
- Supply users with a stand alone tool to convert supplied ASCII files into unformatted binary as required by the Balmino routines.
- Integrate conversion tool into GUT.
- Extend GUT functionality to allow error variance fields to be calculated.
- Extend GUT functionality to allow error covariance fields to be calculated.